Development of biodegradable magnesium alloy scaffolds for tissue engineering

Javier Trinidad

Mondragon Unibertsitatea
Mechanical and Manufacturing Department

September 10, 2013

Development of biodegradable magnesium alloy scaffolds for tissue engineering

Javier Trinidad

Thesis advisors:

Dr. Eneko Sáenz de Argandoña

Dr. Gurutze Arruebarrena

Mechanical and Manufacturing Department. Mondragon Unibertsitatea

Thesis submitted for the degree of
Doctor of Philosophy
at Mondragon Unibertsitatea

September 10, 2013

A mi padre,
que me apoyó mientras pudo

A mi madre,
por todo lo que me ha dado

[...] Come, my friends.
'Tis not too late to seek a newer world.
Push off, and sitting well in order smite
the sounding furrows; for my purpose holds
To sail beyond the sunset, and the baths
Of all the western stars, until I die.
It may be that the gulfs will wash us down;
It may be that we shall touch the Happy Isles,
And see the great Achilles, whom we knew.
Though much is taken, much abides; and though
We are not now that strength which in old days
Moved earth and heaven, that which we are, we are;
One equal temper of heroic hearts,
Made weak by time and fate, but strong in will
To strive, to seek, to find, and not to yield.

Lord Alfred Tennyson
Fragment of "Ulysses"

Abstract

Magnesium and its alloys are currently considered to be a promising metallic biomaterial. The increasing interest in magnesium alloys is due to their biocompatibility, biodegradability and in particular to their mechanical properties which can be matched more closely to those of bone than the mechanical properties of other competitor metallic biomaterials, such as stainless steel and titanium. Due to these characteristics, magnesium alloys represent a promising material to be used for biodegradable implants. Magnesium is also gaining interest in regenerative medicine, especially for the fabrication of scaffolds that support tissue formation. For their application in regenerative medicine, the scaffolds have to present a porous open-cell structure. However, despite the mentioned features, magnesium alloys must overcome their poor corrosion resistance.

The main purpose of the present research work was to develop porous magnesium scaffolds for their use in tissue engineering. First, in order to identify the problems of magnesium as biomaterial, cell cultures on magnesium alloys were carried out as a starting point. In addition to the identified problems of magnesium alloys in regenerative medicine by other authors (hydrogen bubbles, pH increase), it was also detected that adhered crystals on the surface can stop the tissue growth, due to the crystals, samples were only partially covered by a cell layer. This was the reason why the crystal deposition and the corrosion behaviour in PBS solution of magnesium alloys as well as the influence of fluoride treatment on their corrosion and cell viability were analysed. Taking into account these results, novel Mg-Zn alloys with a chemical composition designed to increase their cell viability were developed. It was shown that an acceptable cell viability was achieved with the novel Mg-Zn alloys compared to Ti-6Al-4V. Furthermore, the fluoride treatment decreased the corrosion rate and increased the cell viability in all the analysed alloys.

Finally, replication casting process was analysed for the manufacturing of magnesium scaffolds. The optimal process parameters for several alloys were analysed taking into account the porosity and the mechanical properties of the magnesium foams.

As a final result, highly porous scaffolds manufactured with Mg-Zn alloys and coated with MgF_2 for reducing their corrosion rate have been developed. Their low hydrogen evolution, measured during the present work, makes them a potential application element in tissue engineering.

Laburpena

Gaur egun magnesioa eta bere aleazioak metalezko biomaterialen artean oso interesgarriak bihurtu dira. Interes hau handituz doa bere biobateragarritasunari, biodegradazioari eta batez ere, bere propietate mekanikoei esker. Ohizko biomaterial metalikoekin (titanioa eta altzairu herdoilgaitzak) alderatuz, magnesio aleazioen propietate mekanikoak hezurrarekiko antzekotasun handiagoa dute. Ezaugarri guzti hauek etorkizun handiko materiala bihurtzen dute inplante degradagarrien arloan. Birsorkuntza-medikuntzan ere magnesioren interesa handitzen doa, ehun berria sortzeko erabiltzen diren zelula-aldamioen fabrikazio esparruan hain zuzen ere. Zelula-aldamioek hiru dimentsioko egitura porotsua eduki behar dute eta bere poroak elkar lotuta egon behar dira. Birsorkuntza-medikuntzaren sektorean magnesio aleazioak etorkizun handiko materialak badira ere, korrosioarekiko duten erresistentzia apala da hauen erabilpena oztopatzen duena.

Ikerkuntza lan honen helburu nagusia birsorkuntza-medikuntzan aplikatzeko magnesiozko zelula-aldamioen garapena izan zen. Abiapuntu bezala zelula-kultiboak burutu ziren biomaterial gisa erabiltzean magnesioak dituen arazoak zeintzuk diren jakiteko. Literaturan aurkitu ziren arazoez gain (hidrogeno burbuilen sorketa, pH igoera), ehunaren haztea gelditzen zuen kristalen atxikidura handi bat antzeman zen materialaren gainazalean. Kristal atxikidura hori dela eta, zelulek ez zuten lagin osoa estali. Horregatik, magnesio aleazioen korrosioa, zelula-bideragarritasuna, kristalen sorkuntza eta fluoruro tratamenduen eragina magnesio aleazioetan aztertu ziren. Emaitza hauek kontuan hartuta, Mg-Zn aleazio berriak garatu ziren zelula-bideragarritasuna handitzeko. Aleazio hauek zelula-bideragarritasun egokia erakutsi zuten Ti-6Al-4V aleazioarekin konparatuta. Gainera, fluoruro tratamenduak korrosioarekiko erresistentzia eta zelula-bideragarritasuna handitu zituela antzeman zen aleazio guztietan.

Azkenik, magnesiozko zelula-aldamioak fabrikatzeko galdaketa prozesua aztertu zen. Fabrikazio-parametroak aztertu eta optimizatu ziren fabrikazioa, porositatea eta aparren propietate mekanikoak kontuan hartuta.

Garatutako zelula-aldamioek fluoruro tratamenduarekin garatu ziren. Zelula-aldamio hauek ez zuten hidrogeno sorkuntza handia izan. Hau horrela izanik, garatutako zelula-aldamioak hautagai interesgarri bihurtzen dira birsorkuntza-medikuntzan erabiliak izateko.

Resumen

Actualmente, el magnesio y sus aleaciones están considerados como un prometedor biomaterial metálico. El interés de las aleaciones de magnesio está en aumento debido a su biocompatibilidad, biodegradabilidad y particularmente a sus propiedades mecánicas, las cuales son más cercanas a las del hueso que las de otros materiales metálicos como pueden ser los aceros inoxidables y las aleaciones de titanio. Estas características hacen de las aleaciones de magnesio un material prometedor para su uso en implantes biodegradables. Otra aplicación donde el interés por las aleaciones de magnesio está aumentando es la medicina regenerativa. En esta aplicación nuevo tejido es generado en cultivos celulares sobre soportes celulares. Para su uso en medicina regenerativa, los soportes celulares deben poseer una estructura tridimensional porosa y con interconexión entre poros. Sin embargo, a pesar de las características mencionadas, las aleaciones de magnesio presentan una baja resistencia a la corrosión que dificulta su uso en este tipo de aplicaciones.

El objetivo principal de este trabajo de investigación fue desarrollar soportes celulares de magnesio para su empleo en medicina regenerativa. Para alcanzar este objetivo, como un punto de inicio, se realizaron cultivos celulares con el objetivo de identificar la problemática del magnesio como biomaterial. Además de los problemas detectados en la literatura (generación de burbujas de hidrógeno, incremento de pH), también se detectó que una gran adhesión de cristales sobre la superficie del material puede detener el crecimiento tisular. Debido a esta adhesión, las muestras no quedaron completamente cubiertas de células. Este fue el motivo por el que se analizó la formación cristales y la corrosión de las aleaciones de magnesio en PBS, así como la influencia de los tratamientos de fluoruro en la viabilidad celular y en la corrosión. Teniendo en cuenta estos resultados, se desarrollaron nuevas aleaciones Mg-Zn para obtener una mayor viabilidad celular. Con estas aleaciones se consiguió una viabilidad celular comparable a Ti-6Al-4V, y se observó que los tratamientos de fluoruros aumentaron la resistencia a la corrosión y la viabilidad celular en todas la aleaciones.

Finalmente, para la fabricación de soportes celulares de magnesio se analizó el proceso de infiltración de metal fundido. Se analizaron los parámetros óptimos para la fabricación teniendo en cuenta la porosidad y las propiedades mecánicas de las espumas.

Como resultado final, se desarrollaron soportes celulares recubiertos con MgF_2. Estos soportes no presentaron una gran evolución de hidrógeno, lo que hace de ellos un elemento potencial para su uso en medicina regenerativa.

Contents

Chapter 1

Introduction

The present thesis, entitled "Development of biodegradable magnesium alloy scaffolds for tissue engineering", is part of the research area "Materials science, technology and manufacturing processes" at the Mechanical and Manufacturing Department of Mondragon Unibertsitatea. The motivation, methodology and the outline of this thesis is exposed below.

1.1 Motivation

The corrosion resistance and the high mechanical properties of some metallic biomaterials make them very suitable to be used in long-term and load-bearing applications [Sta06, Won10]. This way, metallic alloys such as Ti alloys, Co-Cr alloys and stainless steels are commonly used materials in prosthesis, implants, plates or screws.

On the other hand, novel medical applications and novel medical requirements are demanding solutions beyond the state of the art. As an example, a novel medical application such as tissue engineering is demanding, besides bioinert ability and high mechanical properties, bioabsorbable and bioactive materials [Hen02]. However, these properties, which were developed in ceramic and polymer materials in the decade of the 80s, have not been achieved in metallic materials yet. Therefore, bioabsorbable metallic biomaterials have become an attractive group of materials to be researched in recent years. In this way, several studies have been carried out with metallic bioabsorbable materials such as magnesium and its alloys [Car11b, Car11c, Cas11, Duy07, Gu09, Gu10c, Han10, Ham12, Hua07, Kan08, Kra10, Li10b, Li11a, Pen10, Pie08, Rei10, Ren07a, Ren07b, Sta06, Vog10, Wil11, Wit05, Wit06, Wit07b, Wit07a, Wit10a, Won10, Xia12, Xu09a],

iron and Fe-Mn alloys [Her10b, Her10c] and tungsten [Peu03b, Peu03a, Peu03c].

Among the mentioned metallic materials, magnesium is the material that is having a greater impact on the scientific community since it combines the property of being compatible and absorbed by the human body and the property of accelerating bone regeneration [Wit07b, Wit07a]. In fact, most of the magnesium in the human body is in the skeleton, being an essential component for bone growth and maturation [Ara00, Ian01]. Regarding biocompatibility, magnesium is a biocompatible metallic material representing the fourth most abundant cation in the body and the second most abundant, after the potassium, in the intracellular medium [Gum04]. Finally, regarding its ability to be bioabsorbed, the cations generated due to corrosion are efficiently regulated by the body [Li08].

However, magnesium is not widely used in medical applications yet because of its rapid corrosion in the organism [Pie08, Sta06, Wit07b, Wit07a, Zen08]. Moreover, the corrosion of magnesium in physiological media generates hydroxides and hydrogen, as it is shown in eq. 1.1. Depending on the corrosion rate, the hydroxides could alkalinize the implant area [Zen08] and the hydrogen generation could create subcutaneous gas bubbles that could damage the adjacent tissue to the implantation site [Wit07b, Wit07a]. As a solution, a corrosion rate lower than the human body capacity to regulate the hydroxides and the hydrogen would avoid both mentioned drawbacks.

$$Mg(s) + 2H_2O \rightarrow Mg(OH)_2 + H_2(g) \tag{1.1}$$

Nevertheless, an analysis of the corrosion rate of different magnesium alloys in the literature is difficult due to the lack of standardization [Mue10]; different techniques, electrolytes and test durations are used. Furthermore, applications like tissue engineering, instead plates and screws for orthopaedic surgery, demands other kind of structures. For these applications three-dimensional porous structures with porous interconnectivity, called scaffolds, are needed. These structures optimize cell migration, tissue growth, and vascularization throughout the material [Hu02, Lu07a, Wen01, Wen07, Wit07b, Wit07a, Wu07, Yos03]. Unfortunately, the optimal parameters to foment the grow of new tissue are unknown.

Motivated by these aspects, in this thesis the design, the development and the characterisation of new magnesium alloys for their use as scaffolds were carried out. The principal objective and specific objectives are showed in the next section.

1.2 The goal

The main objective of the present research was to develop magnesium alloy scaffolds for their application in tissue engineering. To meet this main objective, the following specific objectives were defined:

- To identify the critical factors that inhibit cell growth when using magnesium alloys as biomaterials.
- To develop novel magnesium alloys able to counteract the generation of the previous identified factors.
- To identify and apply proper surface treatments able to counteract the generation of the previous identified factors.
- To develop and set up manufacturing processes for the fabrication of biodegradable magnesium scaffolds.

1.3 Methodology of research

To carry out the aims of this research work, the methodology exposed in figure 1.1 was followed.

Different lines of research and major research groups as well as the most representative authors were analysed in the analysis of the literature review. A critical study of the most recent works was performed.

In this analysis some lacks in the state of the art were detected. Due to these lacks cell cultures on magnesium alloys were carried out as a starting point in order to identify the problems of magnesium as biomaterial.

The literature analysis also showed the necessity of developing new magnesium alloys because current ones do not meet the requirements for being used as scaffolds. Moreover, a lack of standardization in the characterisation of the corrosion behaviour, which makes difficult a comparison among the corrosion rate of the different magnesium alloys, was detected.

In order to determine the corrosion rate of current commercial alloys, a corrosion characterisation of several commercial magnesium alloys was carried out. Later, MgF_2 coatings were carried out in order to solve the identified problems in the preliminary cell culture tests and in the corrosion tests.

Then, taking into account the results of the literature review, the preliminary cell culture tests and the results of the corrosion tests of the commercial alloys, new magnesium alloys were developed. After the development and the characterisation of the new alloys, a set up for manufacturing magnesium scaffolds was performed. Then the characterisation of the scaffolds was carried out. Finally, the conclusions of the research work and purposes for future works were exposed.

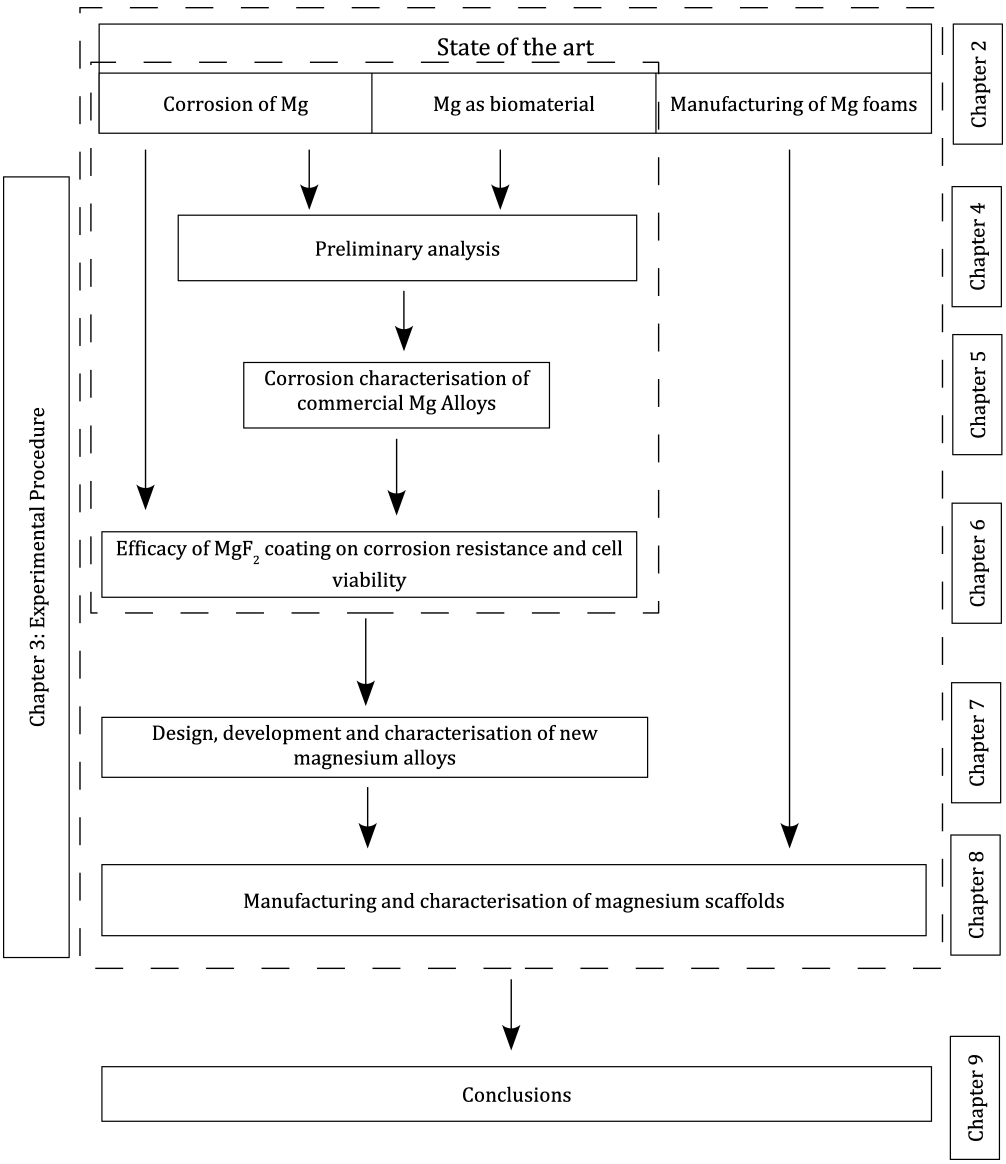

Figure 1.1: Methodology of research

1.4 Outline of the thesis

This research work is divided in nine chapters and a section of bibliographic references.

In Chapter 1 "Introduction", the motivation, the goals of the thesis and the methodology of research are exposed.

In Chapter 2 "Literature review", a bibliographic review, where different research lines of each theme are analysed, is given. The main parts of this analysis are the use of magnesium in tissue engineering, the corrosion of magnesium alloys and the manufacturing of metal foams.

In Chapter 3 "Experimental procedure", the methodology and the procedure of the tests applied in this research work are described.

In Chapter 4 "Cell culture on commercial magnesium alloys: a preliminary analysis", the problems of magnesium alloys as biomaterials are analysed by the realization of cell cultures as a starting point of the thesis.

In Chapter 5 "Evaluation of commercial magnesium alloys for tissue engineering applications", the corrosion resistance of commercial magnesium alloys is analysed. Cell viability of the alloys is also analysed by *in vitro* tests.

In Chapter 6 "Efficacy of MgF_2 coating on magnesium alloys for tissue engineering applications", the corrosion resistance of magnesium commercial alloys with MgF_2 coating is analysed. Cell viability of the alloys is also analysed by *in vitro* tests, in order to analyse the influence of the coating.

In Chapter 7 "Development of new magnesium alloys for tissue engineering applications", the choice of alloying elements and the casting of the new magnesium alloys is exposed. The effect of the MgF_2 coating on corrosion and cell viability is also analysed.

In Chapter 8 "Development of magnesium scaffolds for tissue engineering", the analysis and the set up of the replication casting technology for manufacturing magnesium scaffolds are exposed. Process parameters are defined and the mechanical properties and corrosion resistance of the developed scaffolds are analysed.

In Chapter 9 "Conclusions and future work", the conclusions of the present work and purposes for future works are exposed.

Chapter 2

Literature review

In this chapter the main features necessary to understand the topics of this research are presented. First, an overview of the basis of the regenerative medicine and the peculiarities of the scaffolds is given. Second, magnesium advantages, disadvantages and applications in regenerative medicine are shown. Third, the corrosion mechanism and forms of corrosion of magnesium in physiological environment are described. Fourth, the techniques for magnesium corrosion characterisation are exposed. Fifth, corrosion improvement and corrosion protection strategies are analysed. Sixth, the process to manufacture metal scaffolds are analysed. Finally, the principal conclusions of the literature review are exposed.

2.1 Regenerative medicine

According to the European Technology Platform, the regenerative medicine or tissue engineering is the science that "encompasses the use of cells and their molecules in artificial constructs that compensate for lost or impaired body functions" [Eur06]. The regenerative medicine combines the principles of materials science, engineering and life science in order to develop biological substitutes [Eur06, Gon06].

The three pillars of regenerative medicine are the cells, the signalling factors and the scaffolds (figure 2.1) [Gon06, Ohb09]. According to the cells, apart from the cell type (adult, embryonic, cell line), the culture method (static, spinner flask, perfusion) must be considered. The signalling factors should be appropriate to promote cell proliferation, cell differentiation, collagen generation or others depending on the objectives. Finally,

the main features of the scaffolds, in which this work focuses, are the biomaterial of which are made and their structure.

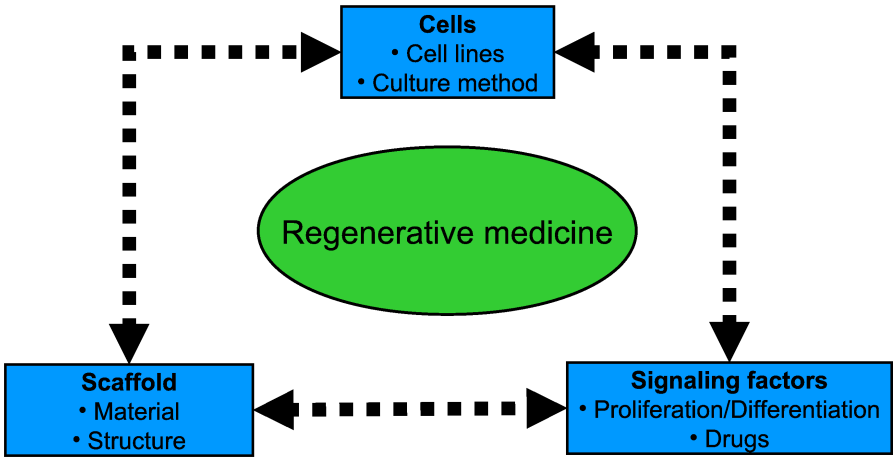

Figure 2.1: Schema of the pillars of regenerative medicine [Gon06, Ohb09]

2.1.1 Characteristics of the scaffolds

The scaffolds, which are the focus of this thesis, provide a suitable three-dimensional structure for the tissue regeneration. Without scaffold the cells cannot generate tissue because they could not interact with each other. The scaffolds provide to the cells a structure where tissue can be generated. The principal parameters of the scaffolds are: biomaterial, porous structure and surface morphology. These parameters are explained next.

Biomaterial

As mentioned in the previous section, biomaterials (biomaterial is defined as any material that could be used in the organism for medical use [Gon06]) are a key part in regenerative medicine for scaffold development. During the last half century a great revolution has been done in biomaterial development. According to Hench *et al.* [Hen02], three generation of biomaterials have been developed. In the 1960's and 1970's, the first generation of modern biomaterials was developed. The developed biomaterials in this generation possess good mechanical properties to replace damaged tissue, combined with minimal toxicity. Generally, these biomaterials were known as biologically inert. In the 1980's, bioactive components were developed in order to produce controlled actions and reactions in physiological media. In this second generation of biomaterials, another advance was the development of the first resorbable polymers. Finally, since 2000, the third generation of biomaterials came as the convergence of the separate concepts of bioactivity and resorption developed in the second generation of biomaterials. In this generation, materials which combine bioactivity and biodegradation are being developed.

Throughout these three generations of biomaterials various types of materials have been developed: ceramic, polymeric, synthetic, metallic... Ceramic materials present high mechanical strength and medium rigidity. These biomaterials can be bioabsorbable (calcium phosphate, bioglass), bioactive (calcium phosphate, bioglass,) or bioinert (alumina, zirconia). Their main problems are their fragility and their long degradation time [Bli08].

Among polymeric and synthetic materials, there are bioinert and bioabsorbable materials [Sab09], as in ceramic material family. One advantage of polymeric materials is the possibility to influence their bioactivity or other properties by the addition of nanofillers. Their drawback is their low mechanical strength.

The traditional metallic biomaterials such as titanium alloys, Co-Cr alloys or stainless steels have been used in orthopaedic applications because they are suitable to be used in load bearing applications and because they are inert materials. Traditional metallic biomaterials are not absorbed by the body, unlike ceramic or polymeric materials, and in some cases a second surgical intervention is needed. In fact, a second surgery to remove an implant is one of the most common operations in orthopaedics of the U.S. [Gar06]. Furthermore, corrosion products of these materials may be considered harmful [Zen08]. Another problem with traditional metallic implants is their high Young's modulus. The disparity between the rigidity of the implant and bone leads to the phenomenon known as "stress shielding effect" [Nag03, Nii01]. The "stress shielding effect" occurs when the mechanical load is supported mainly by the implant and barely by the bone. The reduction of the mechanical stimulus produces a decrease in bone density.

In order to counteract theses drawbacks, several studies have been carried out with bioabsorbable metallic materials such as magnesium and its alloys [Gu09, Kra10, Li08, Pie08, Sta06, Wit07b, Wit07a, Zen08], iron and Fe-Mn alloys [Her07a, Her07b] and tungsten [Peu03b, Peu03a, Peu03c]. However, the tungsten has only been investigated as stents and the results show that this element is not regulated properly by the organism, raising considerably the content of tungsten in the body after implantation [Peu03b, Peu03a]. In addition, the research with iron are also focused in stents [Her07a, Her07b]. Magnesium is the only metal that is being investigated for stent applications and scaffolds for bone regeneration applications. Furthermore, magnesium Young's modulus is closer to the bone's one (table 2.1), leading to a minimization of the "stress shielding effect". As it is shown in table 2.1, magnesium has a higher fracture toughness than hydroxyapatite and a yield strength and a Young's modulus closer to the bone's one than other biomaterials.

Moreover, magnesium is a bioactive material that can accelerate bone regeneration [Sta06, Wit07b, Wit07a]. It is concluded that magnesium combines the property of being compatible and absorbed by the human body with the property of accelerating bone regeneration. The biological and physiological characteristics of magnesium are described in section 2.2.

Table 2.1: Characteristics of different biomaterials and bone tissue [Bla98, MIT06b, MIT06a, Sta06]

	Bone tissue	**Mg alloys**	**Ti alloys**	**Co-Cr alloys**	**Stainless steel**	**Hydroxyapatite**	**PLA**
Density (g/cm^3)	1.8-2.1	1.74-2.0	4.4-4.5	8.3-9.2	7.9-8.1	3.1	1.2-1.3
Young's modulus (GPa)	0.1-3 (trabecular) 17-20 (cortical)	41-45	110-117	230	189-205	73-117	1.2-3
Yield strength comp. (MPa)	130-205 (cortical)	65-100	758-1117	450-1000	170-310	600	28-50
Fracture toughness ($MPa \cdot m^{1/2}$)	3-6	15-40	55-115	-	50-200	0.7	-

Porous structure

A three-dimensional porous structure with pore interconnectivity is needed in order to optimize cell migration, tissue growth and vascularization through the scaffold [Hu02, Lu07a, Wen01, Wen07, Wit07a, Wit07b, Wu07, Yos03]. In this way, cell interaction takes place throughout the material. As an example, figure 2.2 shows a porous magnesium scaffold used in tissue engineering studies [Wit07b, Wit07a]. Nevertheless, the optimal parameters to foment the growth of new tissue are unknown.

A wide range of porosities and pore sizes are found in the literature. For example, porosities of 80 % [Hu02, Yos03], 90 % [Lu07a, Wu07], among 78 and 91 % [Wen07], among 72 and 76 % [Wit07a, Wit07b] (figure 2.2) and in some cases lower porosities have been used, 50 % [Wen01], 25 % [Agh10] and even 10 % [Agh10].

The pore size is also variable in the literature, but it usually ranges between 100 and 500 µm (*e.g.*, 100-350 µm [Hu02, Yos03], 150-400 µm [Wen07], 300-500 µm [Wu07], 150-200 µm [Lu07a]). Other sizes were also used in another works, for example 10-1000 µm [Wit07b, Wit07a].

Figure 2.2: Scaffold with a porosity of 72-76 % with pore size of 10-1000 µm [Wit07a, Wit07b]

Surface morphology

The biomaterial surface has a significant relevance because it is directly related to protein and cell adhesion [Cas02, Kas02, Tir02, Vog98]. Kasemo [Kas02] argues that when a solid material is implanted in the organism, the material is covered by water molecules in a few nanoseconds. After this initial step, proteins cover the surface interacting with the water molecules. Finally, the cells adhere to the protein layer.

This behaviour means that the cell adhesion on a material is related with the adhesion of water molecules. Due to this reason, hydrophilic or hydrophobic characteristics of a material are important in biomaterials science. The majority of the authors postulate that hydrophilic surfaces promote cell adhesion [Mar06, Mic05, Vog98, Wil05]. However, some proteins present higher adhesion to hydrophobic surfaces, thereby promoting cell adhesion [Mic05].

In the same way, the surface roughness is also an influential factor. On smooth surfaces, the cells have a plane morphology whereas on a rough surface the cells have a greater adhesion due to their cytoplasmic extensions [Boy00]. However, it has not been found an optimal morphology for cell adhesion and proliferation in the literature.

2.2 Magnesium as biomaterial

Magnesium is an abundant element in the organism. In fact, magnesium is the fourth most abundant cation in the human body (Ca > K > Na > Mg) [Aba05, Gum04, Swa03, Wol03] and the second most abundant intracellular cation after potassium [Aba05, Gum04, Swa03, Wol03]. An adult human body has around 24 g of magnesium [Sar00, Sta06, Swa03, Wol03, Zen08]. Between 60-65 % of magnesium in the human body is found mineralized in bone tissue [Wol03, Sar00, Ara00, Aba05]. It

is also found in muscles (20 %) [Swa03], in soft tissues [Aba05, Ara00, Sar00, Swa03], complexed with nucleic acid and proteins [Ara00, Wol03] and in blood plasma in a small percentage (≈1 %) [Sar00, Wol03].

Furthermore, magnesium has an important role in modulating transport functions and receptors [Sar00], signal transduction, enzyme activities [Sar00, Wol03], energy metabolism [Sar00], nucleic acid and protein synthesis [Sar00, Wol03], and protecting biological membranes [Sar00], among others. Due to these functions, its deficit can be potentially harmful to health [Swa03].

The recommended daily intake of magnesium is about 350-420 mg for adult males [Sar00, Zen08] and 250-320 mg for adult females [Sar00, Zen08]. Together with calcium, sodium and potassium, magnesium is efficiently controlled in the body by homeostatic mechanisms [Wil06]. Tests in animals show that magnesium levels in the blood can be considered constant after the implantation of magnesium in the body [Li08, Won10]. As a summary, magnesium low toxicity, its efficient regulation by the body and its mechanical properties make it a promising material for temporary implant applications in tissue engineering.

The first application of magnesium as biomaterial was found in a clinical report of 1878 [Hus78]. In this report, Huse [Hus78] used a magnesium wire ligature to stop bleeding vessels of three human patients. Since this first use, many authors studied magnesium as biomaterial. These experiments are listed by Witte *et al.* [Wit10b] in their review about the history of magnesium as biodegradable material. Nowadays, the most common application areas for magnesium in medicine are that of stents and that of bone regeneration scaffolds and implants.

2.2.1 Stents

According to Moravej *et al.* [Mor11], "a stent is a small mesh-like tubular scaffold which is placed and then expanded inside the coronary artery to keep the lumen open". In the last years, a wide number of experiments have been carried out with magnesium stents [Bar07, Di 04, Gri04, Heu03, Man07, Pee05].

However, the principal drawback of biodegradable magnesium stents is their rapid corrosion [Heu03, Man07, Pee05, Wu11]. In the study carried out by Peeters *et al.* [Pee05], the stents were almost completely degraded 6 weeks after implantation in human patient.

2.2.2 Bone regeneration

As mentioned before, magnesium combines the property of being compatible and absorbable by the human body and it also stimulates bone regeneration [Xin11a]. In fact, magnesium incorporation in other biomaterials and

coatings in order to improve bone growth is widely used in the literature [Cai10, Ito08, Kan10, Lau11, Ma11a, Mro10, Suc04, Zre03].

A wide number of *in vivo* studies have been carried out in the literature to evaluate the viability of magnesium as biomaterial [Cas11, Duy07, Han10, Ham12, Hua07, Kra10, Li11a, Rei10, Ren07a, Ren07b, Vog10, Wil11, Wit05, Wit06, Wit07b, Wit07a, Wit10a, Won10, Xia12, Xu09a]. In these studies new formed bone was adhered to the implant as it is shown in figure 2.3a. However, material ability to regenerate bone does not imply its suitability. As it is shown in figure 2.3b, around AZ31B alloy a fibrocellular tissue (F) has formed after nine weeks of implantation in a rabbit model that can lead to an inflammatory response [Hua07]. In this experiment, fibrocellular tissue has not formed in the case of pure magnesium (figure 2.3a).

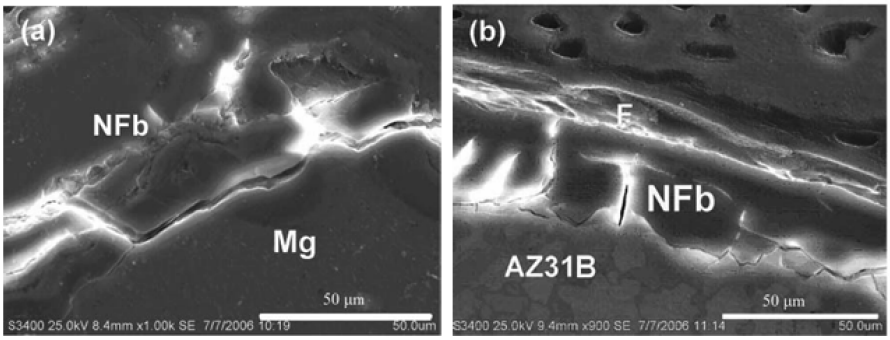

Figure 2.3: Detail of new bone generation (NFb) after nine weeks of implantation in a rabbit (a) pure magnesium (b) AZ31B [Hua07]

In vitro tests have also been carried out to analyse the cytotoxicity or the cell behaviour on magnesium alloys [Car11b, Car11c, Gu09, Li10b, Pie08]. In order to analyse the cell behaviour, direct cell assay or indirect cell assay are carried out. The direct cell assay consists in a cell culture directly on the material to be studied. Whereas in the indirect cell assay an extract of the material to be studied is prepared according to ISO 10993/12. Then the cells are seeded on a control and the extract is added in the medium. In the case of biomaterials to be used for bone regeneration, this kind of analysis are usually carried out with the MG-63 (human osteosarcoma cell line) [Fis10, Mro10, Smo12, Wit07c, Fey10, Gu10c, Wan11b, Wan11a] and MC3T3-E1 (mouse osteoblast precursor cell line) [Car10b, Car11b, Gon12, Gu09, Jo11, Li10c].

However, as in the previous subsection, the principal drawback of magnesium is its rapid corrosion. Next section describes the corrosion mechanisms and forms of corrosion of magnesium in the organism.

2.3 Magnesium corrosion

As mentioned in the previous section, the principal problem of magnesium and its alloys is their rapid corrosion in the organism. In this section, the corrosion mechanisms and the corrosion forms of magnesium in the organism are described.

2.3.1 Corrosion mechanisms

The principal reaction of magnesium in aqueous environment is expressed as eq. 2.1 [Atr11, Son03, Sta06, Zen08]. According to this expression magnesium develops a partially protected film of magnesium hydroxide ($Mg(OH)_2$). However, the presence of chloride ions (Cl^-) in aqueous physiological environments dissolve the $Mg(OH)_2$ film [Ave99] forming soluble magnesium chloride ($MgCl_2$) [Jam11, Sta06]. This transformation is expressed as eq. 2.2. Finally, a reaction between Cl^- and magnesium can also occur [Sta06]. This expression is expressed as eq. 2.3.

$$Mg(s) + 2H_2O \rightarrow Mg(OH)_2 + H_2(g) \tag{2.1}$$

$$Mg(OH)_2(s) + 2Cl^- \rightarrow MgCl_2 + 2OH^- \tag{2.2}$$

$$Mg(s) + 2Cl^- \rightarrow MgCl_2 + 2e^- \tag{2.3}$$

Apart from these species, magnesium could also form magnesium oxide, sulphate or phosphate in a saline environment [Gu09]. Furthermore, due to the generation of hydroxides and the consequent pH increase, insoluble phosphates precipitate on the magnesium surface [Alv10, Xin11b, Zha10]. The formations of phosphates could be formed as it is shown in eq. 2.4 [Zha10]. Hydroxide generation can also promote the deposition of carbonate species [Jam11, Xin11b].

$$H_nPO_4^{(3-n)-} + Ca^{2+} + Mg^{2+} \rightarrow Mg_xCa_y(PO_4)_z \tag{2.4}$$

2.3.2 Forms of corrosion

The principal forms of magnesium corrosion in physiological environment are localized corrosion [Son03], galvanic corrosion [Atr11, Son03, Zen08], microgalvanic corrosion [Atr11, Son03], pitting corrosion [Atr11, Son03, Zen08], corrosion fatigue [Zen08] and erosion corrosion [Zen08]. An overview of these forms of corrosion is explained next.

Localized corrosion

Magnesium is partially protected by a film of $Mg(OH)_2$. This partially protective film implies that the most common form of corrosion for magnesium is localized corrosion [Son03]. In this case, the corrosion starts as irregular pits, which grow laterally over all the surface [Son03].

Galvanic corrosion

Galvanic corrosion takes place when magnesium and another metal with a different electrochemical potential are in electric contact soaked in an electrolyte. One metal acts as anode and the other as cathode. In this case, the metal with the lower electrochemical potential (usually magnesium) is corroded and the other metal is protected against the corrosion [Son03, Zen08].

As an example, Lambotte *et al.* [Lam32] fixed a magnesium implant (Mg standard electrode potential is V^o=-2.363 V [Cal95]) with steel coated with gold (Au standard electrode potential is V^o=+1.420 V [Cal95]). The galvanic couple accelerated the magnesium implant corrosion and magnesium plate disappeared in 8 days. This corrosion caused hydrogen subcutaneous bubbles and other diseases. This form of corrosion must be taken into account in implant and fixation design, avoiding the electric contact between magnesium and other metals.

Microgalvanic corrosion

Microgalvanic corrosion is a galvanic corrosion between the matrix and second phases [Atr11, Son03]. Usually, the matrix has a potential lower than the second phases and works as anode. Meanwhile the second phases, due to the mixture of magnesium and a less reactive material, work as cathode [Son03].

In this form of corrosion, the impurities have an important role. Fe, Ni, Cu and Co, due to their low solubility in magnesium matrix, act as cathodic sites [Atr11]. Figure 2.4 shows that when the concentrations of these impurities exceed their tolerance limits, the corrosion rate increases dramatically [Atr11, Ave99, Son03].

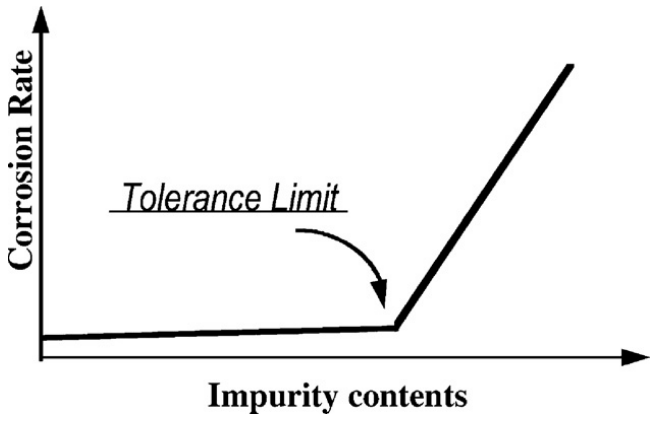

Figure 2.4: Generalised curve for the influence of the impurity elements Fe, Ni, Co and Cu [Son03]

Pitting corrosion

Pitting is a highly localized form of corrosion, which forms small holes on the surface. Pitting is initiated by a defect in the material (*e.g.*, nonmetallic inclusions, damage) or chemistry factors (*e.g.*, high concentrations of chloride). The corrosion is concentrated in the holes, which grow downward. It is supposed that the gravity is the cause of this growth [Cal95]. This form of corrosion was detected in several works [Kan08, Kra10, Ren07b, Wit06, Yue08].

Stress corrosion cracking

The combined action of stress and a corrosive environment produce stress corrosion cracking [Cal95]. The applied stress forms and opens cracks allowing their propagation through the alloy due to corrosion and mechanical effects [Atr11, Cal95]. This corrosion form is not analysed in this work, although it should be taken into account in the design of screw, plates and other elements.

Corrosion fatigue

The corrosion fatigue is also the combined action of a mechanical effect and a corrosive environment, in this case the mechanical effect is a cyclic load [Zen08]. The corrosion fatigue is a critical factor in the life of implants. As in the previous case, this corrosion form is not analysed in this work.

Erosion corrosion

The combined action of corrosion and wear or the action of a fluid in movement produce erosion corrosion [Cal95]. This form of corrosion occurs, for example, in the first step of the implantation of a stent, when it is in direct contact with the blood flow before it is covered by tissue. This form of corrosion is neither analysed in this work.

2.4 Magnesium corrosion characterisation techniques

In this section the benefits and the limitations of different corrosion characterisation techniques are described briefly. Kirkland *et al.* [Kir12] classify these techniques as unpolarised and polarised tests. The difference between these methods is that in a polarised test a polarisation is applied during the test. Besides the characterisation techniques, the corrosion medium must be also taken into account.

2.4.1 Unpolarised tests

Mass loss test

This test consists in the measurement of the mass loss after the immersion of a sample for a period of time [Kir12]. The set up of this test is simple. However, multiple

samples would be needed to achieve information about the corrosion behaviour over time. pH changes during the experiment are not desirable.

Furthermore, corrosion products and precipitates must be removed properly in order to eliminate the error due to their own mass. Prior to measuring the final mass, corrosion products from the surface must be cleaned. Chromic acid is usually used to clean magnesium.

Hydrogen evolution measurement

The set up for hydrogen evolution measurement is similar to the mass lost test. In this case, a collector is placed above the sample to capture the generated gas [Kir12, Son03]. This collector usually consists in an inverted funnel and an eudiometer.

H_2 generation is a critical point *in vivo* [Lam32, Sta06, Wit05, Wit10a, Wit07b, Won10, Xu09a, Zbe09, Zen08], so its measurement is important. This technique also permits a measurement over time and it is not influenced by corrosion products. Nevertheless, other corrosion mechanisms could occur besides hydrogen generation, specifically in heavily alloyed magnesium alloys [Kir12]. Furthermore, H_2 collection could be not 100 % efficient, formed bubbles may escape through the side of the funnel or perhaps be trapped beneath the specimen [Kir12]. Finally, pH also changes during the experiment.

pH monitoring

This measurement consists in an immersion test where the pH medium change is measured over time. However, this technique creates an unrealistic environment due to pH increase, which could increase to 12.

2.4.2 Polarised tests

Potentiodynamic polarisation

This technique is the most commonly used for the study of the corrosion of magnesium in physiological media [Kir12]. After a stabilization of the sample with the electrolyte, a scan between cathodic and anodic potentials is done. This test gives information about corrosion potential (E_{corr}), corrosion current density (i_{corr}) and about the cathodic and anodic reactions.

However, this technique measures the corrosion rate in an instant. It does not take into account the change of corrosion rate over time. In addition, large variations can occur in i_{corr} measurement due to small variations in Tafel slopes measurement [Kir12]. Furthermore, the corrosion rate measurement using this technique has also problems due to the negative different effect (NDE) of magnesium. In magnesium alloys, hydrogen generation increases at more positive anodic potential, which does not occur on other metals, as iron, copper, nickel, etc. [Son03, Son05]. This behaviour is called NDE

[Son03, Son05]. In fact, some works postulate about the inability of Tafel extrapolation to estimate the corrosion rate reliably with the potentiodynamic polarisation test [Atr11, Shi10, Son03].

Electrochemical impedance spectroscopy

The Electrochemical impedance spectroscopy (EIS) is an electrochemical method which uses alternating current. A potential is typically applied to the electrode and its response is measured at different frequencies.

This method is able to quantify the corrosion layers formed on the material. However, as in potentiodynamic polarisation, it records information in a short period of time and it does not take into account the change of corrosion rate over time. Furthermore, its results can be affected by the dissolution of magnesium during the measurement, specially for low frequencies [Kir12].

2.4.3 Corrosion media

As mentioned before, the corrosion mediums must be taken into account. The medium must imitate the physiological environment and it must be stable.

However, there is not an standardization about what medium must be used. Even the corrosion of magnesium is dependent on the implantation site [Wil11]. These are the reasons why there is a wide number of physiological media used to characterise corrosion in the literature: Hank's solution [Her07a, Her07b, Hua10, Kuw00, Ng10, Ren07a, Ren07b, Son07a, Son07b, Tan10, Wan08, Wan09, Zha07], PBS [Agh10, Alo12, Alv10, Car10a, Han10, Mue10, Per10, Xin11a, Xue12], NaCl solutions [Den07, Den09, Hor10], cell culture media [Car10b, Hir10b, Lu07b, Wan09], artificial sea water [Wit07c], among others.

2.5 Improvement of magnesium corrosion resistance

As stated before, the principal problem of magnesium in biomedical applications is its rapid corrosion. The principal strategies to solve this problem are the design of new alloys and the use of coatings [Sta06, Zen08]. These strategies are described next.

2.5.1 Design of new magnesium alloys

In the last years several works have been carried out focusing in the development of magnesium alloys with a higher corrosion resistance for biomedical applications. The principal studies are based in Mg-Ca alloys [Li08, Li10d, Liu10a, Erd10, Kir10], Mg-Li-Al alloys [Ham12, Kra10, Sei11, Wit05, Wit06, Wit10a], Mg-Zn alloys [Che11a, Han09, Han10, Hua10, Li10b, Li10c, Zha10, Zha11a], Mg-RE alloys [Agh10, Fey10, Hor10, Sei11], Mg-Y alloys [Pen10], among others. In the design of new alloys it must be taken into

account that the alloying elements must present a low toxicity and must increase corrosion resistance. The principal alloying elements used in literature are: Ca, Zn, Mn, Li, Al, Y and rare earths, among others.

- **Ca**

  The addition of low quantities of Ca increases the corrosion resistance of magnesium [Kan08, Li08, Liu10a, Zen08] and it also increases pitting resistance [Kan08]. A percentage around 1 wt% of Ca is the most effective in Mg-Ca alloy system in order to achieve the highest corrosion resistance [Li10d]. Higher percentages do not achieve higher corrosion resistance and a percentage of 4-5 wt% embrittles the alloy [Li08, Li10d, Zen08]. Small additions (0.2-0.3 wt%) of Ca are also common in other alloy systems [Bra10, Gao10, Han10, Men11, Han11, Han09, Wan10a, Zha11a].

- **Zn**

  Zn is an essential micro-nutrient [Gu09, Hua10] and it improves the corrosion resistance in magnesium alloys [Gu09, Hua10, Son07a, Xu08, Yin08, Zen08, Zha10]. Additions higher than 3 wt% do not achieve a great improvement on corrosion resistance [Hua10, Yin08]. Mg-Zn binary alloy system with additions of other elements is a common line of research in magnesium alloys for biomedical applications [Che11a, Han09, Han10, Hua10, Li10b, Zha10, Zha11a].

- **Mn**

  Mn is a non toxic element [Xu08]. In fact, it is the principal alloying element in iron degradable stents [Her10a, Her10b, Mor10a, Mor10b, Mor11]. Mn can also improve the corrosion resistance [Gu09, Son05, Son07a, Xu08, Zen08]. Small additions of Mn reduce the impurities in magnesium alloys increasing their corrosion resistance [Ave99, Son05]. Mg-Mn binary system with additions of Zn have been studied in some works [Xu09a, Xu09b].

- **Li**

  The addition of Li increases magnesium corrosion resistance [Son07c, Wit05, Wit06, Zen08]. It has been used in a wide number of research works as alloying element in magnesium alloys for biomedical applications [Ham12, Kra10, Rei10, Sei10, Wit05, Wit06, Wit10a]. However, Li concentrations higher than 2 mmol/l are toxic [Gu09].

- **Al**

  Al is a common alloying element which improves magnesium corrosion resistance [Son03, Son07a, Wen10]. This is the reason why it has been used widely in magnesium alloys for biomedical applications [Cho11, Eli10, Gho10, Gu10a, Her07b, Kan11, Kuw00, Raz10, Son07a, Wit05, Wit07b, Wit07a]. However, Al is a neurotoxicant and it is associated to other diseases due to its accumulation [El 03, Gu09, Mat01]. In addition, Al is a growth inhibitor of bone [Mat01].

- **Y**

  Y additions increase magnesium corrosion resistance [Pen10] and they decrease pitting corrosion as in WE43 alloy with a 4 % of Y [Kra10, Wit06]. Magnesium alloys with Y are common in the literature for biomedical applications [Fey10, Ham12, Han09, Han10, Smo12, Wan10b, Wit06]. In fact, some trials in humans have been done with WE43 alloy [Mor11]. However, the effect of Y in the organism is unknown [Gu09].

- **Rare earths**

  Rare earths increase magnesium corrosion resistance [Son07a, Son07b, Wit05] and decrease pitting corrosion in alloys as LAE442 and WE43 [Kra10, Wit06]. Furthermore, rare earths have been used as alloying elements in magnesium alloys for biomedical applications [Fey10, Gao07, Gu10a, Ham12, Hor10, Rei10, Smo12], and as mentioned before, trials in humans with WE43, which contains rare earths, have been carried out [Mor11]. However, rare earths are not found in the human body, they are not essential and there is controversy about their toxicity [Gu09].

On the other hand, beyond conventional alloys, new metal matrix composites (MMC) [Gu10d, Raz10, Wit07c, Zhe10] and glassy metals [Cao12, Gon12, Li10a, Wan11a, Zbe09] are being developed. Powder metallurgy is used for the manufacturing of magnesium MMC mixing magnesium powder with hydroxyapatite powder (Mg-HA). The Mg-HA MMCs present a higher corrosion resistance and a higher bioactivity [Gu10d, Raz10, Wit07c, Zhe10]. According to the glassy metals (bulk metallic glasses), they also improve the corrosion resistance comparing to standard alloys [Son03]. Zberg *et al.* [Zbe09] do not find hydrogen evolution *in vivo* after the implantation of magnesium glassy metal. In the present research work the glassy metals have not been analysed.

2.5.2 Coatings

Another strategy to increase magnesium corrosion resistance is the use of coatings. Coatings must have an acceptable adhesion on magnesium, adequate toughness, high hardness and mechanical strength, and they must be biocompatible and possess adequate corrosion, fatigue and wear resistance [Zen08]. The principal coatings used in the literature for magnesium protection are shown below.

- **Anodization and micro arc oxidation (MAO)**

  Anodization is an electrolytic oxidation process which increases the thickness of an oxide layer on the surface of a metal. This technique is used by many authors in the literature to increase the corrosion resistance of magnesium [Hir10b, Son07b, Xue11]. Xue *et al.* [Xue11] have been able to reduce the corrosion rate of pure magnesium about 10 times. The nature of the achieved oxides depends on the electrolyte nature.

The micro arc oxidation is a similar technique to the anodization. However, in this technique higher potentials are used in order to achieve plasma reactions, which modify the growing oxide. This technique is also widely used in literature [Bai12, Gao10, Kim08, Pul10, Shi09, Zha07]. In this case, the nature of the achieved oxides also depends on the electrolyte nature.

- **Polymer coatings**

  Polymer membranes have been also applied on magnesium surface by different authors [Ma11b, Li10c, Lu11, Won10, Xu12]. In all cases an improvement on the corrosion resistance is achieved. However, Wong *et al.* [Won10] concluded that more studies are needed to improve the polymer membrane's adhesion properties.

- **MgF_2**

  Another coating used in literature to improve corrosion resistance of magnesium is fluoride treatment [Car11a, Con11, Per10, Per11, Wit10a, Yan10]. Fluoride treatment is a chemical conversion that consists on the immersion of magnesium in hydrofluoric acid (HF) or in fluoride solutions to form a coating of MgF_2. The coating is formed by the reaction of HF with Mg, according to eq. 2.5 [Con10].

$$2HF + Mg(s) \rightarrow MgF_2 + H_2(g) \tag{2.5}$$

  The MgF_2 coating presents a low water solubility and good biocompatibility [Per10, Per11]. The formed coating thickness increases with the fluoride treatment time. However, Yan *et al.* [Yan10] showed that after 72 hours in HF, the coating thickness on AZ31B alloy was not increased notoriously, neither the corrosion resistance. They postulate that the formed barrier film of MgF_2 on the surface after 72 hours is thick enough to terminate the reaction.

- **Other coatings**

  Other kind of coatings are also analysed in the literature. These techniques are ion implantation [Lih10], TiO_2 coating through Sol-Gel technique [Li11b, Shi09], bioactive coatings based on hydroxyapatite and Ca-P [Cor07, Hir10a, Li10b, Li11a, Liu10b, Ma10, Men11, Son08, Tan10, Xu09a, Yan08] and combinations of any of the mentioned techniques (double coatings) [Bai12, Gao10, Hou12, Jo11, Lu11, Liu10b], among others.

2.5.3 Other techniques

Beyond the mentioned techniques, microstructural and surface modifications can also improve the corrosion resistance. A change in the microstructure of a material can modify its corrosion behaviour. In fact, according to some works, grain refinement can improve

corrosion resistance [Alv10, Cor07, Xin09]. However, grain refinement does not always assure an improvement in corrosion resistance [Ral10]. Regarding surface modifications, compressive residual stress generation through mechanical process [Den07, Den09] or laser shock peening [Sea10] can also improve the corrosion resistance.

2.6 Manufacturing of magnesium scaffolds

As mentioned before, a scaffold for tissue regeneration must present a three-dimensional porous structure with pore interconnectivity. Metallic foams, which have a very similar structure to that required for being used as scaffolds, are commonly proposed for applications in aerospace and automotive industries as shock and impact energy absorbers, filters, high-temperature gaskets, silencers, flame arresters, heaters or heat exchangers [Goo13, Wen01]. Processes which have traditionally been used for producing metallic foams with interconnecting pores are described next.

2.6.1 Powder Metallurgy

Sintering of metal powders and fibres (without compaction) [Ban01]

In this process, metal powder or fibres are sintered to achieve an structure with pore interconnectivity. The porosities achieved with this process are between 20 and 50 % [Ban01]. Nevertheless, higher porosities can be achieved with the addition of space holder material.

However, manufacturing metal foams with this technique is difficult when metals such as aluminium or magnesium are used. Aluminium and magnesium powder are covered by an oxide layer which prevents the sintering [Ban01, Bur09]. In these cases, it is necessary to compact the powder in order to break the oxide layer [Ban01, Bur09]. This technique is explained below.

Compaction and sintering of metal powders mixed with space holder

This technique, as it is shown in figure 2.5, consists on the mixing of metal powder with a space holder material. The mixed powders are compacted in order to achieve a preform. Finally, this preform is sintered. Depending on its nature, the space holder material can be eliminated by dissolution or by heat treatment.

Magnesium preforms achieved with a low compacting pressure are more brittle [Hao09]. Furthermore, a low pressure could be not enough to break the oxide layer of the powders [Bur09, Hao09]. Breaking the oxide layer is a critical point. This is the reason why it is recommended to maximize the compacting pressure [Bur09, Hao09]. In addition, for bulk samples, a high pressure reduces the porosity of the sample, being this reduction imperceptible after 300 MPa [Bur09]. Nevertheless, a high pressure can deform the pore shape in metal foams [Hao09]. On the other hand, low pressure (around

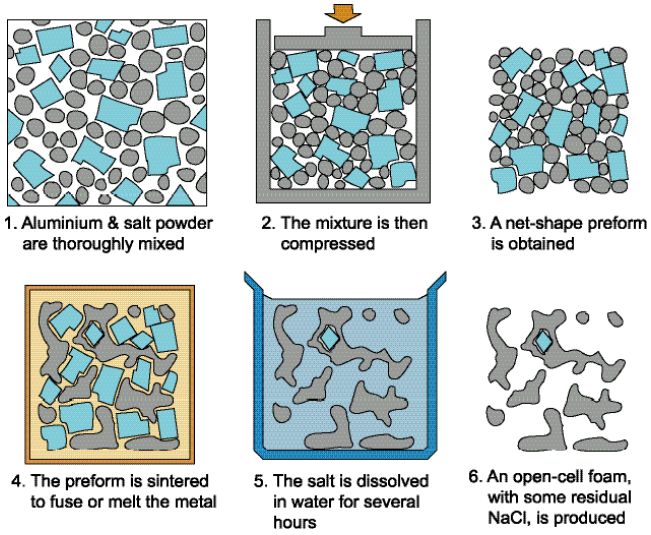

Figure 2.5: Production of an open cell foam by sintering a mixture of metal powder and a removable agent [Ken12]

100 MPa) is also used in other works [Agh10, Wen01, Wen04]. Powder particles obtained by milling under argon atmosphere [Agh10] or by atomization [Bur09] present a small oxide layer, which favour the sintering.

Regarding the sintering process, a high temperature achieves a greater and quicker sinterization [Agh10] and greater mechanical properties [Hao09]. If the temperature is too low, the powders will not sinter or they will need a long time to sinter [Agh10, Hao09]. According to the sintering time, a short time is not enough to weld the powders [Bur09]. However, a long time could decrease the mechanical properties due to grain size growth [Bur09]. Despite this, in some works, the sintering takes several hours [Agh10, Hao09, Wen01, Wen04].

Finally, different materials can be used as space holder material, for example, salt (NaCl) [Oza08], carbamide ($CO(NH_2)_2$) [Wen01, Wen04], ammonium bicarbonate ($(NH_4)HCO_3$) [Toj10, Wen01], potassium carbonate (K_2CO_3) [Fer09] and polymers [Fer09], among others. As mentioned before, these materials are removed by dissolution or thermal treatment.

2.6.2 Replication casting

In this process, liquid metal is infiltrated into a negative mould. The mould is removed after metal solidification, thereby obtaining the metal foam [Bac03, Bac05, Con06, Wen00, Wit07b, Wit07a, Yam99]. The negative mould material is usually soluble in water, like sintered salt [Bac03, Bac05, Wit07b, Wit07a], plaster [Ban01, Wen00, Yam99] or a mixture of mullite, phenolic resin and calcium carbonate [Ban01].

A schematic description of this process is shown in figure 2.6 [Fer08] for salt moulds. According to this process, a negative mould is achieved by the sinterization of the salt. Then molten metal is infiltrated into the resulting salt mould. In order to achieve a complete infiltration, pressure on top of the mould [Bac03], vacuum at the bottom [Bac05] or the combination of both techniques could be applied. After salt removal in water, a metallic porous structure is obtained. Furthermore, according to Bach *et al.* [Bac05], a finer grain microstructure can be achieved vibrating the mould. The porosities achieved with this techniques are between 60-70 % [Fer08].

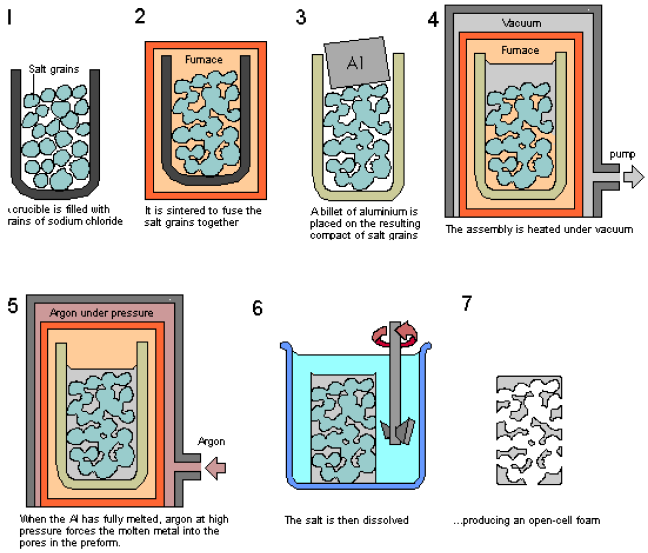

Figure 2.6: Infiltration process of melted metal in removable salt mould [Fer08]

On the other hand, to manufacture moulds of a mixture of mullite, phenolic resin and calcium carbonate or plaster a polymer foam is used as starting point. The polymer foam is filled with mould material in liquid state. After the solidification of the mould, the polymer is removed by thermal treatment. In this case the porosities are between 80-97 % [Ban01].

2.7 Conclusions

The main conclusions from the literature review are exposed in this section. According to several authors, magnesium and magnesium alloys is a biocompatible and biodegradable metallic material [Cas11, Duy07, Han10, Ham12, Hua07, Kra10, Li11a, Rei10, Ren07a, Ren07b, Vog10, Wil11, Wit05, Wit06, Wit07b, Wit07a, Wit10a, Won10, Xia12, Xu09a]. Furthermore, it has been observed that magnesium is osteoconductive [Duy07, Ham12, Kra10, Rei10, Ren07a, Ren07b, Wil11, Wit05, Wit06, Wit07b, Wit07a, Wit10a] and that it can improve bone growth [Cai10, Ito08, Kan10, Lau11, Ma11a, Mro10, Suc04, Zre03]. These facts make magnesium a promising material to be used in regenerative medicine applications. However, despite there is a wide number of cytotoxicity or cell viability tests in the literature [Car11b, Car11c, Gu09, Li10b, Pie08], few complete *in vitro* works with magnesium have been detected. This is the reason why a complete *in vitro* test (proliferation and differentiation) was carried out in Chapter 4 as a starting point.

In spite of the biocompatibility and mechanical properties of magnesium, several authors agree that the rapid corrosion in physiological medium is the principal problem of magnesium alloys [Sta06, Wit07b, Wit07a, Zen08, Pie08]. In order to improve magnesium corrosion resistance, new magnesium alloys (*e.g.*, Mg-Ca alloys [Li08, Li10d, Liu10a, Erd10, Kir10], Mg-Li-Al alloys [Ham12, Kra10, Sei11, Wit05, Wit06, Wit10a], Mg-Zn [Che11a, Han09, Han10, Hua10, Li10b, Li10c, Zha10, Zha11a], Mg-RE alloys [Agh10, Fey10, Hor10, Sei11], among others) are being developed. Moreover, coatings are also being applied to the magnesium alloys in order to improve magnesium corrosion resistance. In this thesis, MgF_2 coating have been selected because it is a coating widely used in the literature, simple and economic [Car11a, Con11, Per10, Per11, Wit10a, Yan10]. Furthermore, the coating of porous samples is also viable with this coating.

Regarding the cell cultures, direct cell assays had been chosen because this represented a more realistic environment. Osteoblast-like cell MG-63 was used since this line is widely used for cytotoxicity analysis [Fis10, Mro10, Smo12, Wit07c, Fey10, Gu10c, Wan11b, Wan11a] and, taking into account the final application, it is relevant to the *in vivo* implantation site.

For the design of new alloys, a corrosion characterisation of magnesium alloys of three different families was carried out in Chapter 5. A reliable comparison of alloys based on literature is difficult because the lack of standardization in the corrosion tests [Mue10]. For their characterisation, electrochemical techniques were dismissed because these techniques measure the corrosion rate in only an instant [Kir12] and because the infeasibility of the polarized test to determinate the corrosion rates of the magnesium alloys [Atr11, Shi10, Son03]. Hydrogen evolution measurement was selected in order to determinate the corrosion rate of magnesium alloys because it is a technique that permits a measurement over time and because a high H_2 generation causes diseases

in vivo [Lam32, Sta06, Wit05, Wit10a, Wit07b, Won10, Xu09a, Zbe09, Zen08], so its measurement is important.

Later, the principal alloying elements were selected taking into account the present literature review, the results of the corrosion characterisation of the commercial alloys (Chapter 5), the cell viability of the commercial magnesium alloys (Chapter 5 and Chapter 6) and the effectivity of the MgF_2 on magnesium alloys (Chapter 6). Finally, in Chapter 8, replication casting process was analysed for the manufacturing of magnesium scaffolds. The powder metallurgy routes were dismissed because the process is more complex, it has more steps and the uncertainty of the oxidation of powder particles.

Chapter 3

Experimental procedure

As commented in Chapter 1, the main proposal of this thesis is to develop magnesium scaffolds for tissue engineering. In order to achieve this goal, several analysis and tests were carried out. In this chapter the main performed tests are described.

3.1 Corrosion testing

The corrosion test used to calculate the corrosion rate of the alloys by a volumetric method are described below.

3.1.1 Immersion testing with hydrogen evolution measurement

The samples were hung in an inverted funnel (figure 3.1). The volumetric hydrogen evolution, as an indicator of the corrosion rate, was measured in an eudiometer tube with a resolution of 0.1 ml. The procedure to measure the corrosion rate is described by Song *et al.* [Son03].

The samples were immersed in commercial PBS solution, which has been used for magnesium implant evaluation in the literature [Agh10, Alo12, Alv10, Han10, Mue10, Per10, Xin11a, Xue12] and it is recommended in corrosion standards such as ASTM F2129-08 or ASTM F746-04 for evaluation of implants. Dulbecco's Phosphate-Buffered Saline (DPBS) (200 mg l^{-1} KCl, 200 mg l^{-1} KH_2PO_4, 8000 mg l^{-1} NaCl, 1150 mg l^{-1} Na_2HPO_4) was used with a starting pH of 7.4 at 37 °C and without agitation. Approximately 40 ml of PBS per cm^2 sample surface was used in order to avoid changes

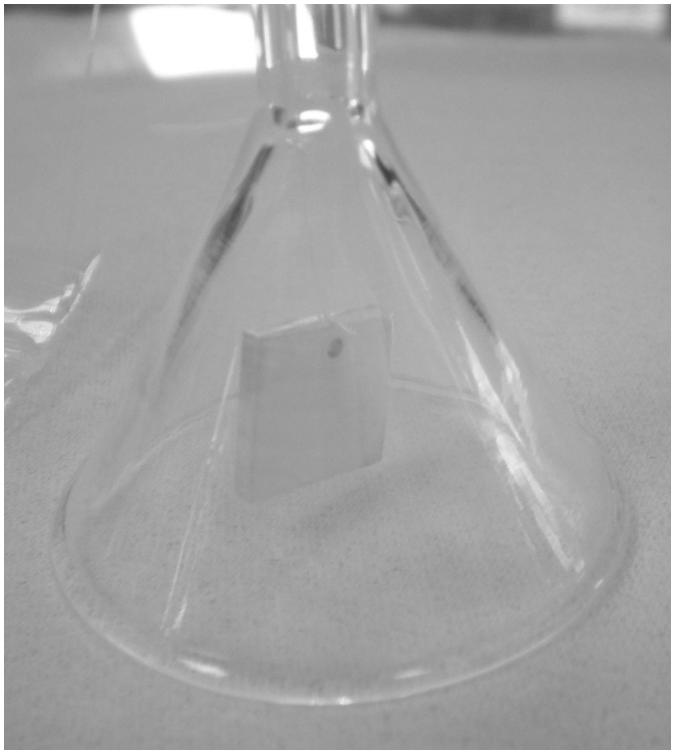

Figure 3.1: Detail of a magnesium sample hung in a funnel

in the corrosivity of the media according to ASTM G 31-72. The entire volume of PBS was changed every 48 hours to prevent pH increase due to the generation of hydroxides.

3.1.2 Calculation of the corrosion rate

In the present thesis the corrosion evaluation was analysed through the hydrogen evolution (ml of H_2 per mm_2 of sample) and the corrosion rate calculated using the hydrogen evolution. Corrosion rate was calculated the moles of hydrogen generated according to eq. 3.1.

$$P \cdot V = n \cdot \mathrm{R} \cdot T \tag{3.1}$$

Where:
P: H_2 pressure [atm]
V: H_2 volume [l]
n: moles of H_2 [mol]
R: gas constant, 0.08205746 $\frac{\mathrm{l \cdot atm}}{\mathrm{mol \cdot K}}$
T: temperature of H_2 gas [K]

The temperature (T) of the hydrogen gas was measured with a thermocouple during the set up of the experiment. The temperature was 303 K (30 °C), the temperature was lower than 37 °C because the top of the eudiometer was not close to the heat source. On the other hand, the volume (V) of the hydrogen gas was directly measured from the eudiometer. Finally, the pressure (P) of the hydrogen gas was calculated according to ep. 3.2.

$$P = P_{atm} - P_{vapor} - P_{column} \tag{3.2}$$

Where:
P: H_2 pressure [atm]
P_{atm}: atmospheric pressure, 1 atm
P_{vapor}: vapor pressure of H_2O at 30 °C, 0.0419 atm
P_{column}: pressure of the PBS column in the eudiometer

After calculating all the parameters, the moles (n) of hydrogen were calculated from eq. 3.1. Taking into account eq. 1.1 the moles of generated H_2 is equal to the moles of corroded Mg. Therefore, the corrosion rate of magnesium was calculated according to eq. 3.3.

$$CR = \frac{n \cdot m_a}{\rho \cdot S \cdot t} \tag{3.3}$$

Where:
CR: corrosion rate [mm year^{-1}]
n: moles of Mg [mol]
m_a: magnesium atomic mass, 24.3050 u
ρ: magnesium density [g/mm^3]
S: sample surface [mm^2]
t: experiment duration [year]

3.1.3 Characterisation of the corrosion surface

A Jeol JSM-5600LV scanning electron microscope equipped with an Oxford Instruments 6587 energy dispersive X-ray spectrometer (EDX) was used for analysing the final morphology of the samples. The energy dispersive X-ray (EDX) was used to analyse the coating and the composition of depositions and corrosion products.

3.2 Fluoride treatment

In order to improve the corrosion resistance of magnesium alloys, the samples were immersed in 48 wt% concentration hydrofluoric acid (HF) solution for 24 hours and/or 72 hours under slow stirring to achieve a MgF_2 coating. The MgF_2 coating was formed

by the reaction of HF with Mg, according to eq. 3.4 [Con10]. The coated samples were ultrasonically rinsed in ethanol for 15 minutes and dried.

$$2HF + Mg(s) \rightarrow MgF_2 + H_2(g) \tag{3.4}$$

A maximum of 72 hours of immersion in HF was chosen in this work. According to literature, Yan *et al.* [Yan10] showed that after 72 hours in HF the coating thickness on AZ31B alloy did not undergo further significant increase and as a result there was little further increase in the corrosion resistance. According to Yan *et al.* [Yan10] after 72 hours in HF the coating thickness on AZ31B alloy and the corrosion resistance did not increase significantly. They postulated that after 72 hours, the newly-formed coating was thick enough to terminate the reaction. Based on this previous research, and in order to achieve comparable results, a 72 hours immersion in HF was proposed for all the analysed alloys.

3.3 Development of new magnesium alloys

The alloy development of this work was performed in the Magnesium Innovations Centre (MagIC) of the Helmholtz-Zentrum Geesthacht (HZG). Pure Mg (99.99 wt%), pure Zn (99.99 wt%), pure Y (99.90 wt%), pure Ca (99.5 wt%) and Mg-2wt%Mn master alloy were used to prepare magnesium alloys. Magnesium was melted under a protective atmosphere (Ar) and the alloying elements were added as pure elements at a melt temperature of 750 °C. The melt then was stirred for 30 min at 200 rpm to prevent the alloying elements from settling prior to casting. The chemical compositions of the cast alloys were measured via spark emission spectrum analysis and XRF in the case of Ca.

3.4 Biological testing

The biological tests of this work were performed in the Stem Cells and Cell Culture Laboratory of the Cruces Hospital and in the Tissue Engineering Laboratory of The Kroto Research Instute of the University of Sheffield. Two different kinds of cell cultures were used in this work, one with mesenchymal stem cells (MSC) in Cruces Hospital and the other one with the MG-63 cell line in The Kroto Research Institute.

Human MSC were chosen for their ability to proliferate and differentiate into mesodermal cell lineages [Dom06]. These cells were used to carry out the biological tests of Chapter 4, in which an analysis of the problems of magnesium alloys in a cell culture taking into account cell adhesion, proliferation and differentiation was carried out as a starting point of the present thesis.

MG-63 cells were used in Chapter 5, Chapter 6 and Chapter 7 in order to analyse the cell viability of the commercial and non commercial magnesium alloys used in the present thesis. MG-63 cells were chosen because they are commonly used in the literature

to analyse the cell viability of materials used for bone regeneration [Cai10, Fey10, Fis10, Gu09, Gu10d, Gu10c, Mro10, Smo12, Wan11b, Wan11a, Wei10, Wit07c, Zha11b]. The assays performed with these two kind of cells are explained below.

3.4.1 Cell cultures with human MSC line

The chosen cells for culture on magnesium alloys were primary cultures of human mesenchymal stem cells (MSCs) obtained from bone marrow. The MSCs are a type of adult stem cell with a high rate of proliferation *in vitro* during the first passages. Furthermore, they are able to differentiate under appropriate culture conditions into mesodermal cell lineages (adipocytes, osteocytes and chondrocytes) [Dom06].

Human bone marrow-derived MSCs (BM-MSCs) were obtained from Inbiobank, a node of the National Cell Line Bank (Spain). These cells were harvested from cadaveric donors upon the informed consent of close relatives under the supervision of the Spanish National Transplant Organization (ONT). After expansion, MSCs displayed a typical CD29+, CD73+ (SH3 and SH4), CD105+ (SH2), CD166+, CD34-, CD45- and CD31- phenotype. In the presence of specific differentiation factors, they are able to differentiate into adipocytes, chondrocytes and osteocytes.

MSCs proliferation

MSCs were spread at high density on magnesium alloys ($10 \times 10 \times 1.5$ mm^3) and were maintained in culture for two weeks in a controlled atmosphere with 5 % CO_2 at 37 °C. The culture medium for cell proliferation was enriched with proteins, amino acids and antibiotics to avoid possible contamination. The components are detailed in table 3.1.

For the cell proliferation analysis on magnesium alloys, the cells were stained with Hoechst 33342. This is a fluorescent stain that labels double-stranded DNA concentrated in the cell nucleus, allowing the identification of cells on metallic alloys using fluorescence microscopy. The presence of this stain does not affect cell viability.

Differentiation into chondrocytes: chondrogenesis

Once the cells proliferated on the alloys, chondrogenesis was induced. Cells were cultured in differentiation medium supplemented with recombinant growth factor TGF-β, described in table 3.1. The cells were maintained for 6 weeks under these conditions, replacing the culture medium every 2-3 days.

3.4.2 Cell cultures with MG-63 cell line

Human osteosarcoma cells (MG-63) were used for the biological test of this work. High passage numbers (69-72) were used. The cells were storaged in liquid nitrogen at -196 °C.

Table 3.1: Components of the proliferation medium and differentiation medium.

Medium type	Medium components
Proliferation	DMEM
	L-Glutamine
	Penicillin/Streptomycin
Chondrogenesis	Basal Medium
	Dexamethasone
	Sodium piruvate
	L-Glutamine
	Proline
	Gentamicin/Amphotericin
	Ascorbic acid
	TGF-β

Cell culture

The magnesium alloy samples (10 × 10 × 1.5 mm^3) were sterilized in isopropyl alcohol (2-propanol) for 3 hours. The samples were wetted in fetal calf serum (FCS) in order to allow protein attachment which would facilitate cell attachment.

Human osteosarcoma cells (MG-63) were cultured in a standard culture medium containing DMEM, 10 % fetal calf serum (FCS), 1 % L-Glutamine and 1 % penicillin/streptomycin (PEN-STREP) at 37 °C in a humidified atmosphere of 5 % CO_2. 200,000 cells were seeded on the sterilised magnesium samples in 24-well plates. Cells were grown up to 14 day, culture media was replaced once every 2-3 days.

Cell viability testing

On day 1, 7 and 14, the samples were moved to new well-plates and incubated for 4 hours in medium containing 0.1 mM resazurin to measure cell viability. The colour change of the solution was measured in a FLX 800 Fluorescence Microplate Reader as indicator of cell metabolic activity. Finally, the Resazurin Sodium solution was removed and samples were cleaned with PBS and new cell culture media was added.

3.5 Scaffold manufacturing by replication casting

The magnesium scaffolds of the present thesis were manufactured at The University of Sheffield in collaboration with Dr. Russell Goodall's group. The installation for manufacturing magnesium foams (figure 3.2) consists of a furnace, a vacuum pump and a system for supplying a protective and pressurising gas. The infiltration was carried

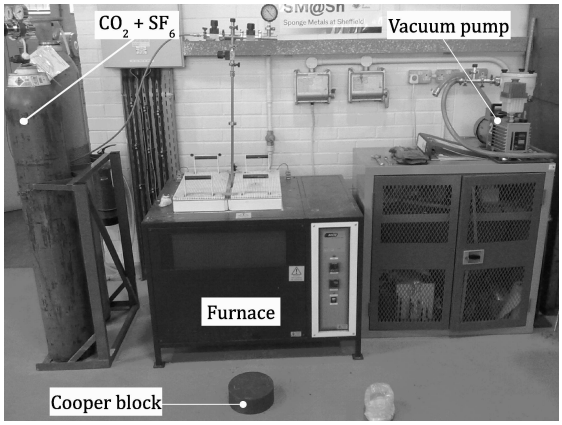

Figure 3.2: Installation for foam manufacturing by replication casting

out in a 33 millimetres diameter steel cylinder coated with boron nitride in aerosol form. First, 250-500 µm grain size NaCl was loaded (unlike some other versions of the method, the salt particles were added loose and not pre-compacted) and next a magnesium ingot was added on top of the salt. Finally the cylinder was closed using graphite gasket rings on top and bottom. The cylinder was then introduced into a resistance furnace and heated at a rate of 20 °C per minute, maintaining the cylinder at the process temperature for two and a half hours to assure a homogeneous temperature before the infiltration casting. During the entire procedure, the molten magnesium was under a protective atmosphere of $CO_2 + 4\ \%\ SF_6$ at 0.5 bar (with a lower pressure the magnesium could sublimate). After the temperature homogenization, the gas pressure was increased forcing the molten magnesium to permeate through the salt grain preform.

After the infiltration, the steel cylinder was cooled by placing it on a copper block to allow solidification to proceed from bottom to top. This strategy helps solidification shrinkage to take place outside the salt preform avoiding unwanted extra porosity and other solidification defects that could arise as a result of slow cooling and final solidification in the centre of the sample. After the cooling, the samples were removed from the steel cylinder. Distilled water with NaOH (4 g per litre to give a pH of 13) was used to dissolve the salt in order to decrease the corrosion of the magnesium during the removal of the salt.

3.6 Porosity evaluation

The porosity of the foams manufactured by replication casting was obtained according to eq. 3.5.

$$\wp = 1 - \frac{\rho_{foam}}{\rho_{Mg}} \tag{3.5}$$

Where:
$\wp$: the porosity of the foam.
ρ_{foam}: the density of the foam based on its weight and dimension.
ρ_{Mg}: the density of bulk Mg.

3.7 Mechanical testing

Uniaxial compression tests were carried out in an Instron 4206 testing machine. Tests were performed with a compression testing device (set up is shown in figure 3.3). A 50 mm extensometer was coupled to this device. The tests were conducted at a strain rate of 10^{-3} s^{-1}.

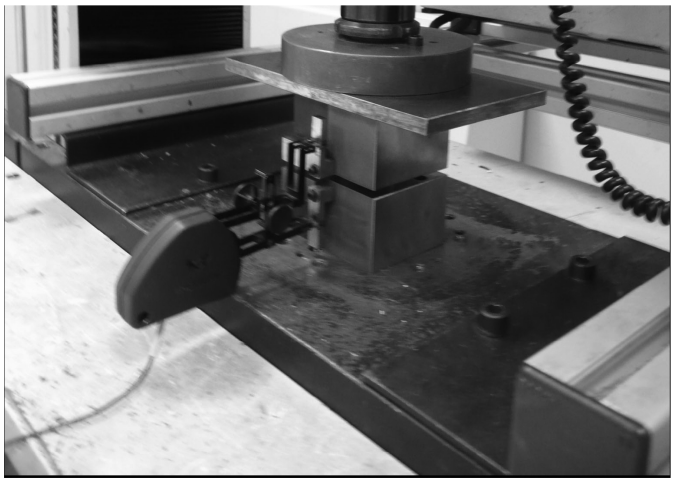

Figure 3.3: Compression test set up

Chapter 4

Cell culture on commercial magnesium alloys: a preliminary analysis

After the literature review exposed in Chapter 2, some gaps were identified. The principal gaps detected in the literature were the definition of the optimal surface roughness for cell attachment, the identification of the problems in a complete cell culture with cell proliferation and differentiation and the difficulty of making a reliable comparative between corrosion rate of magnesium alloys, among others.

For these reasons, the performed tests in the present chapter were carried out as a starting point of this thesis. In these tests the problems of magnesium alloys in a cell culture were analysed taking into account the cell adhesion, proliferation and differentiation into chondrocytes. Human MSC were chosen to carry out the cell cultures due to their ability to proliferate and differentiate into mesodermal cell lineages [Dom06]. Furthermore, four surface modifications were analysed in order to choose the optimal one and to apply it in subsequent experiments.

The magnesium alloys evaluated in this study were AZ31B (nominal 3 wt% Al and 1 wt% Zn) and ZM21 (nominal 2 wt% Zn and 1 wt% Mn). Aluminium is an alloying element that increases the corrosion resistance of magnesium. In fact, magnesium alloys combined with aluminium, especially aluminium-zinc series, have been commonly used in several studies [Gu09, Kra10, Pie08, Wit07b, Wit07a], despite Al could cause toxicity

problems [El 03, Gu09, Mat01] and could inhibit the bone growth [Mat01]. AZ31B was chosen because it contains a low percentage of Al ($\sim$ 3 wt%), decreasing the toxicity caused by this element. The second alloy, ZM21, has been chosen due to the corrosion resistance that magnesium alloys with similar composition have shown in physiological fluids [Son07c].

4.1 Sample preparation

$10 \times 10 \times 1.5$ mm^3 samples were prepared for various analysis (cellular adhesion and proliferation, chondrogenesis and material degradation). In order to determine the influence of surface roughness on cellular adhesion and proliferation, four different surfaces morphologies were evaluated. These surfaces and their nomenclature are described in table 4.1. Figure 4.1 shows the morphology of the achieved sample surfaces. ST1 presented a roughness with deep lines (figure 4.1a), ST2 also presented lines but less deep than ST1 (figure 4.1b), ST3 showed a flat morphology (figure 4.1c) and ST4 presented a surface with a large number of peaks and valleys (figure 4.1d).

Table 4.1: Description of the performed surface treatments

Name	Treatment
ST1	1000 grit SiC paper
ST2	1000 grit SiC paper + 4000 grit SiC paper
ST3	1000 grit SiC paper + 4000 grit SiC paper + polishing (Al_2O_3 0.05 µm)
ST4	1000 grit SiC paper + 4000 grit SiC paper + polishing (Al_2O_3 0.05 µm) + etching (HNO_3 69.5 %)

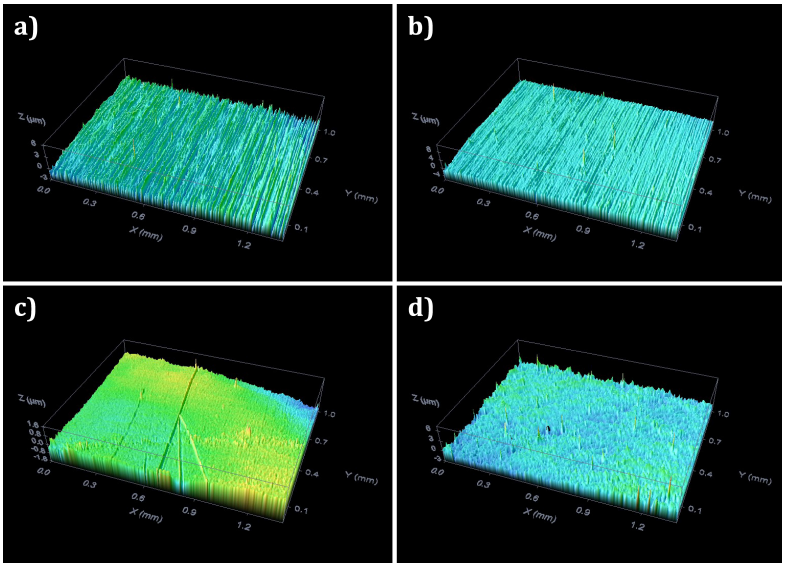

Figure 4.1: Morphology detail of a) ST1 b) ST2 c) ST3 d) ST4

After the sample surface modification, the samples were subjected to a sterilization process with ethylene oxide to avoid possible alterations due to the thermosensitivity of the material [Sil00].

4.2 Cell proliferation and differentiation into chondrocytes

After 14 days in the proliferation medium, cell confluence was great enough for the formation of a monolayer of undifferentiated cells on ZM21 ST4 sample. This cell layer covered the sample partially with significant extensions of tissue. Figure 4.2 shows on ZM21 ST4 sample the formed layer. However, different behaviours were detected between the different alloys and surfaces. Comparing the two alloys, cell proliferation was lower or non-existent in AZ31B alloy compared to the ZM21 alloy, as it is shown in figure 4.3.

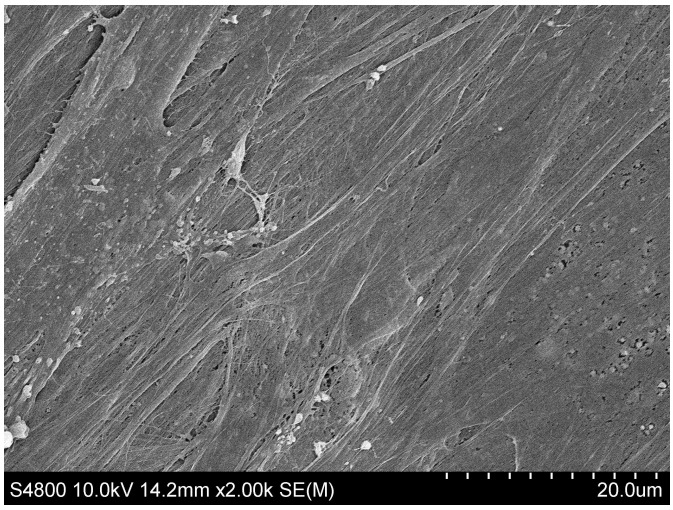

Figure 4.2: Detail of cell monolayer on ZM21 ST4 sample. Optimal cell proliferation region observed by SEM (Image provided by Cruces Hospital)

Taking into account the different surface morphologies of the ZM21 alloy, a more uniform cell distribution was observed on ST2, ST3 and ST4 surfaces (figure 4.3). Meanwhile, as it is shown in figure 4.3e, cells were clumped in clusters on ST1. This may be due to an excessive surface roughness. Nevertheless, a very low roughness, as the polished one (ST3), apparently resulted in a compromised cell adhesion and proliferation (in figure 4.3g less cell density is shown for the polished surface after the proliferation process). As it is shown in figure 4.3f and figure 4.3h, ST2 and ST4 respectively, presented high cell adhesion and proliferation.

Finally, after the chondrogenesis process, the composition of the secreted matrix by differentiated cells was analysed. In this analysis sulfated glycosaminoglycans were found.

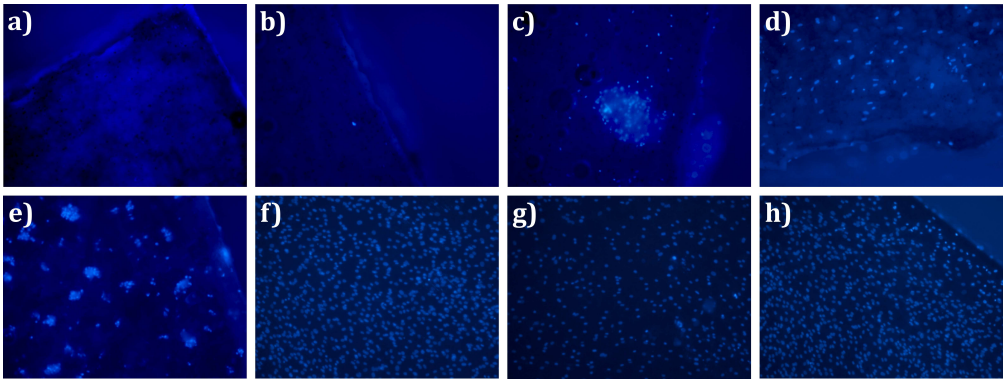

Figure 4.3: Cell adhesion after 14 days in cell culture medium on a) AZ31B ST1 b) AZ31B ST2 c) AZ31B ST3 d) AZ31B ST4 e) ZM21 ST1 f) ZM21 ST2 g) ZM21 ST3 h) ZM21 ST4 (images provided by Cruces Hospital)

These components are the principal constituents of the extracellular matrix of cartilage. These preliminary results indicated a greater potential for the ZM21 alloy compared to the AZ31B alloy in regenerative medicine.

4.3 Magnesium corrosion during cell culture

During cell culture, generation of gas bubbles was observed in all the magnesium alloys. In figure 4.4a the bubbles generated due to magnesium corrosion are clearly observed. After several days, due to the activity of the material, formations were seen in the medium. As it is shown, in figure 4.4b needle like products were detected. These needle like products have been detected also in cell cultures by others authors [Fis10].

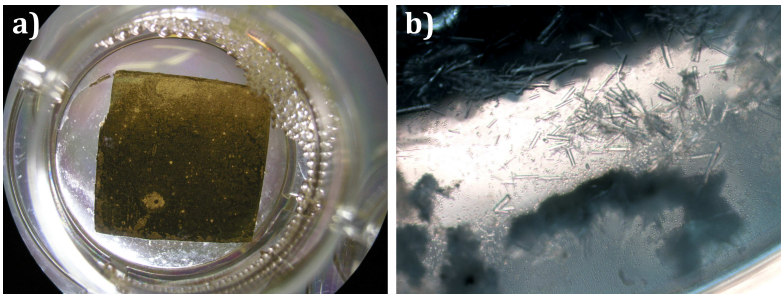

Figure 4.4: a) Detail of generated hydrogen bubbles due to the corrosion of the AZ31B ST1 in culture medium b) Products in culture medium due to the activity of ZM21 ST1 (images provided by Cruces Hospital)

Furthermore, crystals were deposited on the surface during the cell culture. Figure 4.5a shows that these crystals prevented tissue growth. Some crystals were large enough to create a barrier effect and the tissue was not able to continue growing and samples were only partially covered by a cell layer. As it is shown in figure 4.5b, the crystals were rich in Mg, P and O. This elemental analysis suggested that crystals could be $(PO_4)^{3-}$ for-

mations. These phosphates have also been detected in other works [Alv10, Tie10, Zha10].

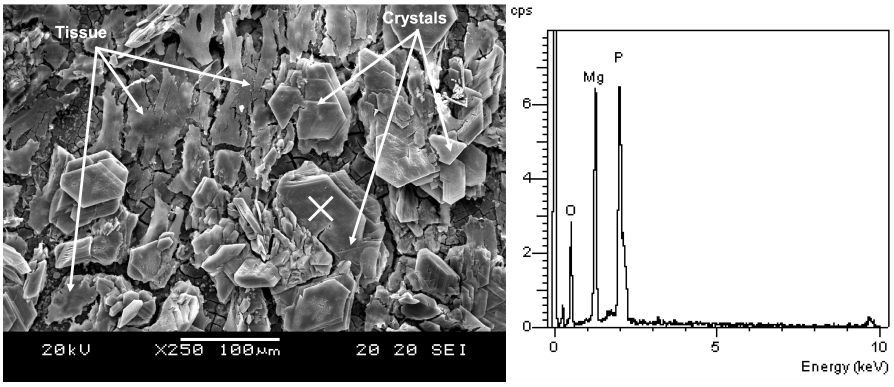

Figure 4.5: Detail of cells and crystals after 14 days in cell culture medium on ZM21 ST4 (analysed point marked as X)

Besides $(PO_4)^{3-}$ formations, other formations were also found. Figure 4.6 shows the presence of deposited crystals rich in P, Mg, Na and O. These crystals could be the deposition of NaH_2PO_4 which was in the culture medium. Finally, depositions rich in Ca were also detected as it is shown in figure 4.7. The presence of these crystals could be due to the bioactivity of magnesium.

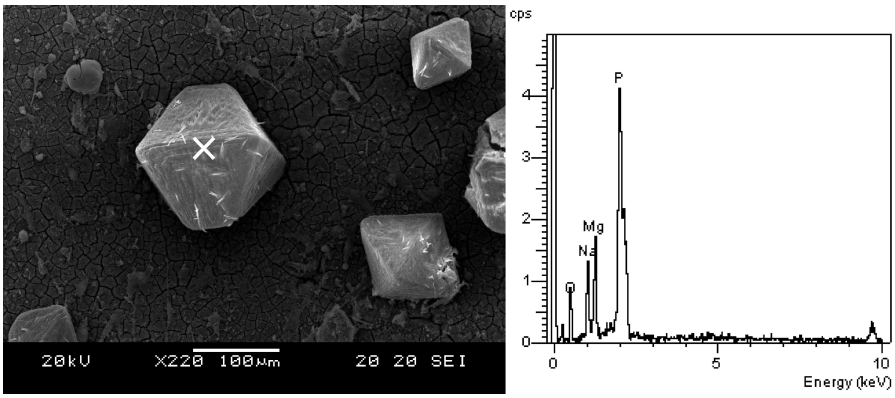

Figure 4.6: Crystals after 14 days in cell culture medium on ZM21 ST1 (analysed point marked as X)

4.4 Conclusions

The principal conclusions of this chapter were:

- ZM21 alloy favoured cell adhesion and subsequent cell proliferation of mesenchymal stem cells on it.
- AZ31B alloy had lower cell adhesion and proliferation rate than ZM21.

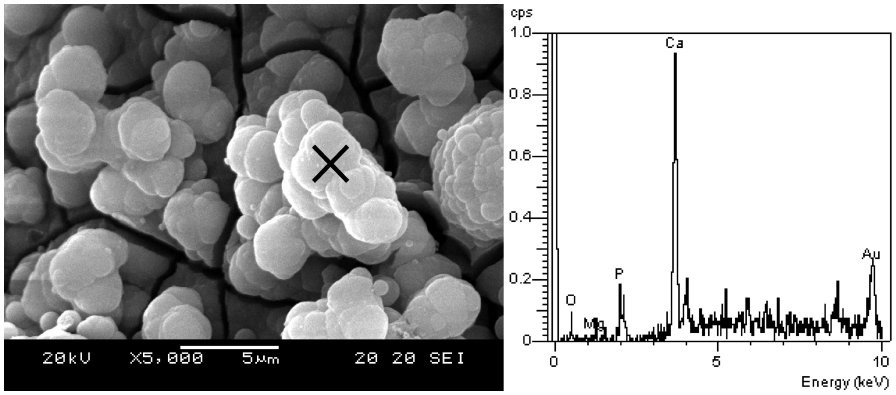

Figure 4.7: Depositions after 14 days in cell culture medium on ZM21 ST1 (analysed point marked as X)

- The identification of sulfated glycosaminoglycans confirmed the chondrogenesis process on magnesium alloys.
- Fine grinding (ST2), polishing (ST3) and etching (ST4) gave an uniform distribution of cells on the alloys.
- Rough grinding (ST1) gave a non-uniform distribution of cells with cells clumped in clusters.
- The polishing (ST3) made the cell adhesion and proliferation more difficult than rough grinding (ST1), polishing (ST3) and etching (ST4).
- Adhered crystals on the surface stopped the tissue growth.

These conclusions indicate that the material toxicity, degradation and activity are the most important factors to consider when magnesium is used as biomaterial. This is the reason why in the present thesis new magnesium alloys for biomedical applications were developed. Furthermore, the inhibition of tissue growth by crystal adhesion was a problem that was not previously identified in the literature. In order to achieve samples fully covered with cells, the formation of these crystals and how to reduce them will be discussed in following chapters. Finally, regarding the surface treatment, the following tests of this research, samples were ground with SiC papers from 1000 grits to 4000 grits (ST2). HNO_3 etching (ST4) was dismissed due its greater complexity.

Chapter 5

Evaluation of commercial magnesium alloys for tissue engineering applications

As mentioned in Chapter 4, the present chapter analyses the corrosion of magnesium alloys in physiological medium. For this purpose, three commercial magnesium alloys from different families and previously used in literature were selected: AZ31B [Alv10, Car11a, Con11, Gho10, Kim08, Qu11, Wit05, Yan10], WE43 [Gu09, Gu10a, Kra10, Wit05, Wu10, Xu08] and ZM21 [Eri09, Jam11]. Besides the corrosion behaviour, this chapter also analyses the cell viability of the three alloys. Thus, the suitability of different magnesium alloy families as biomaterial was evaluated.

After analysing the literature, as it is shown in table 5.1, a high dispersion in the corrosion rate measured by different authors was found. In the case of AZ31B magnesium alloy, the corrosion rate varies between 0.25 and 2 mm year^{-1}. The measured corrosion rate for the WE43 magnesium alloy varies between 0.3 and 1.5 mm year^{-1}. Finally, only few works with the ZM21 magnesium alloy were found in literature. However, the most common measured corrosion rate for the ZM21 is around 0.9 mm year^{-1}.

There may be many reasons for these dispersions but the most important one is the lack of standardisation [Mue10] and, in the cases when potentiodynamic polarisation is used, the inability of Tafel extrapolation to estimate the corrosion rate reliably due to the NDE [Son03, Atr11, Shi10]. In order to make a feasible compar-

Table 5.1: Comparison of the corrosion rates of the literature

	r_{corr} [mm year^{-1}]	Electrolyte	Characterisation test	Ref.
AZ31B	12.52	PBS	Potentiodynamic polarisation	[Sch10]
	0.25	Hank's solution	Immersion test	[Wan08]
	0.3	Hank's solution	Immersion test	[Ren07a]
	0.323	Hank's solution	Immersion test	[Gu10b]
	0.098	Hank's solution	Potentiodynamic polarisation	[Wan08]
	0.711	Hank's solution	Potentiodynamic polarisation	[Gu10b]
	6.597	Hank's solution	Potentiodynamic polarisation	[Tan10]
	0.284	SBF	Potentiodynamic polarisation	[Yan10]
	1.425	SBF	Potentiodynamic polarisation	[Hah11]
	8.965	SBF	Potentiodynamic polarisation	[Eri09]
	0.522	m-SBF	Potentiodynamic polarisation	[Wen10]
	0.737	m-SBF	Potentiodynamic polarisation	[Wen10]
	1.997	m-SBF	Immersion test	[Wen10]
	8.29	m-SBF	Immersion test	[Wen10]
	0.709	0 mol NaCl l^{-1}	Potentiodynamic polarisation	[Qu11]
	0.294	10^{-5} mol NaCl l^{-1}	Potentiodynamic polarisation	[Qu11]
	0.505	10^{-4} mol NaCl l^{-1}	Potentiodynamic polarisation	[Qu11]
	0.914	10^{-3} mol NaCl l^{-1}	Potentiodynamic polarisation	[Qu11]
	1.395	10^{-4} mol NaCl l^{-1}	Potentiodynamic polarisation	[Qu11]
	1.740	10^{-1} mol NaCl l^{-1}	Potentiodynamic polarisation	[Qu11]
	1.152	0 mol NaCl l^{-1} saturated with CO_2	Potentiodynamic polarisation	[Qu11]
	1.079	10^{-5} mol NaCl l^{-1} saturated with CO_2	Potentiodynamic polarisation	[Qu11]
	1.547	10^{-4} mol NaCl l^{-1} saturated with CO_2	Potentiodynamic polarisation	[Qu11]
	3.778	10^{-3} mol NaCl l^{-1} saturated with CO_2	Potentiodynamic polarisation	[Qu11]
	5.178	10^{-2} mol NaCl l^{-1} saturated with CO_2	Potentiodynamic polarisation	[Qu11]
	8.096	10^{-1} mol NaCl l^{-1} saturated with CO_2	Potentiodynamic polarisation	[Qu11]
	0.672	-	*In vivo*	[Gu10b]
WE43	0.361	SBF	Potentiodynamic polarisation	[Xu08]
	1.2	SBF	Potentiodynamic polarisation	[Eri09]
	0.035	SBF	Immersion test	[Han10]
	4.221	SBF	Immersion test	[Gu10b]
	4.467	SBF	Immersion test	[Xu08]
	0.704	-	*In vivo*	[Kra10]
	0.896	-	*In vivo*	[Gu10b]
	1.44	-	*In vivo*	[Kra10]
ZM21	0.919	SBF	Potentiodynamic polarisation	[Eri09]
	0.004	Ringer solution	Potentiodynamic polarisation	[Jam11]
	0.939	Ringer solution	Potentiodynamic polarisation	[Jam11]

ison, the three alloys were characterised under the same conditions in this chapter. The results were taken into account for the design of new magnesium alloys in Chapter 7.

The evaluation was carried out by measuring the hydrogen generation in PBS solution. According to the results of Chapter 4, a high crystals deposition on magnesium surface can avoid the tissue growth in a cell culture. This was the reason why the generated corrosion products and the deposited crystals during the degradation were characterised too. Finally, cell viability tests were carried out with the MG-63 cell line. This cell line is widely used in literature for biological characterisation of materials for bone regeneration [Cai10, Fey10, Gu10c, Smo12, Tan10, Wan11b, Wan11a, Wei10, Wit07c].

5.1 Sample preparation

$10 \times 10 \times 1.5$ mm^3 samples of commercial AZ31B (nominal composition: 3 wt% Al and 1 wt% Zn), WE43 (nominal composition: 4 wt% Y and 3 wt% rare earths), and ZM21 (nominal composition: 2 wt% Zn and 1 wt% Mn) magnesium alloys were prepared. Considering the conclusions in Chapter 4, the samples were ground with SiC papers from 1000 grits to 4000 grits, ultrasonically rinsed in ethanol for 15 minutes and finally dried. 6 repetitions were prepared for each magnesium alloy.

5.2 Immersion tests

All magnesium alloys degraded during the immersion tests. The hydrogen evolution of the alloys during the immersion tests is shown in figure 5.1. The corrosion rate evolution is also shown in order to get a better evaluation of the corrosion behaviour due to pH changes. All the alloys revealed higher hydrogen generation during the first 24 hours of the test with a decreasing and stabilizing corrosion rate over increasing immersion time (figure 5.1a). ZM21 bare alloy had the higher hydrogen generation (0.0155 ml/mm^2 after 96 hours in PBS) followed by AZ31B (0.0109 ml/mm^2 after 96 hours in PBS) and WE43 (0.0092 ml/mm^2 after 96 hours in PBS).

As it is shown in figure 5.2, there were not large pH variations. In all cases the pH kept below 8. However, the corrosion rate showed changes due to these pH changes. The corrosion rate increased slightly when the corrosion medium was changed (figure 5.1b).

The achieved corrosion rates for the studied alloys were compared with the literature (table 5.1). The results of the present research work fit well with the results achieved by other authors. The measured corrosion rate for AZ31B, 0.69 mm year^{-1} (after 96 hours in PBS), is between literature values (0.25 and 2 mm year^{-1}, table 5.1) and close to the results measured *in vivo*, 0.672 mm year^{-1} [Gu10b]. WE43 corrosion rate was 0.51 mm year^{-1} (after 96 hours in PBS) which is between literature values (0.3 and 1.5 mm year^{-1}, table 5.1). However, the *in vivo* corrosion rate measured by other authors is greater (0.704 mm year^{-1} [Kra10], 0.896 mm year^{-1} [Gu10b], 1.44 mm year^{-1} [Kra10]).

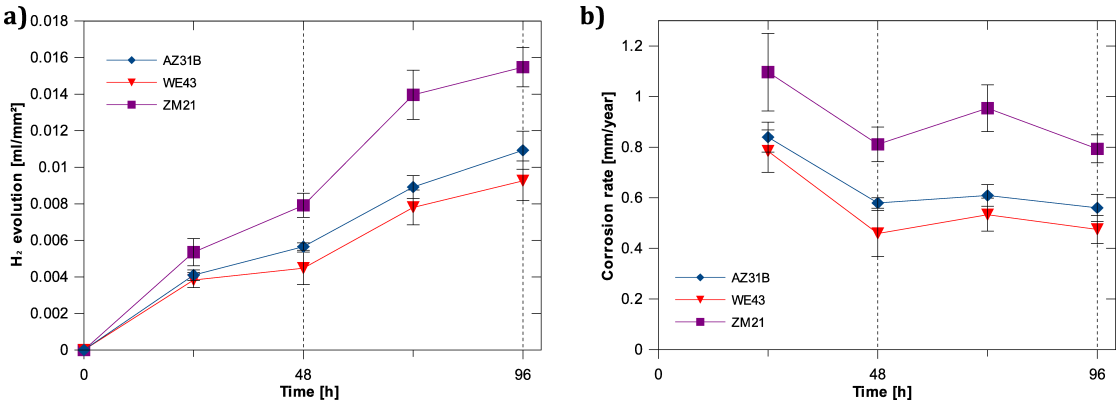

Figure 5.1: Corrosion tests of commercial magnesium alloys in PBS a) hydrogen evolution b) corrosion rate

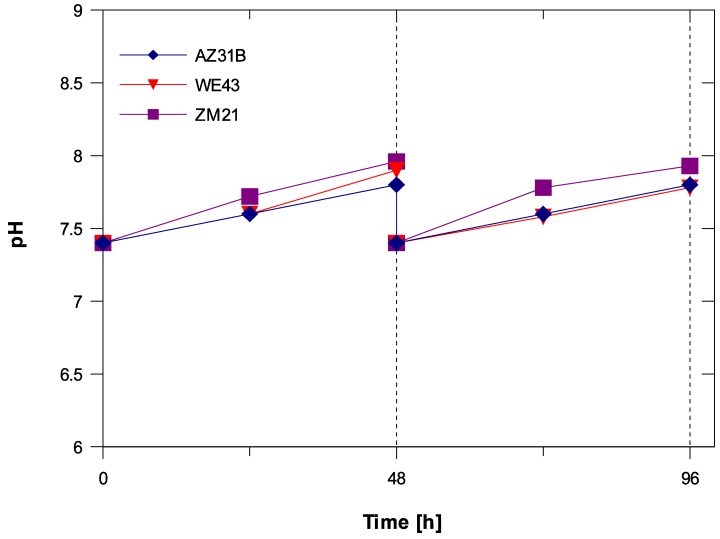

Figure 5.2: pH variation during the immersion tests

Finally, the corrosion rate for ZM21 was 0.90 mm year^{-1} (after 96 hours in PBS), close to the literature values (round 0.9 mm year^{-1}, table 5.1).

5.3 Characterisation of the corrosion surface

In order to achieve better understanding of the depositions immersion tests of 168 hours were carried out. The morphological features of the samples at different immersion times in PBS are shown in figure 5.3. The highest adhesion of precipitates was observed on AZ31B alloy (figure 5.3a, 5.3b and 5.3c). Two kind of deposits were found on AZ31B alloy, needle-like deposits and sponge-like deposits. ZM21 alloy presented less deposits (figure 5.3g, 5.3h and 5.3i) and WE43 is the alloy that showed the lowest activity after the immersion (figure 5.3d, 5.3e and 5.3f). ZM21 alloy presented higher depositions (black dots in figure 5.3h) than the WE43 (figure 5.3e) alloy and also other kind of depositions (figure 5.3i).

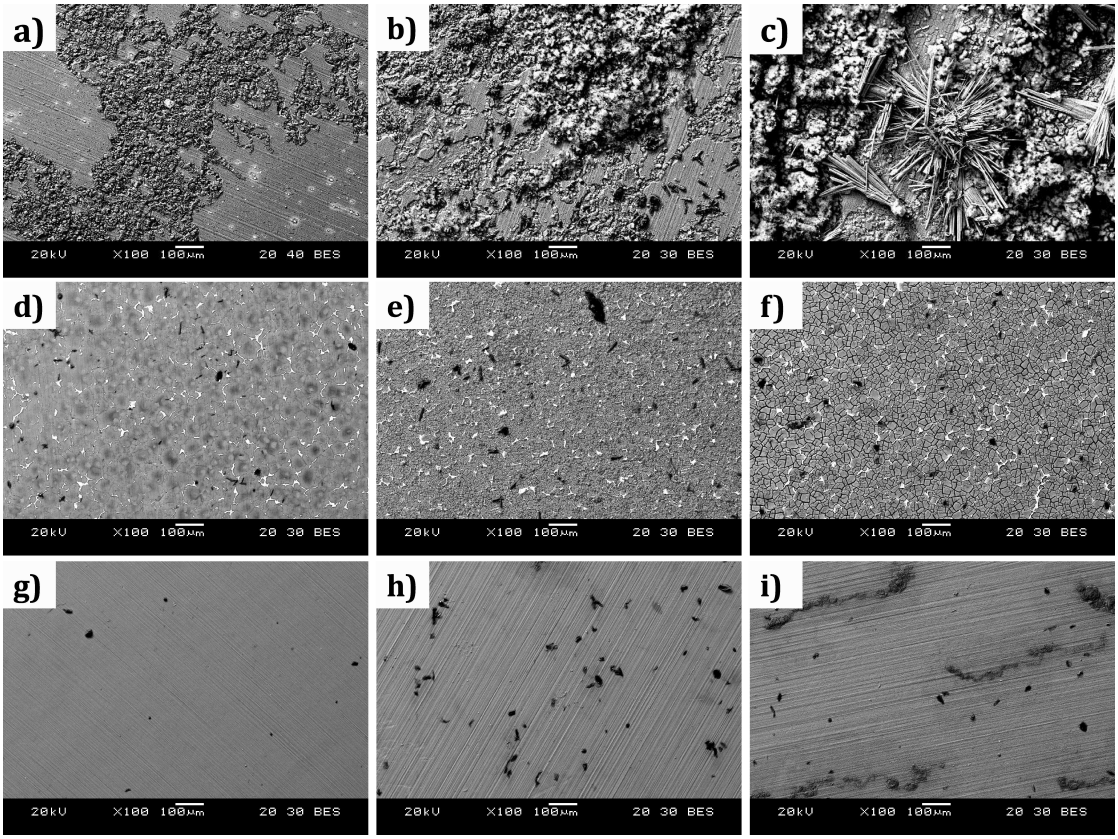

Figure 5.3: Detail of corroded surfaces. AZ31B after a) 24 h b) 72 h and c) 168 h in PBS. WE43 after d) 24 h e) 72 h and f) 168 h in PBS. ZM21 after g) 24 h h) 72 h and i) 168 h in PBS.

In order to identify the corrosion mechanisms, early stages of the corrosion process were also analysed. Figure 5.4 shows the start of a corrosion point on AZ31B alloy. The distribution maps show the presence of O, P and Ca. In the case of the ZM21, the distribution maps in figure 5.5 show corrosion products rich in Cl and O. Longer immersion tests in PBS of AZ31B and ZM21 alloys gave as a result the presence of several formations. After 7 days of immersion, needle like depositions rich in Mg, K, P, Na, K and O (figure 5.6) and sponge-like depositions rich in Mg, P, Ca, Na, K and O (figure 5.7) were adhered on AZ31B sample surface. In ZM21 samples depositions rich in Mg, P and O were also adhered but in more localized areas (figure 5.8). In the case of the WE43 bare alloy no significant adhesions were found.

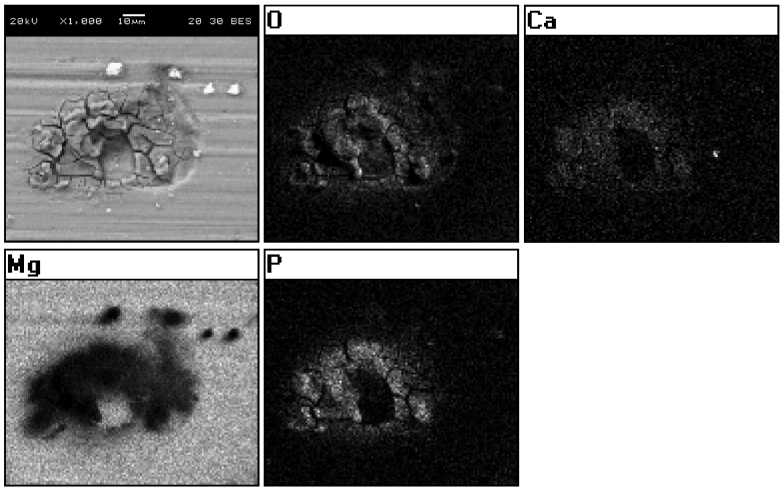

Figure 5.4: Early stage of the corrosion in AZ31B sample after 24 hours in PBS

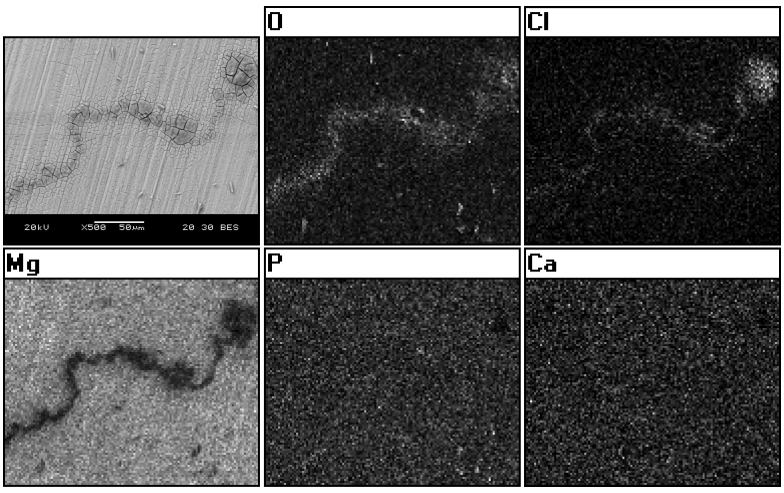

Figure 5.5: Early stage of the corrosion in ZM21 sample after 72 hours in PBS

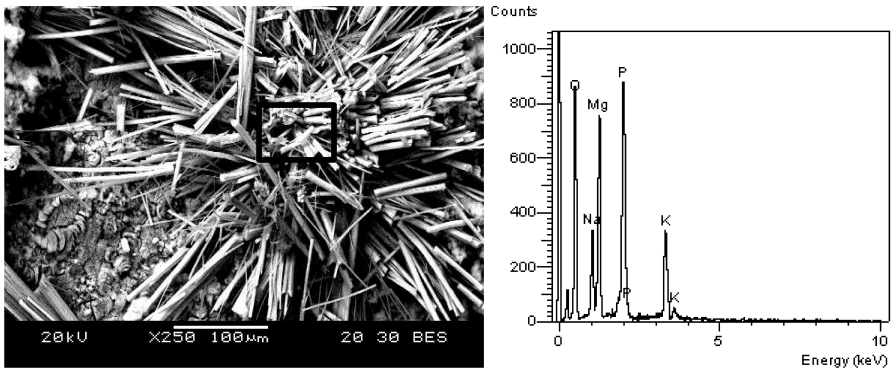

Figure 5.6: Needle-like depositions on AZ31B alloy after 7 days in PBS (analysed area marked as a box)

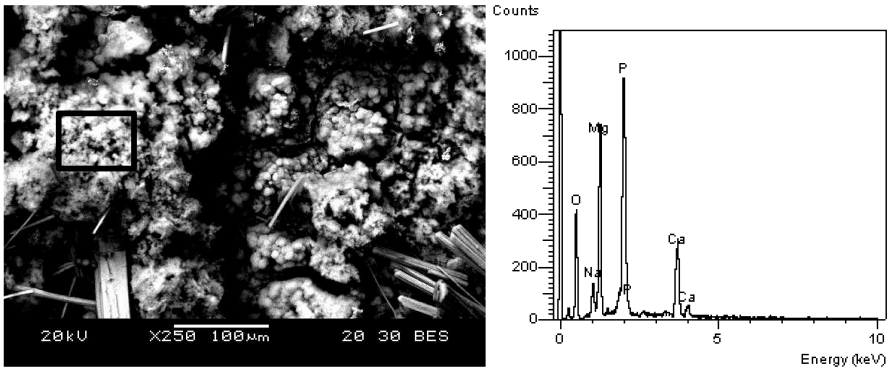

Figure 5.7: Sponge-like depositions on AZ31B alloy after 7 days in PBS (analysed area marked as a box)

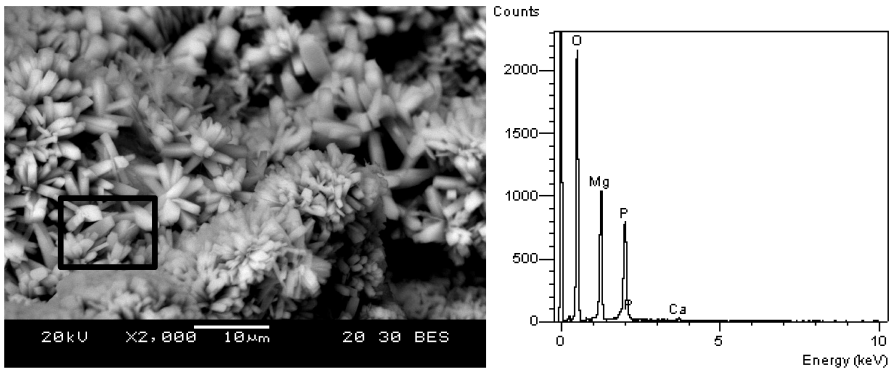

Figure 5.8: Formations on ZM21 alloys after 7 days in PBS (analysed area marked as a box)

The elemental analysis suggests that a mixture of $MgCl_2$ and $Mg(OH)_2$ could be the predominant species in the corrosion of bare alloys at the beginning of the corrosion. The formed $Mg(OH)_2$ could be dissolved in aqueous medium and transformed into soluble $MgCl_2$ by chloride ions [Xin11a]. As corrosion progresses, the elemental analysis suggests that different phosphates $(PO_4)^{3-}$ with Mg, Ca, K or Na were deposited on the surface. Depositions or corrosion products containing $(PO_4)^{3-}$ are also detected in other works [Alv10, Tie10, Zha10]. Finally, some particles rich in C, Mg and O were also detected (figure 5.9). According to the elemental analysis, these particles could be $(CO_3)^{2-}$. The presence of carbonates is common after the immersion of magnesium in physiological medium [Jam11, Tie10, Qu11]. However, in this work, only small formations of carbonates were found because PBS does not contain any. Nevertheless the presence of some carbonates could be explained due to the reaction of distilled water with the CO_2 of the atmosphere. In the same way, although PBS does not contain Ca, elemental analysis detected small amounts of Ca. In this case, it may be found as an impurity in PBS.

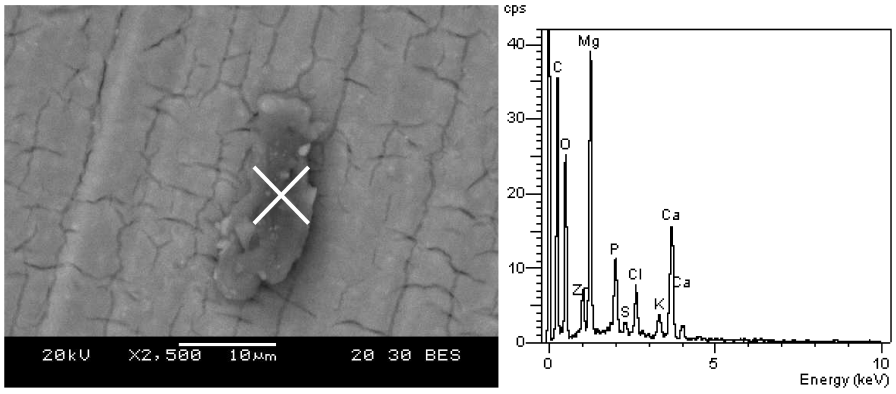

Figure 5.9: Deposit on ZM21 alloy after 72 hours in PBS (analysed point marked as X)

5.4 Cell viability

In order to get a general overview of the three alloys as biomaterials, cell viability tests were also carried out. Figure 5.10 shows the cytotoxicity results of AZ31B, WE43 and ZM21 magnesium alloy samples compared with Ti-6Al-4V for direct cell assay using MG-63 cells. The magnesium alloys showed a lower seeding efficiency than the Ti alloy. However, after 14 days, WE43 and ZM21 alloys presented an acceptable cell viability, although AZ31B alloy presented a low cell viability.

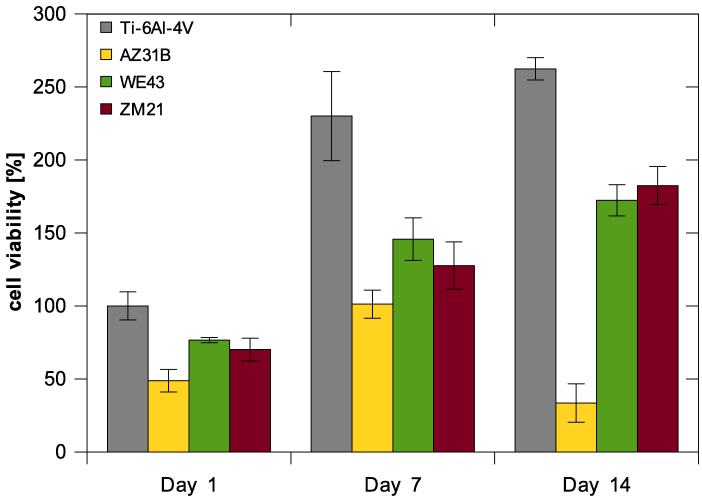

Figure 5.10: Cell viability after 14 days of MG-63 cells cultured directly in magnesium alloy samples

Figure 5.11 shows the morphologies of the MG-63 cells cultured on AZ31B, WE43 and ZM21 magnesium alloys samples for 14 days. As in Chapter 4, no cells were observed on the surface of AZ31B (figure 5.11a). However, for WE43 (figure 5.11b) and ZM21 (figure 5.11c) magnesium alloys, a higher number of cells with an elongated cell morphology was observed, indicating good cell adhesion.

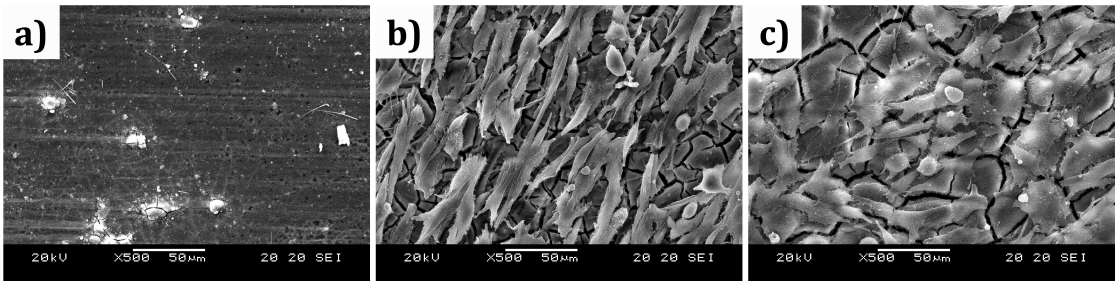

Figure 5.11: Morphology of MG-63 cells cultured on a) AZ31B b) WE43 and c) ZM21 magnesium alloys samples after 14 days

In contrast to the results obtained in the immersion test, no significant deposits were found on the surface of the alloys after the cell culture. This may be due to the presence of cells on the surface or due to the composition of the cell culture medium. DMEM, which was the main component of the cell culture medium, contained a lower concentration of $(PO_4)^{3-}$ than PBS, so less phosphate deposition was expected. Furthermore, the culture medium also contains proteins, which could inhibit the corrosion of the substrate by the medium [Liu10a, Kir10]. This could also be the reason that the ZXM200 alloy presented less corrosion in culture medium.

5.5 Conclusions

According to the results of this chapter the main conclusions were that:

- AZ31B alloy presented a low cell viability, and it is not recommended for biological application.
- Despite the difference in corrosion resistance between the WE43 and ZM21 alloy, both alloys showed a similar cell viability.
- These facts indicate that there was not a direct relation between the corrosion resistance and cell viability.
- In this case, the composition may be more important than the corrosion rate. As commented in Chapter 2, Al is a growth inhibitor of bone [Mat01]. This could be the reason why the cell viability of the AZ31B alloy was low.
- According to the corrosion and the crystal deposition, there was not a direct relation between them. AZ31B presented higher corrosion resistance than ZM21. However, AZ31B presented more crystal adhesion.
- The adhesion of deposits in the cell culture was lower than the adhesion of deposits in the immersion test in PBS for all the alloys.

Furthermore, the corrosion rate of the magnesium alloys was higher at the beginning of the corrosion. Although corrosion rate stabilized after a few days, this initial excess of corrosion could inhibit the efficiency of the cell seeding. In next chapter, the alloys were coated in order to decrease the corrosion rate, to prevent the initial excess of corrosion, to prevent the crystal adhesion and to analyse the effect of the coating on the cell viability.

Chapter 6

Efficacy of MgF_2 coating on magnesium alloys for tissue engineering applications

The present chapter analyses the efficacy of surface treatments on magnesium alloys for biomedical applications. As commented in Chapter 2, the use of surface treatments is a common strategy to solve the rapid corrosion of magnesium in physiological media [Won10, Li10b, Con11, Car11a, Per10, Per11, Wit10a, Che11a, Che11b, Gao10, Hah11, Hir10b, Kei11, Li10c, Li11b, Liu10b, Lu11, Ma10, Son10, Son08, Xu09a, Xu09b]. One of the surface treatments, widely used in literature to improve the corrosion resistance of magnesium, is the use of fluoride treatments [Con11, Car11a, Per10, Per11, Wit10a, Yan10]. The fluoride treatment is a chemical conversion that consists on the immersion of magnesium in hydrofluoric acid (HF) to form a coating of MgF_2. The MgF_2 coating presents a low water solubility and a good biocompatibility [Per10, Per11].

In this chapter, besides the increase of corrosion resistance, the aim was also the prevention of crystal deposition. According to the results of Chapter 4, the achievement of a surface fully covered with cells in a cell culture is not possible if a high crystal deposition occurs. This is the reason why in this chapter a MgF_2 coating was applied to the magnesium alloys in order to achieve a higher corrosion resistance and a lower crystal deposition.

As in Chapter 5, the corrosion evaluation was carried out measuring the hydrogen generation in PBS solution. Furthermore, in these corrosion tests, the effect of the fluoride treatment on crystal deposition was also analysed. Finally, a cell culture with the MG-63 cell line to analyse the cell viability after applying the fluoride treatment was carried out.

6.1 Sample preparation

Before applying the fluoride treatment, 10 × 10 × 1.5 mm^3 samples of each alloy (AZ31B, WE43 and ZM21) were ground with SiC papers from 1000 grits to 4000 grits, ultrasonically rinsed in ethanol for 15 minutes and finally dried (as in Chapter 5). The fluoride treatment was applied to the samples for 24 and 72 hours, as it was indicated in Chapter 3. Finally, treated samples were ultrasonically rinsed in ethanol for 15 minutes and dried. 6 repetitions were prepared for each material and surface treatment. The nomenclature used in this chapter for each sample is described in table 6.1.

Table 6.1: Nomenclature of the samples

sample	alloy	Coating treatment
AZ31B	AZ31B	-
AZ31BHF24h	AZ31B	24 h immersed in HF
AZ31BHF72h	AZ31B	72 h immersed in HF
WE43	WE43	-
WE43HF24h	WE43	24 h immersed in HF
WE43HF72h	WE43	72 h immersed in HF
ZM21	ZM21	-
ZM21HF24h	ZM21	24 h immersed in HF
ZM21HF72h	ZM21	72 h immersed in HF

6.2 Fluoride treatment

As it is shown in figure 6.1, a stable film was formed on all the samples after the fluoride treatment. The thickness of the coating increased with the immersion time for AZ31B and ZM21 alloys. AZ31B alloy presented an uniform film of 1.5 μm after 24 hours immersed in HF (figure 6.1a) which grew to 2.5 μm after 72 hours immersed in HF (figure 6.1b). On the other hand, the protected layer on the WE43 alloy was barely perceptible after 24 hours of immersion (figure 6.1c). After 72 hours the film was not homogeneous and it was clearly concentrated in the intermetallics (figure 6.1d). In this thin film no cracks were detected. Finally, the film on ZM21 alloy grew to 2.8 μm in the first 24 hours (figure 6.1e) and to 5 μm after 72 hours (figure 6.1f). Some cracks on the layer were found.

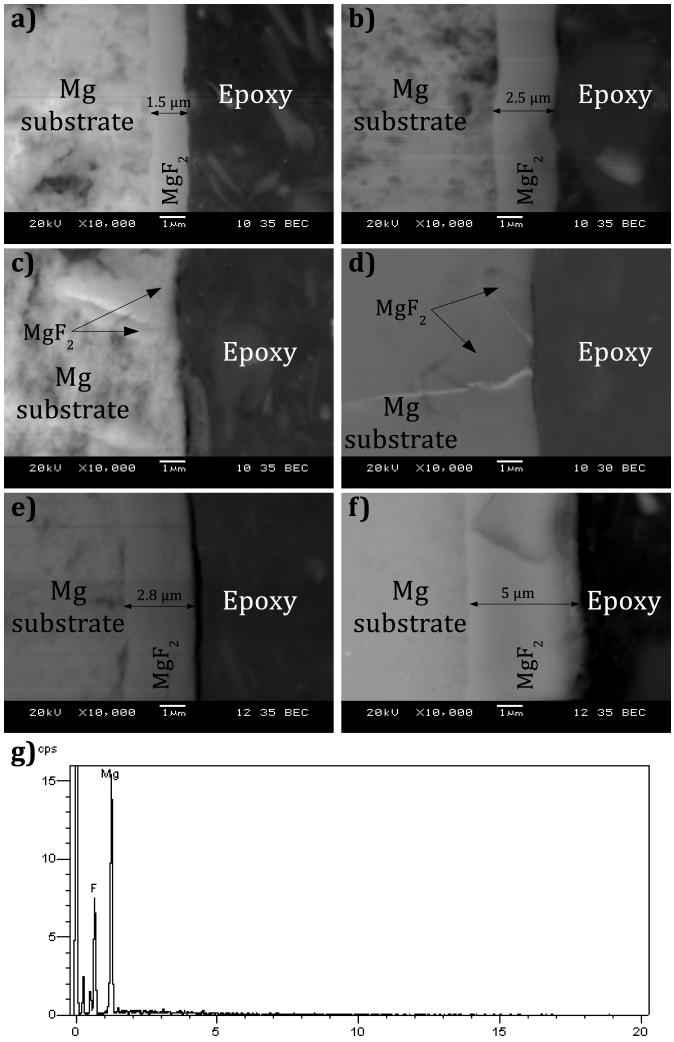

Figure 6.1: Detail of the thickness of the different coatings: a) AZ31BHF24h b) AZ31BHF72h c) WE43HF24h d) WE43HF72h e) ZM21HF24h f) ZM21HF72h g) Elemental analysis on the formed layer of AZ31B72h

Figure 6.1g shows the composition of the layer on the sample AZ31BHF72h after the immersion. As it was expected, the layer was rich in Mg and F indicating MgF_2 generation. The coating of the remaining samples was also rich in Mg and F.

As commented, in spite of being a stable layer, cracks were found on the ZM21HF24h and ZM21HF72h samples, and also sporadically on AZ31BHF72h samples, where thicker layers were generated during the fluoride treatment. On the other hand, no cracks were found on AZ31BHF24h, WE43HF24h and WE43HF72h samples, where thinner layers were created. The cracks may have appeared due to the brittleness of the coating [Sei11] in samples with a thick layer.

In order to analyse the possibility of forming a thicker coating on α-Mg of WE43 alloy, samples were immersed in HF during 168 hours. However, the coating on these samples was also non-uniform and barely appreciable in some areas (figure 6.2). It was also shown that the coating concentrates around the intermetallics. This may be due to micro-galvanic couples between the α-Mg and the intermetallics [Atr11, Coy10, Son99]. According to this, the loss of electrons by magnesium is concentrated around the intermetallic and it is there where MgF_2 is formed according to eq. 3.4. The effect could disappear dissolving the intermetallics in a T4 heat treatment before fluoride treatment.

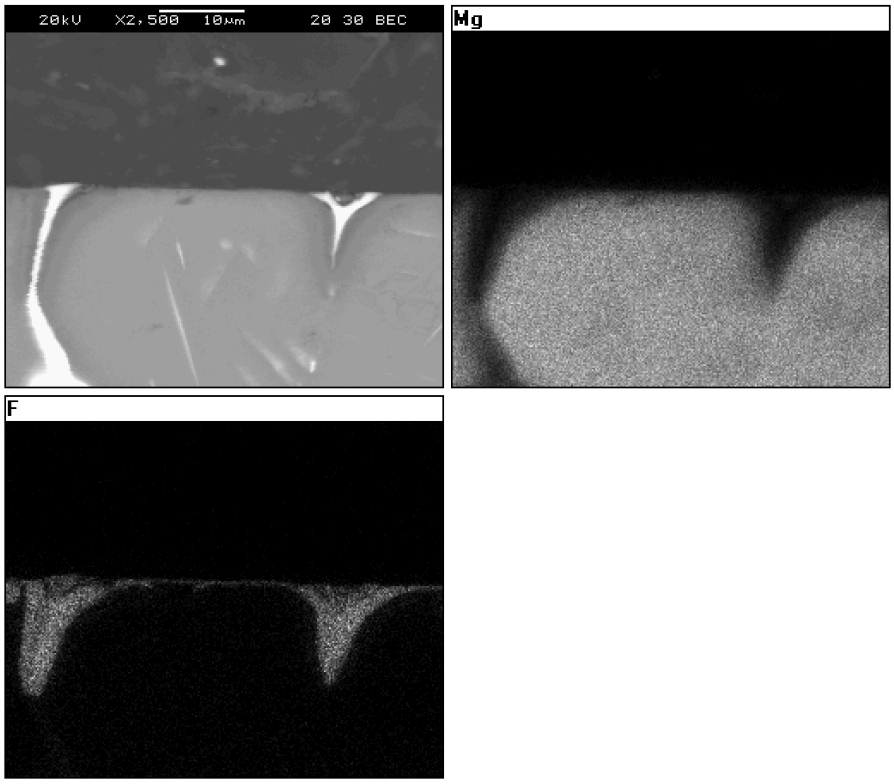

Figure 6.2: Detail of the MgF_2 layer around the intermetallic in the WE43 alloy

6.3 Immersion tests

All magnesium alloys degraded after 96 hours of immersion test. As it was stated in Chapter 5, all the bare alloys revealed higher hydrogen evolution during the first 24 hours of testing and a reduction and subsequent stabilization of the corrosion rate over immersion time (figure 6.3). ZM21 bare alloy had the higher hydrogen generation (0.0155 ml/mm^2 after 96 hours in PBS), followed by AZ31B (0.0109 ml/mm^2 after 96 hours in PBS) and WE43 (0.0093 ml/mm^2 after 96 hours in PBS).

Higher corrosion resistance was achieved for all the alloys after fluoride treatment. Longer fluoride treatment resulted in lower hydrogen generation. Therefore, a positive influence of the fluoride treatment on the magnesium corrosion was observed as stated previously [Con11, Car11a, Per10, Per11, Wit10a, Yan10]. However, fluoride treatment had a different influence in each magnesium alloy. This way, and compared to the bare alloys, the immersion of the samples in HF during 24 hours increased the corrosion resistance by 25 % for AZ31B, 34 % for ZM21 and 37 % for WE43. Furthermore, the immersion of the samples in HF during 72 hours increased the corrosion resistance by 50 % for WE43, 52 % for AZ31B and 75 % for ZM21. ZM21HF72h sample showed the lowest hydrogen generation (0.0039 ml/mm^2 after 96 hours in PBS) of all the samples, although the ZM21 bare alloy showed the highest hydrogen generation. The corrosion rate evolution for all the bare alloys is shown in figure 6.3.

In contrast with bare alloys, coated alloys started with a low corrosion rate and it increased slightly over immersion time due to magnesium fluoride film dissolution (figure 6.3). It was also observed that fluoride treatment made the alloys to show less dispersion in the results from sample to sample (figure 6.3). There were not large pH variations (table 6.2). However, as in Chapter 5, the corrosion rate in the samples showed changes due to these pH changes (figure 6.3).

Table 6.2: pH variation in the immersion test

sample	0 h	24 h	48 h	medium change	72 h	96 h
AZ31B	**7.4**	7.6	7.8	**7.4**	7.6	7.8
AZ31BHF24h	**7.4**	7.7	7.8	**7.4**	7.78	7.9
AZ31BHF72h	**7.4**	7.6	7.7	**7.4**	7.8	7.85
WE43	**7.4**	7.6	7.9	**7.4**	7.58	7.78
WE43HF24h	**7.4**	7.6	7.64	**7.4**	7.6	7.8
WE43HF72h	**7.4**	7.63	7.84	**7.4**	7.64	7.8
ZM21	**7.4**	7.72	7.96	**7.4**	7.78	7.93
ZM21HF24h	**7.4**	7.72	7.82	**7.4**	7.74	7.8
ZM21HF72h	**7.4**	7.6	7.6	**7.4**	7.68	7.8

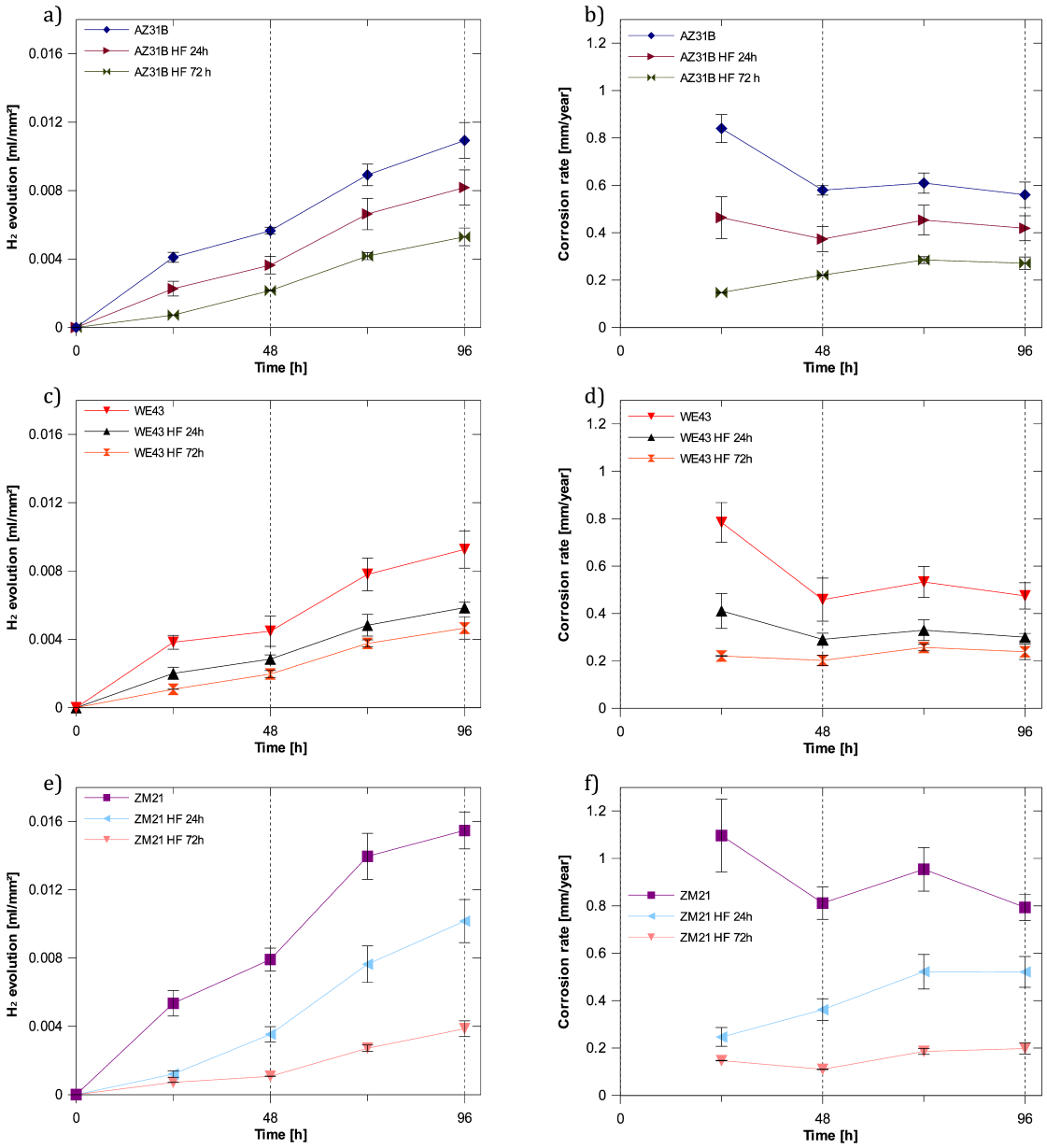

Figure 6.3: Hydrogen evolution and corrosion rate of (a and b) AZ31B, (c and d) WE43 and (e and f) ZM21

The increase of the corrosion resistance by the fluoride treatment depended on the morphology of the coating generated for each alloy (figure 6.1). In the case of the AZ31B and ZM21 magnesium alloys this dependency was clearer. As it is shown in figure 6.4, the hydrogen evolution decreased proportionally to the coating thickness. For both alloys, the greater the coating thickness was, the greater the corrosion protection it offered. The AZ31BHF24h samples, with a coating thickness of 1.5 µm, showed a corrosion rate 25 % lesser than the untreated AZ31B magnesium alloy samples. The AZ31BHF72h samples, with a coating thickness of 2.5 µm, showed a corrosion rate 52 % lesser than the untreated AZ31B magnesium alloy samples. In the case of ZM21 magnesium alloy, the ZM21HF24h samples with a coating thickness of 2.8 µm showed a corrosion rate 34 % lesser than the untreated ZM21 magnesium alloy samples and the ZM21HF72h samples with a coating thickness of 5 µm showed a corrosion rate 75 % lesser than the untreated ZM21 magnesium alloy samples.

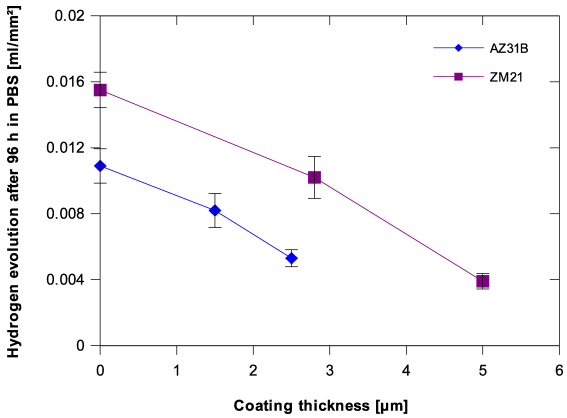

Figure 6.4: Hydrogen evolution according to the coating thickness

The tendency towards greater protection when the fluoride treatment was longer was also proved for the WE43 magnesium alloy. The WE43HF24h samples showed a corrosion rate 37 % lesser than the untreated alloy samples and the WE43HF72h samples showed a corrosion rate 50 % lesser than the untreated alloy. However, unlike the AZ31B and ZM21 alloys, there was not a direct relation between the corrosion rate decrement and the coating thickness for the WE43 magnesium alloy samples: the coating on the WE43HF24h was barely perceptible and the WE43HF72h presented a non-uniform coating.

Despite the WE43 alloy samples did not present a homogeneous coating, they achieved the highest reduction in corrosion rate after 24 hours of immersion in HF (37 %). The explanation for this may be the micro-galvanic corrosion that occurs in magnesium alloys with rare earths [Coy10]. As mentioned before, the coating was concentrated around the intermetallics (figure 6.2), leaving α-Mg almost without protection. This encapsulation could have eliminated the micro-galvanic couples between α-Mg and the intermetallics, thereby increasing the corrosion resistance of the WE43 alloy.

6.4 Characterisation of the corrosion surface

The morphological features of the samples after an immersion in PBS for 72 hours are shown in figure 6.5. As happened in Chapter 5, the highest adhesion of precipitates was observed on AZ31B bare alloy (figure 6.5a). WE43 (figure 6.5d) and ZM21 bare alloys (figure 6.5g) presented less activity. In all cases, the fluoride treatment decreased the adhesion of crystals on the surface (figure 6.5).

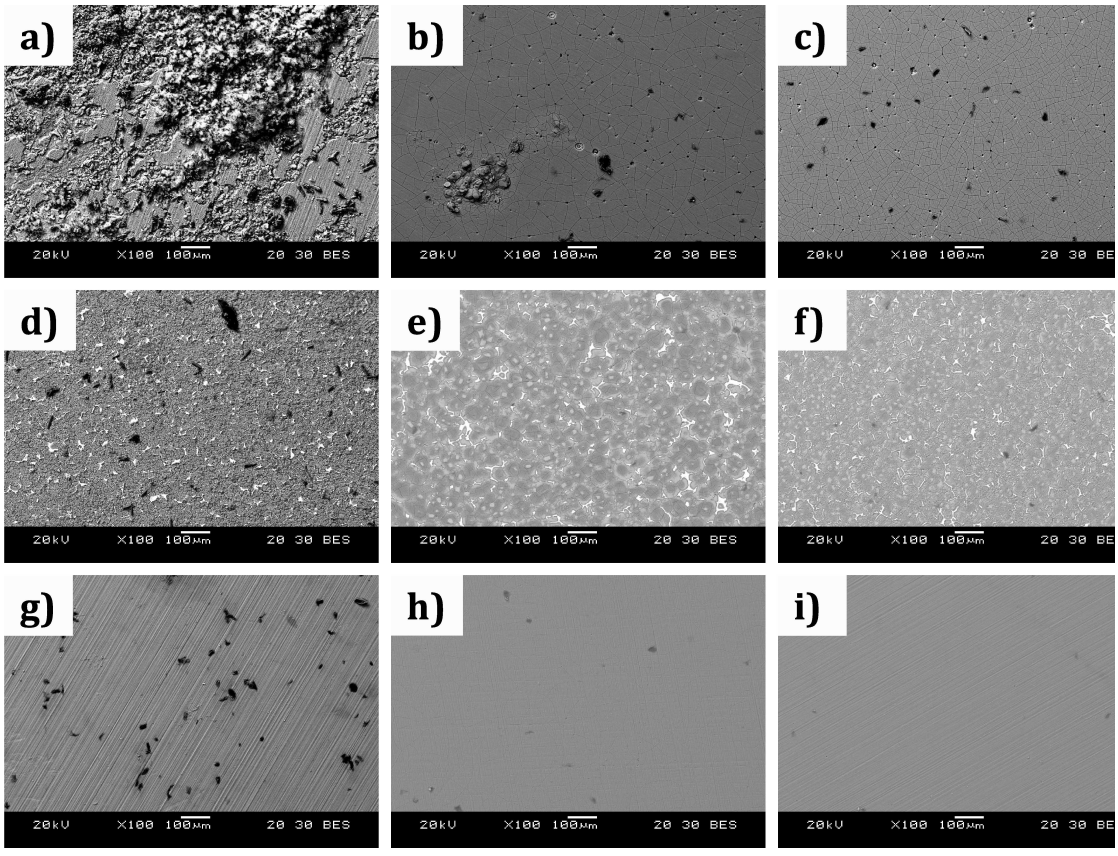

Figure 6.5: Surface of the samples after 72 h in PBS a) AZ31B b) AZ31BHF24h c) AZ31BHF72h d) WE43 e) WE43HF24h f) WE43HF72h g) ZM21 h) ZM21HF24h i) ZM21HF72h

Regarding the corrosion of the coated alloys, a early stage of the corrosion on the AZ31B alloy with a fluoride treatment of 24 hours is shown in figure 6.6 and figure 6.7. After MgF_2 dissolution, corrosion products rich in O and Cl were detected (figure 6.6). As commented in Chapter 5, a mixture of $Mg(OH)_2$ and $MgCl_2$ were the principal species. Other kind of formations rich in O, P, Na and Ca were also found, as it is shown in figure 6.7. For the AZ31BHF72h and for the coated WE43 and ZM21 alloys no significant formations were found. After 72 hours of immersion in PBS, MgF_2 coating was still present on the sample surface, especially in ZM21 alloy with a surface rich in Mg and F, as it is shown in figure 6.8.

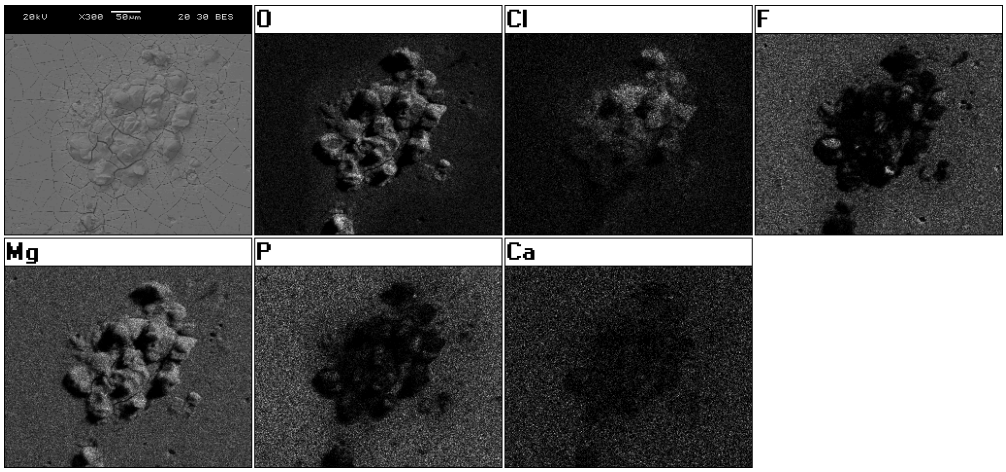

Figure 6.6: Early stage of the dissolution of the MgF_2 layer in AZ31BHF24h sample after 72 hours in PBS

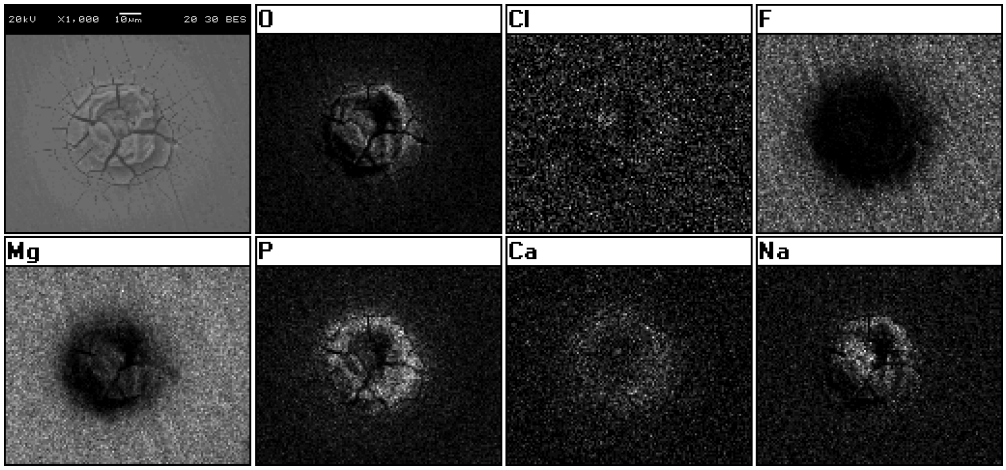

Figure 6.7: Dissolution of the MgF_2 layer in AZ31BHF24h sample after 24 hours in PBS with deposits of P, O, Na and Ca

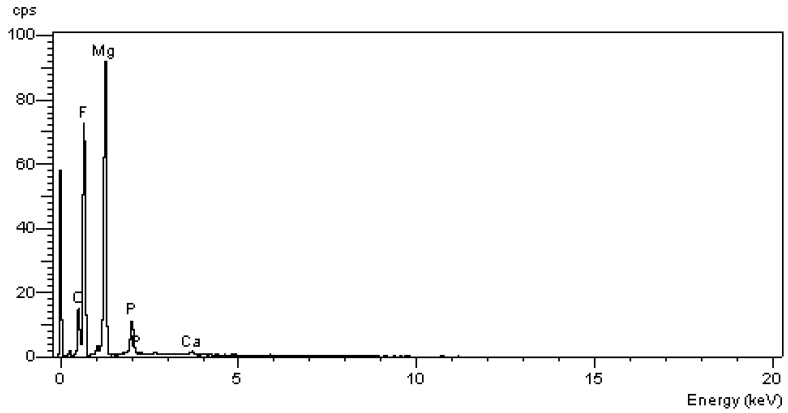

Figure 6.8: Elemental analysis of the MgF_2 layer on ZM21HF24h sample after 72 hours in PBS

6.5 Cell viability

The cell viability of the bare alloys and alloys with a fluoride treatment of 72 hours was analysed. The alloys with treatment of 72 hours were selected for better analysis of the effect of the fluoride treatment and because they showed higher corrosion resistance than those with 24 hours of treatment. Figure 6.9 shows the cell viability results of AZ31B, AZ31BHF72h, WE43, WE43HF72h, ZM21 and ZM21HF72h samples compared with Ti-6Al-4V for direct cell assay using MG-63 cells. It can be concluded that the fluoride treatment increased the seeding efficiency in all magnesium alloys and increased the cell viability. However, the ZM21HF72h samples showed a decrease in cell viability after 14 days of test. This may be due to the high confluence of cells on the sample: when the cell number on the sample is too high the cells may loss their adhesion. As it is shown in figure 6.10, a confluent layer of cells was observed, which may indicate an overcrowding on the sample. Furthermore, groups of stacked cells were common in the ZM21HF72h samples.

Figure 6.11 shows the morphologies of the MG-63 cells cultured on the samples for 14 days. A higher number of cells was observed in the coated alloys than in the bare alloys. This effect is clearly shown in figure 6.11e, where cells with an elongated cell morphology nearly forming a monolayer are shown on the WE43HF72h samples. In the case of the AZ31BHF72h samples, only isolated cells were observed on the surface (figure 6.11d). As in Chapter 5, no significant deposits were found on the surface of the alloys after the cell culture.

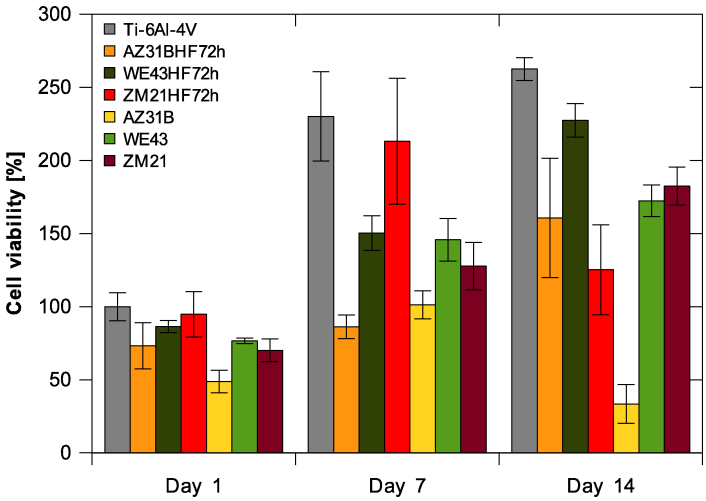

Figure 6.9: Cell viability after 14 days of MG-63 cells cultured directly on magnesium alloy and coated magnesium alloy samples

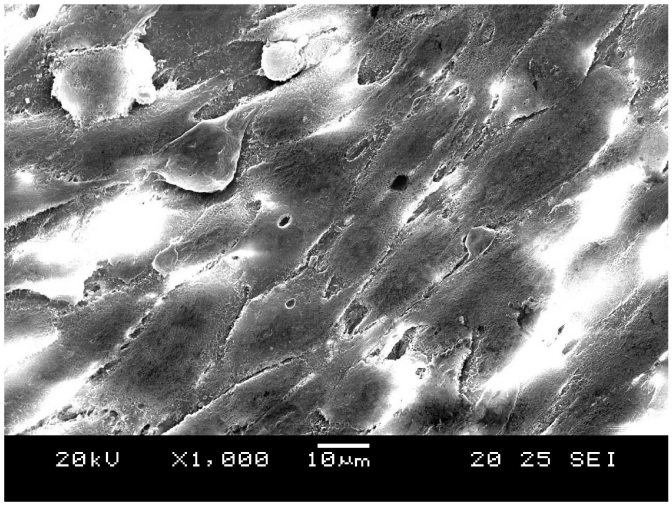

Figure 6.10: Confluent layer of cells on ZM21HF72h

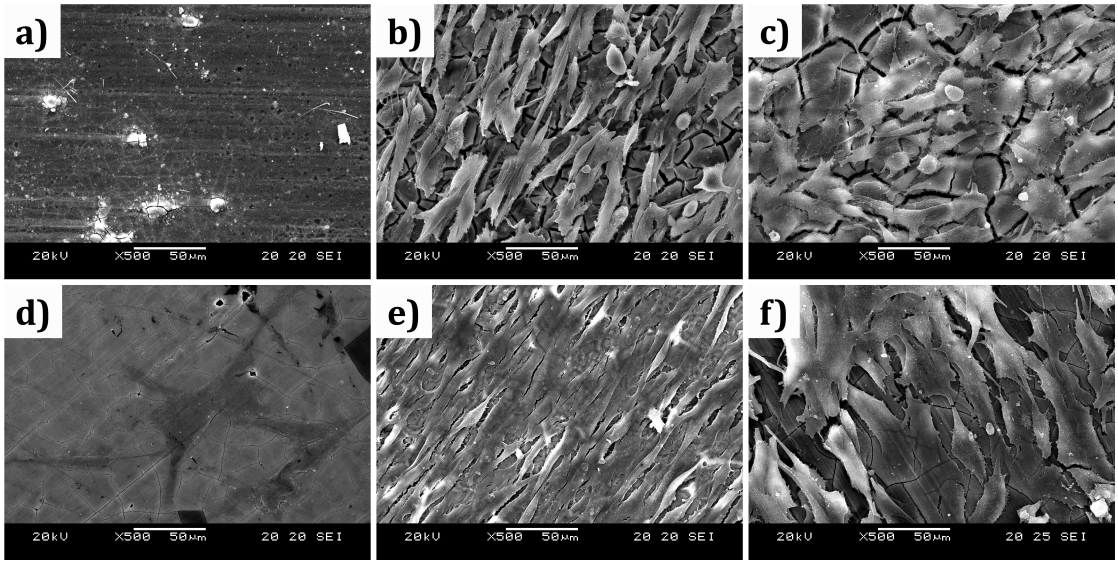

Figure 6.11: Morphology of MG63 cells cultured on a) AZ31B b) WE43 c) ZM21 d) AZ31BHF72h e) WE43HF72h f) ZM21HF72h samples after 14 days

6.6 Conclusions

The results of this chapter demonstrated that:

- Fluoride treatment applied to magnesium alloys increased the corrosion resistance and decreased dramatically the crystal deposition on the surface.
- The corrosion rate of magnesium can be decreased through the modification of the immersion time in HF. Fluoride coating was able to adequate the corrosion rate of magnesium alloys making them available for the future development of temporal implants and scaffolds.
- After 24 hours of fluoride treatment, the WE43 alloy achieved the highest increase in the corrosion resistance. The reason could be that fluoride treatment encapsulated the intermetallic phases in the WE43 alloy reducing the micro-galvanic couples. Regarding the ZM21 alloy, fluoride treatment had a smaller effect. Finally, the least effect was achieved for AZ31B alloy.
- After 72 hours of fluoride treatment, the ZM21 alloy achieved the highest increase in the corrosion resistance, despite some transversal cracks appeared in the coating layer. Regarding the AZ31B alloy, fluoride treatment had a smaller efficiency. Finally, the less effectiveness was achieved for WE43 alloy.
- Fluoride treatment increases cell viability of magnesium alloys.
- Absence of adhered crystals allowed an adequate cell distribution almost all over the surface for all samples except for bare AZ31B and coated AZ31B alloy. As

commented, Al is a growth inhibitor of bone [Mat01]. This could be the reason why the cell viability of the AZ31B alloy was low.

- As in Chapter 5, the adhesion of deposits in the cell culture was lower than the adhesion of deposits in the immersion test in PBS for all the alloys.

In the next chapter new magnesium alloys were developed taking into account the achieved results of Chapter 4, Chapter 5 and Chapter 6. Mg-Zn alloys without toxic elements and with a high increase in corrosion resistance after after fluoride treatment were developed.

Chapter 7

Development of new magnesium alloys for tissue engineering applications

As commented in Chapter 2, the main strategies to solve the rapid corrosion in physiological media of magnesium alloys are the development of novel magnesium alloys, that retain the biocompatibility but are more resistant to corrosion, and the application of surface treatments. In the case of the development of magnesium alloys, there are controversies on the biological effects of some common alloying elements, such as Y or rare earth elements [Gu09]. Because of that, some works advise to avoid these elements entirely or to use only small amounts of them [Hua10, Zha10, Zha11a]. However, new alloys using some of these elements are being developed for biomedical applications [Fey10, Gu09, Ham12, Han09, Han10, Wan10b, Wit06]. In fact, some trials in humans were carried out with WE43 alloy, which contains 4 % of Y and 3 % of rare earth, and no toxicity was detected [Mor11].

In order to avoid risks, until more knowledge on the effect of rare earth elements in the body is obtained, a line of research focused on the development of alloys based on the Mg-Zn binary alloy system with additions of other elements can be an alternative [Che11a, Han09, Han10, Hua10, Li10b, Zha10, Zha11a]. Zn is an essential micro-nutrient [Gu09, Hua10] and it improves the corrosion resistance in magnesium alloys [Gu09, Hua10, Son07a, Xu08, Yin08, Zen08, Zha10]. Furthermore, according to the results of Chapter 6, after fluoride treatment an improvement of 75 % in the

corrosion resistance was achieved in the case of ZM21 alloy, which makes Mg-Zn alloy system a promising binary alloy system for biomedical applications when it is combined with MgF_2 coating.

In the present chapter, novel Mg-Zn alloys were developed and compared with commercial WE43. Taking into account the results of Chapter 6, ZM20 alloy was cast as starting point. This alloy contains 2 % of Zn, because higher amounts than 3 % of Zn does not achieve a great improvement on corrosion resistance [Hua10, Yin08]. It also contains 0.2 % of Mn because it improves magnesiun corrosion resistance [Gu09, Son05, Son07a, Xu08, Zen08] since small additions of Mn reduce the impurities in magnesium alloys increasing corrosion resistance [Ave99, Son05].

In order to analyse the influence of alloying elements, ZM20 alloy was modified adding Y to achieve the alloy named as ZWM200 and Ca to achieve the one named as ZXM200. In the case of the Y, the amount used was small (0.5 wt%) in order to avoid the possible negative effects. A 0.5 % of Y achieve a Zn/Y atom ratio of 6. This permits the formation of I-phase (Mg_3YZn_6) [Gua11, Mor09, Wan10b, Zha08], which improves the corrosion resistance of the alloy [Gua11, Wan10b, Zha08]. Regarding the ZXM200 alloy, 0.25 % of Ca was added because the highest corrosion resistance for magnesium alloys with a 2 % of Zn is achieved with 0.2-0.3 % of Ca [Gua11]. Furthermore, a similar concentration is used in other works [Gao11a, Gao11b, Gua11, Li11c].

As in Chapter 6, the corrosion evaluation of coated and uncoated alloys was carried out measuring the hydrogen generation in PBS solution. The effect of the fluoride treatment in crystal adhesion was also evaluated. Finally, a cell culture with the MG-63 cell line was carried out to analyse the cell viability of the fluoride treatment.

7.1 Sample preparation

Before applying the fluoride treatment, 10 × 10 × 1.5 mm^3 samples of each alloy (ZM20, ZWM200 and ZXM200) were ground with SiC papers from 1000 grits to 4000 grits, ultrasonically rinsed in ethanol for 15 minutes and finally dried (as in Chapter 5 and Chapter 6). In this case, the fluoride treatment of 72 hours was applied to the samples because samples with this treatment showed higher corrosion resistance than those with 24 hours of treatment, as it is shown in Chapter 6. Finally, treated samples were ultrasonically rinsed in ethanol for 15 minutes and dried. 6 repetitions were prepared for each material and surface treatment. The chemical compositions of the cast alloys measured via spark emission spectrum analysis and XRF for Ca are shown in table 7.1.

7.2 Fluoride treatment

After fluoride treatment, a stable film was formed on all the samples (figure 7.1). ZM20 alloy presented a uniform film of 2.4 μm thickness after 72 hours immersed in

Table 7.1: Composition of the alloys (wt%)

ZM20					
Al %	0.0100	Cu %	0.00226	**Mn %**	**0.259**
Fe %	0.00315	Ni %	0.00107	**Zn %**	**1.88**
Be %	0.00004	Si %	0.0252	Ag %	<0.00010
Ca %	0.00124	Sn %	<0.00050	Zr %	<0.00060
Ce %	0.00150	La %	<0.00020	**Mg %**	**97.82**
ZWM200					
Ag %	0.00116	Al %	0.0215	Ca %	0.00489
Ce %	0.00256	Cu %	0.00239	Fe %	0.00136
La %	0.00130	**Mn %**	**0.238**	Nd %	0.00600
Ni %	0.00040	Pb %	<0.00040	Pr %	0.00028
Si %	0.0123	Sn %	0.00348	Th %	0.0415
Zn %	**1.97**	Ti %	0.00143	**Y %**	**0.532**
Mg %	**97.16**				
ZXM200					
Al %	0.0165	Cu %	0.00196	**Mn %**	**0.220**
Fe %	0.00542	Ni %	0.00188	**Zn %**	**1.88**
Be %	0.000035	Si %	0.0239	Ag %	<0.00010
Ca %	**0.20**	Sn %	<0.00050	Zr %	<0.00060
Ce %	0.00231	La %	<0.00020	**Mg %**	**97.72**

HF (hereinafter this sample will named as ZM20HF72h) (figure 7.1a). After 72 hours immersed in HF, ZWM200 alloy presented a uniform film of 2.7 µm (hereinafter this sample will named as ZWM200HF72h) (figure 7.1b). Finally, the film on ZXM200 alloy grows up to 2.3 µm after 72 hours (hereinafter this sample will named as ZXM200HF72h) (figure 7.1c).

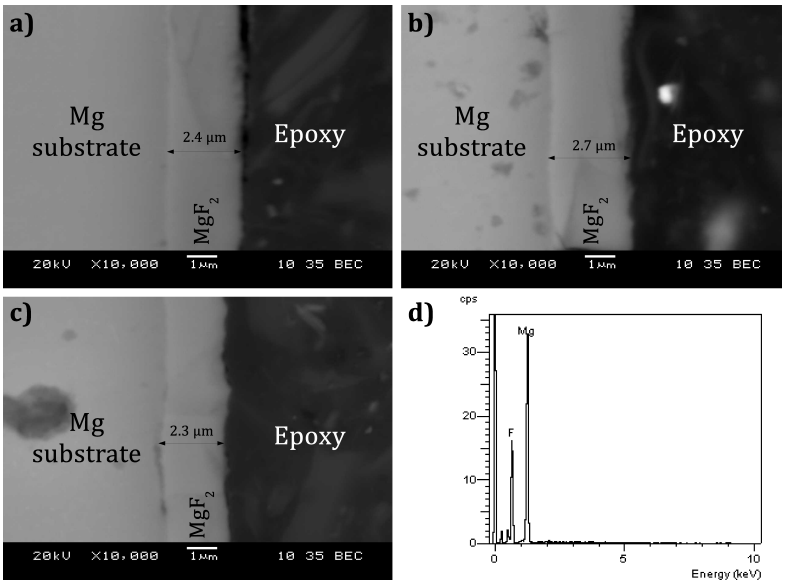

Figure 7.1: Coating on magnesium samples a) ZM20HF72h b) ZWM200HF72h c) ZXM200HF72h d) elemental analysis of the formed layer on ZM20 alloy

Figure 7.1d shows the elemental analysis of the layer on the sample ZM20HF72h after the immersion in HF determined by EDX. As expected, the layer was rich in Mg and F indicating MgF_2 generation. The other alloys presented a similar composition.

It must be pointed out that, as it is shown in figure 7.2, cracks were found on the layer of all Mg-Zn samples (ZM20, ZWM200, ZXM200). The presence of cracks on MgF_2 coating is also mentioned by Seitz *et al.* [Sei11]. The authors speculate that cracks may appear due to the brittleness of the coating [Sei11], and could be driven by residual stresses between the coating and the substrate.

7.3 Immersion tests

All samples degraded (*i.e.*, interacted chemically with the medium, releasing hydrogen) during the immersion tests. Figure 7.3 shows the hydrogen evolution of the alloys during testing (figure 7.3a), and also their corrosion rate (figure 7.3b) in order to get a better evaluation of the corrosion behaviour due to pH changes. ZXM200 bare alloy had the highest hydrogen generation (0.023 ml/mm^2 after 96 hours in PBS), followed

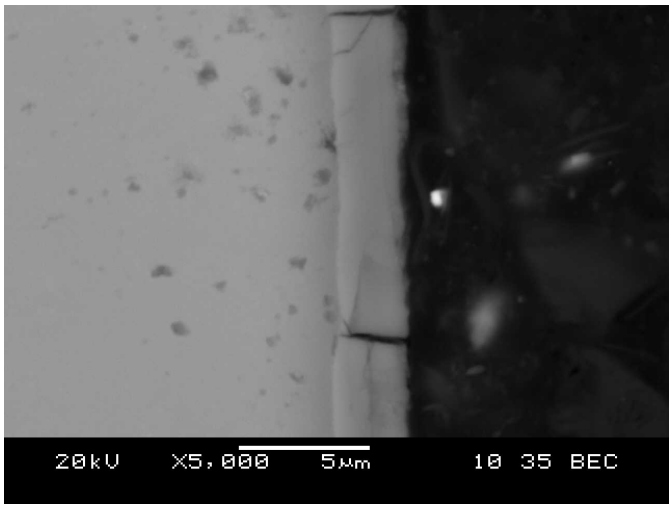

Figure 7.2: Detail of cracks on the coating of ZWM200 sample after 72 hours in HF

by ZM20 (0.0156 ml/mm^2 after 96 hours in PBS) and ZWM200 (0.0139 ml/mm^2 after 96 hours in PBS). Compared with WE43 (0.0093 ml/mm^2 after 96 hours in PBS), uncoated Mg-Zn alloys presented a higher hydrogen evolution. ZXM200 alloy presented a significant increase of corrosion rate at the end of the experiment.

The first three days of immersion for the three developed alloys in untreated form resulted in similar quantities of hydrogen generation. After an immersion test of 96 hours in PBS, ZM20 and ZWM200 bare alloys presented a corrosion rate of 0.800 mm year^{-1} and 0.715 mm year^{-1} respectively. However, the corrosion rate of ZXM200 bare alloy increased dramatically after the first 48 hours to 1.118 mm year^{-1} after 96 hours. WE43 alloy in the untreated condition presented a lower corrosion rate than any of the Mg-Zn alloys (0.47 mm year^{-1} after 96 hours).

Higher corrosion resistance was achieved for all the alloys after fluoride treatment. Compared with bare alloys, the immersion of the samples in HF for 72 hours increased the corrosion resistance by 50 % for ZM20, 71 % for ZWM200 and 74 % for ZXM200. In the case of the reference WE43 alloy, the increase in corrosion resistance was of 50 %. ZWM200 with fluoride treatment showed the lowest hydrogen generation (0.0041 ml/mm^2 after 96 hours in PBS).

This positive influence of the fluoride treatment on the corrosion rate of magnesium is in agreement with previous works [Con11, Car11a, Per10, Per11, Wit10a, Yan10]. In the experiments reported here, coated ZWM200 and ZXM200 alloys presented a similar corrosion rate compared with coated WE43 alloy. Even the ZWM200 alloy showed a corrosion rate lower than WE43.

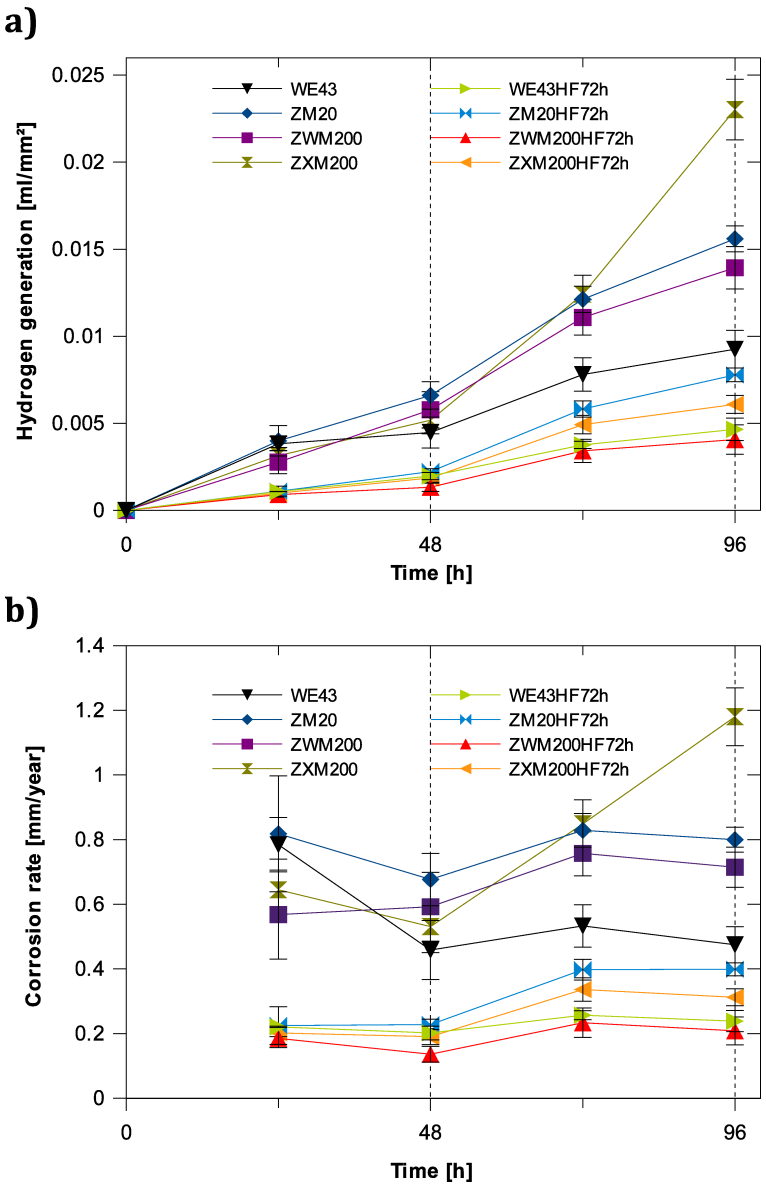

Figure 7.3: Immersion test in PBS: a) hydrogen evolution b) corrosion rate

In contrast with bare alloys, the corrosion rate increased slightly over immersion time for coated alloys. This is likely to be due to magnesium fluoride film dissolution (figure 7.3). It was also observed that fluoride treatment led the alloys to show less dispersion from sample to sample in the results (figure 7.3). The pH variations were not large (table 7.2). However, the corrosion rate in the samples did show a slight change, most likely due to these pH variations (figure 7.3).

Table 7.2: pH variation in the immersion test

sample	0 h	24 h	48 h	medium change	72 h	96 h
ZM20	**7.4**	7.66	7.9	**7.4**	7.67	7.97
ZM20 HF	**7.4**	7.48	7.6	**7.4**	7.68	7.8
ZWM200	**7.4**	7.58	7.81	**7.4**	7.69	7.95
ZWM200 HF	**7.4**	7.5	7.54	**7.4**	7.6	7.73
ZXM200	**7.4**	7.6	7.82	**7.4**	7.75	8.08
ZXM200 HF	**7.4**	7.5	7.52	**7.4**	7.6	7.65

7.4 Characterisation of the corrosion surface

The morphological features of the surfaces of the samples after immersion in PBS for 72 hours are shown in figure 7.4. Small deposits could be observed on the ZM20 alloy (figure 7.4a) after 72 hours in PBS. These deposited formations are shown in figure 7.5 in more detail. The EDX distribution map shows that these deposits are rich mainly in P and O. The highest adhesion of such precipitates was observed on the ZWM200 alloy (figure 7.4c), where needle-like deposits were found. As shown in figure 7.6, the needle-like deposits are rich in K, P and O. Finally, on the ZXM200 alloy sample, needle-like deposits were also observed (figure 7.4e) together with conical formations rich in Mg, O and some C around the intermetallics (figure 7.7). Fluoride treatment reduced the depositions of crystals on the surface in all cases (figures 7.4b, 7.4d, 7.4f).

In order to identify the corrosion mechanisms, the early stages of the corrosion process have also been analysed. Figure 7.8 shows the corrosion on the surface of a ZXM200 bare alloy sample after 24 hours in PBS. The figure shows the presence of a corroded area with cracks rich in Mg, O and P, and another non-corroded area rich in Mg where grinding lines from the original preparation of the sample are still present. A similar corrosion behaviour was found for the other bare alloys.

Concerning the species found on the sample surfaces, the elemental analysis suggests that different phosphates $(PO_4)^{3-}$ with Mg, Ca, K or Na were deposited on the corroded surface. Depositions or corrosion products containing $(PO_4)^{3-}$ were also detected by other researchers [Zha10, Alv10, Tie10]. Xin *et al.* [Xin11b] postulate that HPO_4^{2-} from

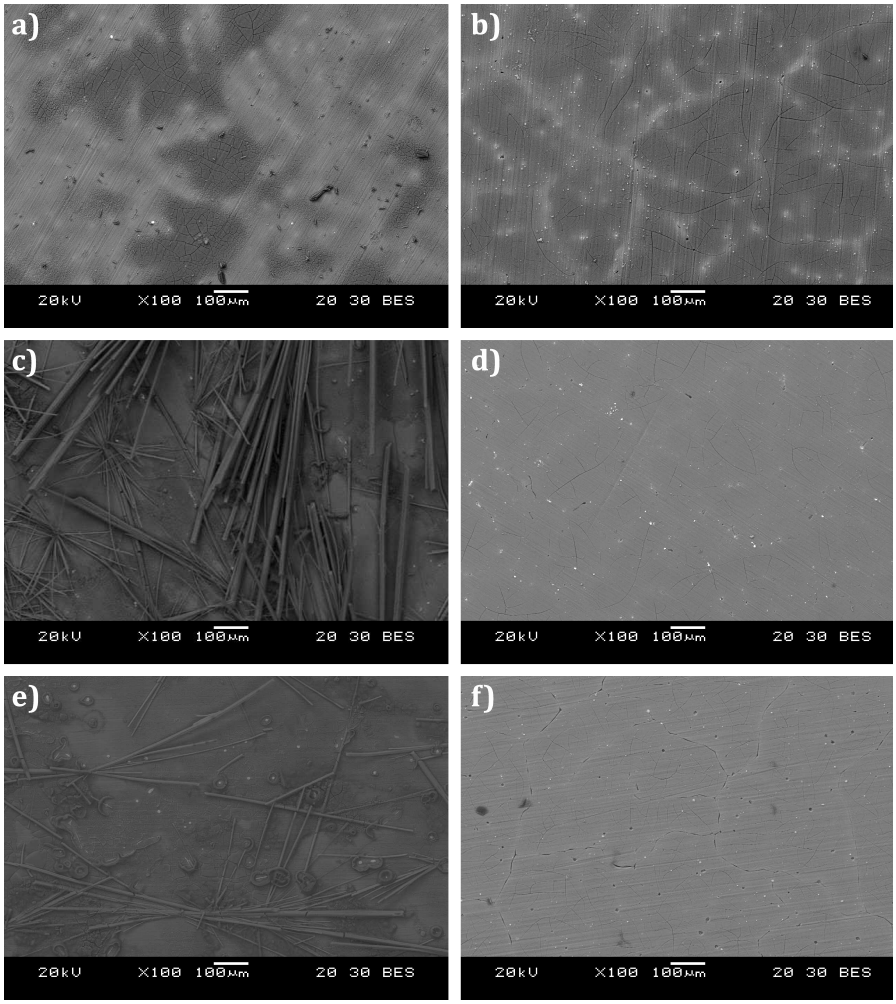

Figure 7.4: Sample surfaces after 72 h in PBS: a) ZM20 b) ZM20HF72h c) ZWM200 d) ZWM200HF72h e) ZXM200 f) ZXM200HF72h

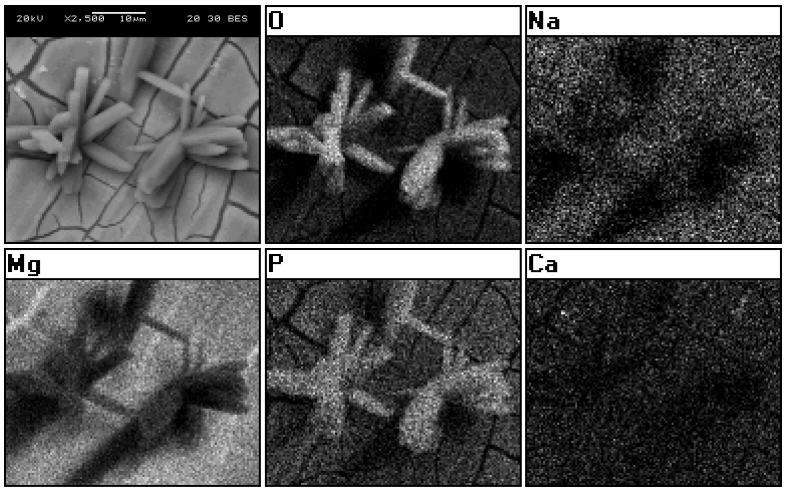

Figure 7.5: Element mapping of O, Mg, P, Na and Ca on the ZM20 bare alloy sample after 72 hours in PBS

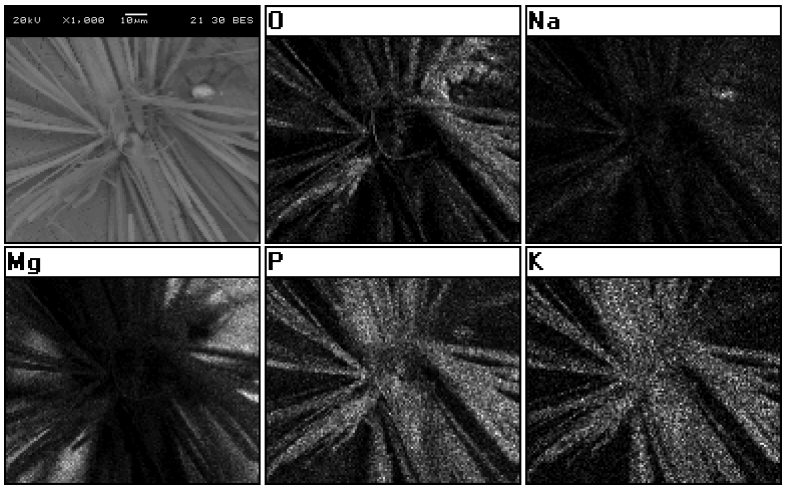

Figure 7.6: Element mapping of O, Mg, P, Na and K on the ZWM200 bare alloy sample after 72 hours in PBS

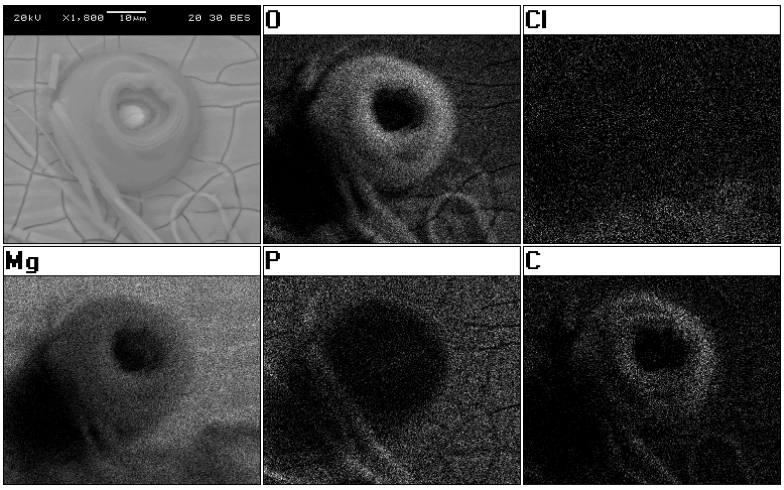

Figure 7.7: Element mapping of O, Mg, P, C and Cl on the ZXM200 bare alloy sample after 72 hours in PBS. Formation around a intermetallic

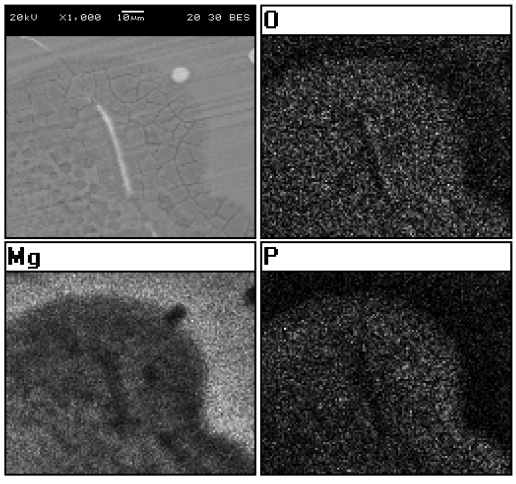

Figure 7.8: Element mapping of O, Mg, P and Cl on the ZXM200 bare alloy sample after 24 hours in PBS

the test solution could react with OH^-, which is generated due to magnesium corrosion. This fact induces the precipitation of phosphates. Finally, some $(CO_3)^{2-}$ particles (figure 7.7) were also detected around the intermetallics on the ZXM200 alloy. The presence of carbonate is common after the immersion of magnesium in physiological medium [Tie10, Jam11, Qu11]. However, in this work, there were few carbonates identified because the PBS does not contain any. The presence of the observed carbonates could be explained due to the reaction of distilled water with the CO_2 of the atmosphere. In the same way, although PBS does not contain Ca, the elemental analysis detected small amounts of Ca. In this case, it may be found as an impurity in PBS.

Regarding the corrosion of coated alloys, figure 7.9 shows the early stages of the corrosion process on the ZXM200 alloy sample with a fluoride treatment of 72 hours. After MgF_2 dissolution, the area affected was rich in Cl and O. The influence of P was also detected on the sample. Coated ZWM200 and ZXM200 alloys presented a similar behaviour. The presence of Cl^- could cause the dissolution of the MgF_2 layer [Yan10]. After this dissolution, the unprotected magnesium begins to corrode and possibly forms a mixture of $MgCl_2$ and $Mg(OH)_2$. As corrosion is continuous, $(PO_4)^{3-}$ would precipitate in a second step.

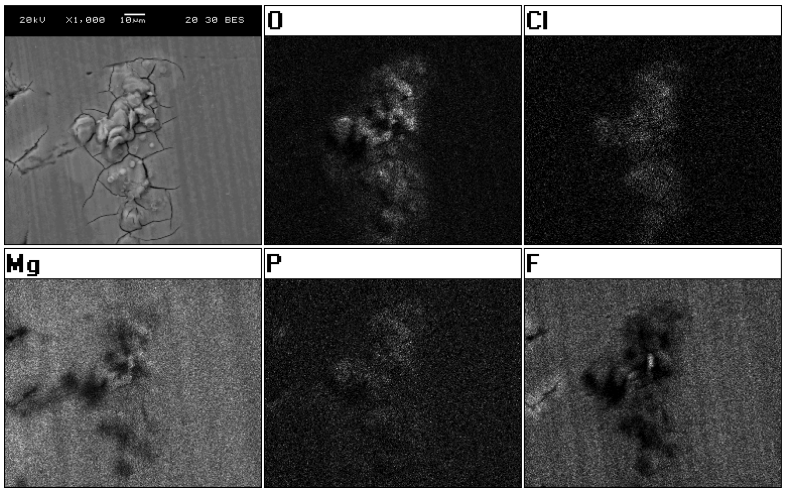

Figure 7.9: Element mapping of O, Mg, P, Cl and F on the ZXM200HF72h sample after 24 hours in PBS

7.5 Cell viability

Figure 7.10 shows the mean values of the cell viability results from the samples of the coated and uncoated alloys, compared with WE43 alloy and Ti-6Al-4V for direct cell assay using MG-63 cells. The alloys with fluoride treatment showed higher cell viability than bare alloys in all cases. It should also be noted that ZWM200HF72h and ZXM200HF72h samples achieved the same cell viability as the Ti alloy samples after 14 days.

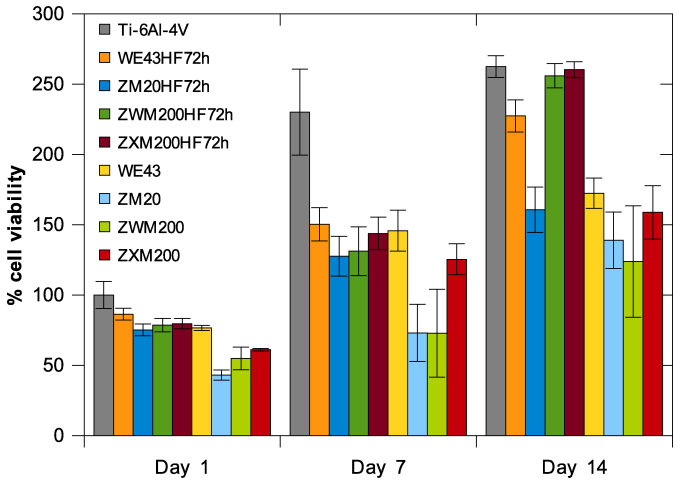

Figure 7.10: Cell viability after 14 days of MG-63 cells cultured directly on magnesium alloys and coated magnesium alloy samples

The MgF_2 coating had a positive effect on cell viability. The low corrosion rate and surface stability at the beginning of the cell culture experiments due to the presence of the coating may be the reason that seeding efficiency increased in all examined alloys. The coated samples presented a cell viability higher than bare alloys in all cases during cell culture tests. After 14 days of cell culture, the coated ZWM200 and coated ZXM200 alloys presented a cell viability close to the titanium alloy and even higher than the coated WE43 alloy, indicating that these materials could have potential as an implantable material as the titanium alloy is already used in such medical applications.

In the case of uncoated alloys, a similar cell viability was found among the different alloys after 14 days of cell culture. However, after 7 days higher cell viability was found in ZXM200 and WE43 alloys. In all cases the cell viability was smaller than the correspondent coated alloy.

Figure 7.11 shows the morphologies of MG-63 cells cultured on the samples. A higher number of cells were observed in coated alloys than in bare alloys after 14 days of culture. This effect is clearly shown in figure 7.11e, where cells with an elongated cell morphology nearly forming a monolayer are shown on ZWM200HF72h. No data are available for

ZXM200 alloy since the cells detached during the cell fixation step. As in Chapter 5 and Chapter 6, the deposits in the cell culture were less than the deposits in the immersion test in PBS.

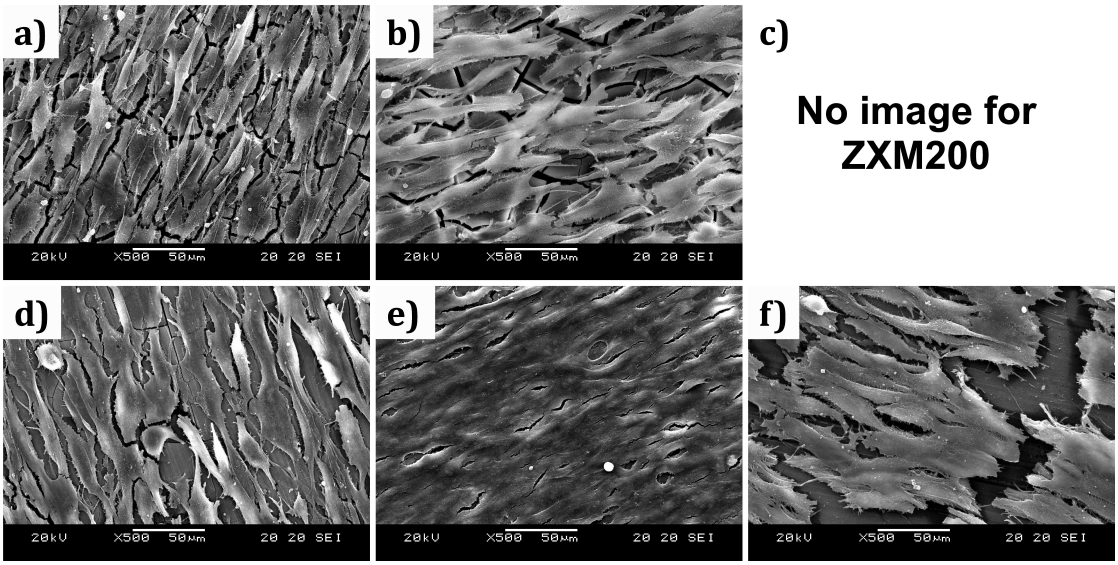

Figure 7.11: Detail of cell attachment after 14 days of cell cultures on a) ZM20 b) ZWM200 c) ZXM200 d) ZM20HF72h e) ZWM200HF72h f) ZXM200HF72h

7.6 Conclusions

The results of this chapter showed that:

- The addition of Y slightly improved the corrosion resistance of the ZM20 alloy.
- The addition of Ca decreased the corrosion resistance of the ZM20 alloy.
- Fluoride treatment improved the corrosion resistance and reduced the deposition of crystals in all the alloys.
- Fluoride treatment had a positive effect on the cell viability.
- The addition of Y and Ca to the ZM20 alloy with fluoride treatment presented higher cell viability, close to that of Ti-6Al-4V, and higher than WE43, implying that coated ZWM200 and ZXM200 alloys could be potential materials for biomedical fields.
- Corrosion rate and cell viability are not directly related. ZXM200 alloy presented a high cell viability but a low corrosion resistance.
- As in Chapter 5 and Chapter 6, the adhesion of deposits in the cell culture was lower than the adhesion of deposits in the immersion test in PBS for all the alloys.

In the next chapter, the development of scaffolds made of these new alloys is shown.

Chapter 8

Development of magnesium scaffolds for tissue engineering

In the present chapter, replication casting process [Con06, Goo13] to manufacture magnesium alloys scaffolds was analysed. Three-dimensional and open porous structures are desired when manufacturing the scaffolds in order to improve the cellular migration, the ingrowth of the new tissue, the transport of body fluid and the vascularization through the material [Wen01, Hu02, Lu07a, Wen07, Wit07b, Wit07a, Wu07, Yos03]. Several porosities and pore sizes have been used in the literature with porosities around 70 % being the most common ones [Hu02, Lu07a, Wen07, Wit07b, Wit07a, Wu07, Yos03] and the most used pore size being in the range of 100 to 500 μm [Hu02, Lu07a, Wen07, Wu07, Yos03].

Based on these advantages, magnesium foams have been already analysed in the literature for tissue regeneration [Wit07b, Wit07a]. However, the fabrication of magnesium foams has not been widely studied and the process parameters necessary to obtain the desired porosities and pore sizes are not yet well known [Bac05, Bac03, Wen00, Yam99].

For this reason, the main objective of the present chapter is to define the optimal process parameters for the fabrication of magnesium foams. The manufacturing of magnesium scaffolds was carried out at The University of Sheffield in collaboration with Dr. Russell Goodall's group. The set up of the process was carried out with AZ91E magnesium alloy. After the set up, magnesium scaffolds were manufactured using WE43 and the alloys developed in Chapter 7. Finally, fluoride treatment was applied to the developed scaffolds and corrosion tests in PBS were carried out.

8.1 Infiltration casting process definition

In this section, a set up of the replication casting technology for magnesium alloys was carried out. AZ91E alloy, which is commonly used alloy in casting technology due to its castability, was used for this set up. Later, magnesium scaffolds for WE43 and the cast alloys in Chapter 7 were manufactured with different process parameters. The porosity and the mechanical properties (yield strength) of the magnesium foams were characterised. As a final result, the replication casting process window for the analysed magnesium alloys was defined. Finally, the developed scaffolds were coated with MgF_2 and their corrosion behaviour in PBS was analysed.

The process for manufacturing the scaffolds was explained in section 3.5. This process consists in the infiltration of melted magnesium into a negative mould of salt. Optimal infiltration casting process parameters were defined for manufacturing foams (such as the example in figure 8.1) with AZ91E, WE43 and with the alloys developed in Chapter 7. These optimal process parameters mainly depend on the castability of each alloy and on the alloy interaction with the salt. The infiltration process for all the alloys started from 0.5 bar and the pressure was raised to 3 bar over 2 minutes. Then the pressure was increased until the corresponding infiltration pressure was achieved, which was maintained until the melt was solidified (pressure-time profiles are shown in figure 8.2).

Figure 8.1: Sample of AZ91E foam

The infiltration pressures varied between 4 bar and 6 bar for all the alloys. Lower pressures than 4 bar were not high enough to infiltrate the magnesium through the salt and higher pressures than 6 bar were found to compress the upper region of the salt preform rather than causing infiltration, creating a compact layer between the magnesium and the salt preform that was not penetrable (figure 8.3).

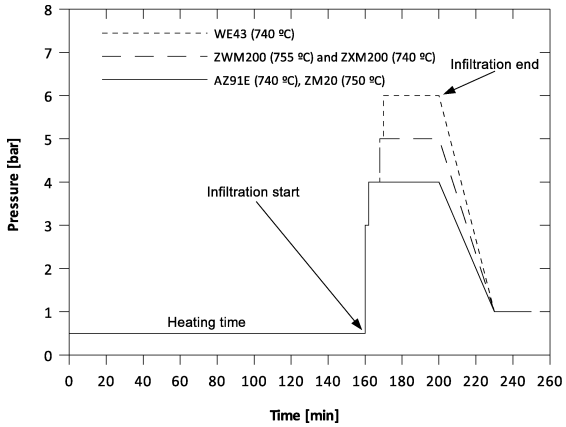

Figure 8.2: Optimal infiltration pressures for maximizing the porosity while obtaining uniform infiltration in each alloy

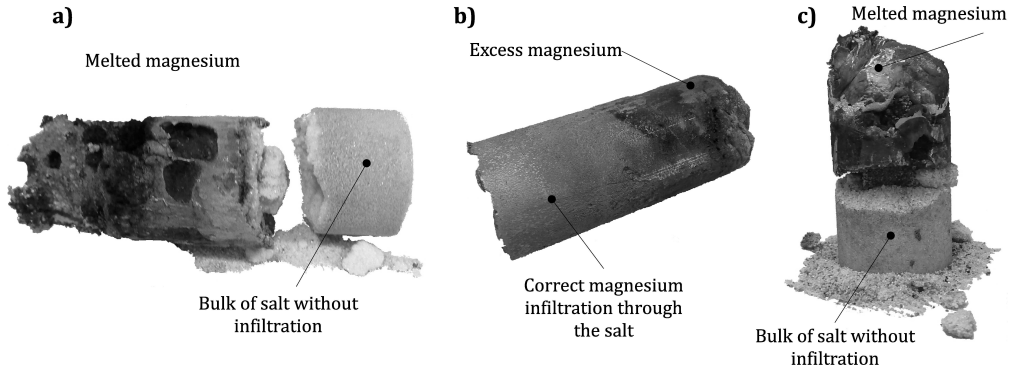

Figure 8.3: AZ91E foams manufactured varying infiltration pressure. a) no-infiltration under a pressure of 3 bar b) acceptable foam with infiltration pressure of 4 bar c) no-infiltration due to preform compaction under a pressure of 8 bar

In terms of process pressure, three different behaviours were observed during the study. AZ91E and ZM20 magnesium alloys needed the lowest infiltration pressure for achieving sound scaffolds. For both alloys an optimal infiltration pressure of 4 bar was defined. In the case of the novel ZXM200 and ZWM200 magnesium alloys, a slightly higher pressure of 5 bar was needed. Finally, the WE43 commercial alloy needed the highest pressure of all the alloys examined in this study, 6 bar.

In terms of required process temperature, two different groups were observed. AZ91E, WE43 and ZXM200 needed a temperature of 740 °C to achieve uniform infiltration and the required porous structures. On the other hand, ZM20 and ZWM200 alloys required higher temperatures in order to improve their fluidity and infiltrate them through the salt, 750 °C for ZM20 and 755 °C for ZWM200.

Different parameters, that yield foams with structures suitable for scaffolds, are shown in figure 8.4. According to this work, overall the parameters are a temperature between 740 °C and 755 °C and an infiltration pressure between 4 and 6 bar.

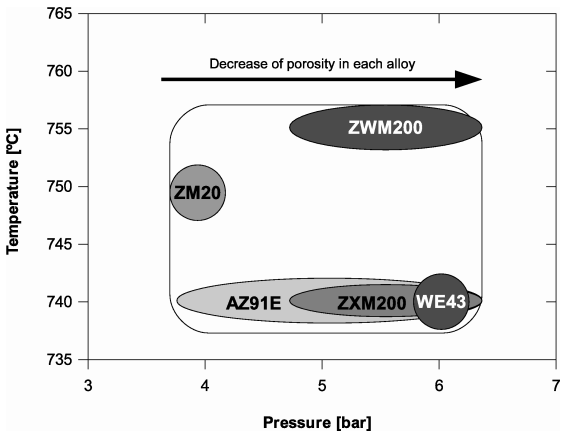

Figure 8.4: Process window for the different magnesium alloys examined to produce foams with suitable structures

A particular feature of applying the replication process to magnesium alloys is, as mentioned above, the need to maintain a gas pressure over the melt to reduce evaporation of the metal into the system. Unlike other examples of the replication process (as described in [Con06]), the system is not under vacuum when the metal melts, and some gas will be trapped inside the preform (this is part of the reason why relatively high gas pressures are needed to infiltrate the foams, even though the pore size is not small compared to what can be achieved with this technique). It was found in this work that the infiltration pressure must be maintained until complete solidification of the foam has taken place. If this does not happen, the trapped gas expands and starts bubbling through the porous structure causing large defects as shown in figure 8.5.

8.2 Porosity

The porosity of the samples was measured according to section 3.6. The porosity obtained for each alloy is given in table 8.1. The lowest porosity was achieved for ZWM200 and ZXM200 alloys (30 % at 6 bar infiltration pressure) and the highest porosity was achieved for ZWM200 alloy (69 % at 5 bar infiltration pressure). For

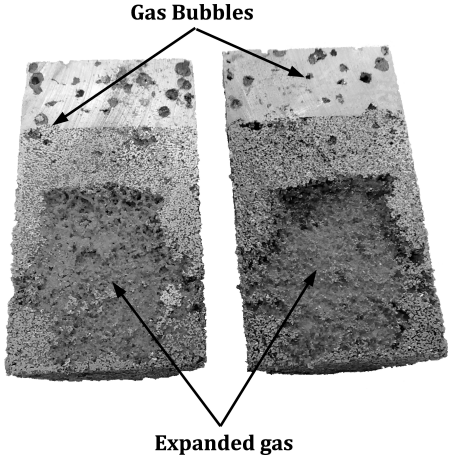

Figure 8.5: Section of an AZ91E foam that was depressurized before solidification. Defects due to gas expansion and gas bubbling are shown

replication into a compacted preform, the preform density will closely define the foam porosity [Con06]. In the experiments described here, loose packing of salt will give a consistent, but relatively low, fraction of space filled, and to obtain higher porosities the fraction of the available free space that is filled must be controlled by precise selection of the infiltration conditions. The main factors influencing the porosity are the fluidity of each alloy and the infiltration casting process parameters used during infiltration. Through the present research, a range of porosities have been obtained depending on the alloy and on the manufacturing parameters, as it is shown in table 8.1.

One of the key controllable parameters influencing the achievable porosity is the infiltration pressure. As an example, figure 8.6 shows the structures achieved for the ZWM200 alloy at an infiltration pressure of 6 bar and at an infiltration pressure of 5 bar, showing that as the pressure increases the amount of metal increases and the pores are more closed off from each other. The porosity achieved at an infiltration pressure of 5 bar was 69 %, while at an infiltration pressure of 6 bar it was only 30 %. It can be noted the great effect that the infiltration pressure has in the foam porosity (at least for this alloy). However, the effect of the infiltration pressure is barely detected in the AZ91E alloy which presented a similar porosity for infiltration pressures of 4 and 6 bar (figure 8.7). It should be further noted that the lowest porosities of only 30 % are very low, well below what is typically expected of a foam. A possible explanation for such values in the replication process would be incomplete dissolution of the salt, which can become difficult at high densities as the interpore windows become small. To attempt to avoid this, water was forced to flow through the samples to promote salt dissolution, but the possibility that a small quantity of NaCl could be trapped in the highest density structures remains, reducing the apparent porosity values by a small amount.

Table 8.1: Porosity, Young's modulus and Yield Stress of the magnesium alloy foams

Magnesium alloy	Infiltration temperature [°C]	Infiltration pressure [bar]	Porosity	Yield Stress [MPa]
AZ91E	740	4	68 %	3.62 (±1.16)
	740	6	67 %	3.12 (±0.75)
WE43	740	6	39 %	8.67 (±0.78)
ZM20	750	4	43 %	3.48 (±0.43)
ZWM200	755	5	69 %	2.31 (±0.41)
	755	6	30 %	12.15 (±2.45)
ZXM200	740	5	44 %	8.66 (-)
	740	6	30 %	9.19 (±3.15)

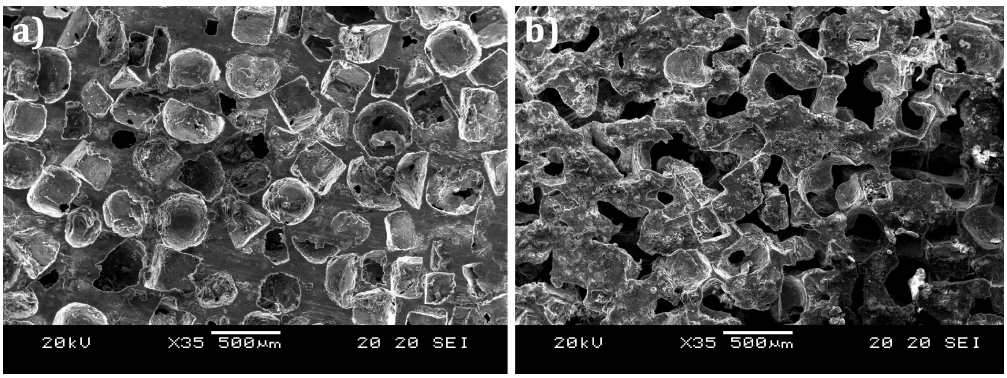

Figure 8.6: Structures of ZWM200 foams with an infiltration pressure of a) 6 bar (30 %), and b) 5 bar (69 %)

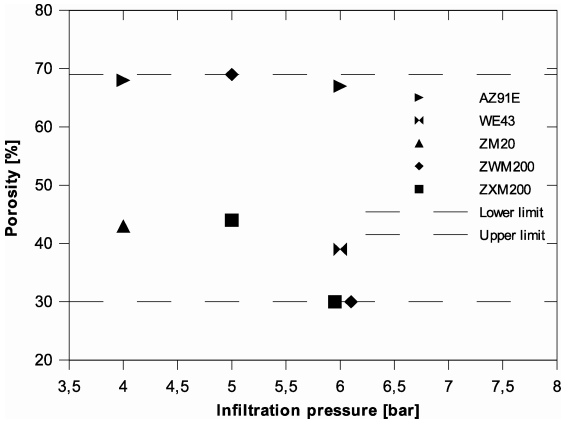

Figure 8.7: Upper and lower limits of the achieved porosities for each alloy depending on the infiltration pressure

The results demonstrate that the manufacturing of magnesium foams with variable porosity through this route is possible, although there will be a lower limit, reached when the porosity decreases dramatically and the pores tend towards becoming closed. For the concerns above relating to the possibility of trapped salt within such structures, and the fact that nearly isolated pores would not be recommended for the growth and proliferation of cells in the foam, scaffolds with a porosity percentage inferior to 40 % are not considered suitable candidates for the current application.

8.3 Mechanical properties

The influence of the process parameters on the mechanical properties of the foams was also analysed in the present work. It must be noted that the mechanical properties of the foams are directly related to the porosity achieved within them. Therefore, a direct relation between the process parameters (particularly the infiltration pressure) with the porosity and the mechanical properties has been observed.

The samples were machined to 6 mm in diameter and 6 mm in height. Three repetitions were prepared for each material. Compression tests for all the magnesium alloy foams manufactured under different process parameters were performed (obtaining typical compressive stress-strain curves shown in figure 8.8). Table 8.1 shows the mechanical properties of all the tested scaffolds. It can be seen that there is an inverse relationship between the achieved porosity in the scaffolds and their mechanical response; the higher the porosity the lower the mechanical properties found.

The effect of processing on mechanical properties is clearly shown in the case of ZWM200 alloy. This Mg alloy was processed under two different infiltration pressures at 755 °C (5 bar and 6 bar) and gave as a result very different porosities and mechanical properties. When evaluating the mechanical properties (figure 8.9), it was noticed that the yield stress of the scaffolds was 6 times bigger when processed at

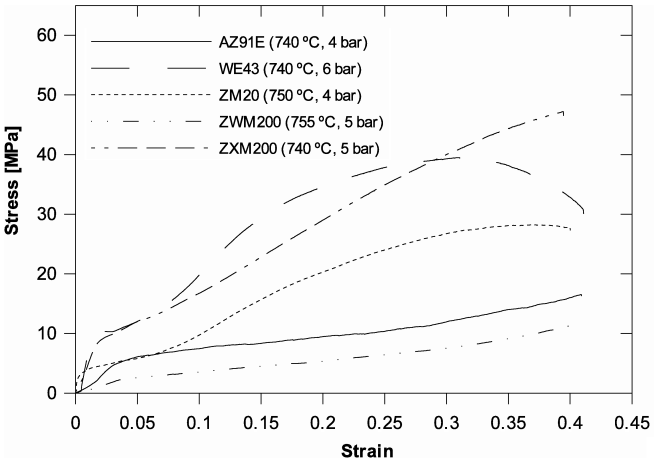

Figure 8.8: Vompressive stress-strain curves for magnesium alloy foams examined in this study (example)

the highest infiltration pressure (table 8.1). These results, which showed much bigger changes with density than the ones predicted through the Gibson-Ashby equations for foam properties [Gib97], clearly indicate the possibility to modulate the stiffness and the strength of the scaffolds over a wide range. The reason that the predictions are exceeded in this case was that the density change was so wide that the structure was likely to be altered significantly (particularly at the high density end of the range), and the foam does not deform following the same mechanism in both forms.

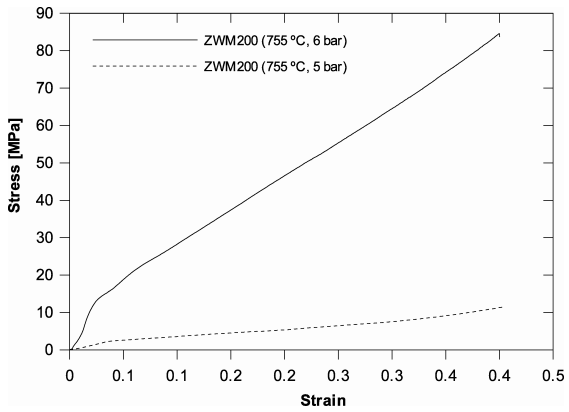

Figure 8.9: Compression stress-strain curves of the ZWM200 foams manufactured with different infiltration pressures, showing the decrease of mechanical properties of the foam with increasing porosity

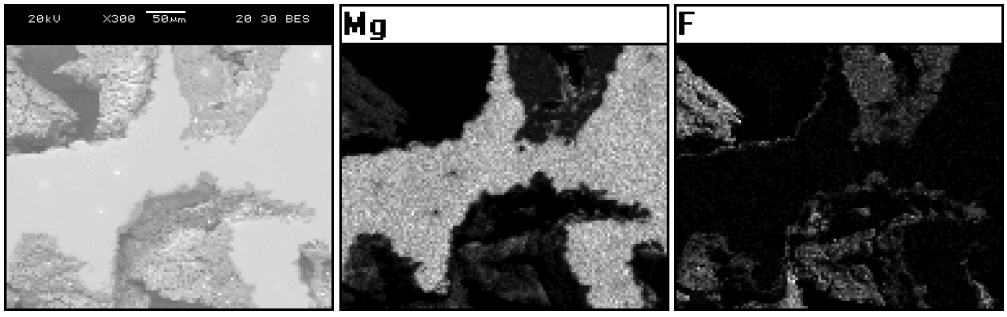

Figure 8.10: Detail of the generated MgF_2 coating inside a ZWM200 scaffold after 72 hours of immersion in HF

Another important requirement would be strength. The ultimate tensile strength of trabecular bone ranges from 1.55 to 5.33 MPa [Kea98], and that of cortical bone from 130 MPa to 205 MPa [Cur98]. The yield strength of the scaffolds manufactured in the present research work ranges from 2.13 to 12.15 MPa, comparable to the trabecular bone. As shown above, this value can of course be influenced by the foam structure, principally by the density.

8.4 Corrosion characterisation of magnesium alloy scaffolds

In order to improve the corrosion resistance of the scaffolds, a fluoride treatment of 72 hours was applied to the scaffolds (6 mm in diameter and 6 mm in height). To analyse the coating penetration inside them, several millimetres of the material were ground and then polished. Figure 8.10 shows the formation of MgF_2 on the ZWM200 alloy. The other alloys presented similar characteristics. Regarding the morphology of the coating, as it is shown in figure 8.11, the coating on the scaffolds presented more cracks and was less uniform than the coating achieved in Chapter 7. This could be due to the concave geometry of the pores, which increased the compression stress on the coating.

Regarding the corrosion, all the scaffolds degraded during the immersion tests. The hydrogen evolution of the developed scaffolds is shown in figure 8.12. The hydrogen evolution was calculated with the external area of the cylinder and not with the real area. The smallest hydrogen evolution was achieved by ZM20 foam (0.0099 ml/mm^2 after 92 hours in PBS), followed by ZWM200 with a porosity of 69 % (0.01541 ml/mm^2 after 92 hours in PBS). The highest hydrogen evolution was achieved by WE43 (0.08579 ml/mm^2 after 92 hours in PBS). The high hydrogen evolution of this scaffold was probably due to trapped NaCl particles, which increased the corrosion inside the scaffolds. It should be noted that the hydrogen generation by the other scaffolds (ZM20 43 %, ZWM200 69 %, ZXM200 30 %, ZXM200 44 %) was close or even less than the hydrogen generation of ZM21 bare alloy, which presented a hydrogen evolution of 0.0155 ml/mm^2 after 96 hours in PBS (Chapter 5 and Chapter 6). However, this comparisson could not be reliable because the data were extrapolated from a porous component to a nonporous component.

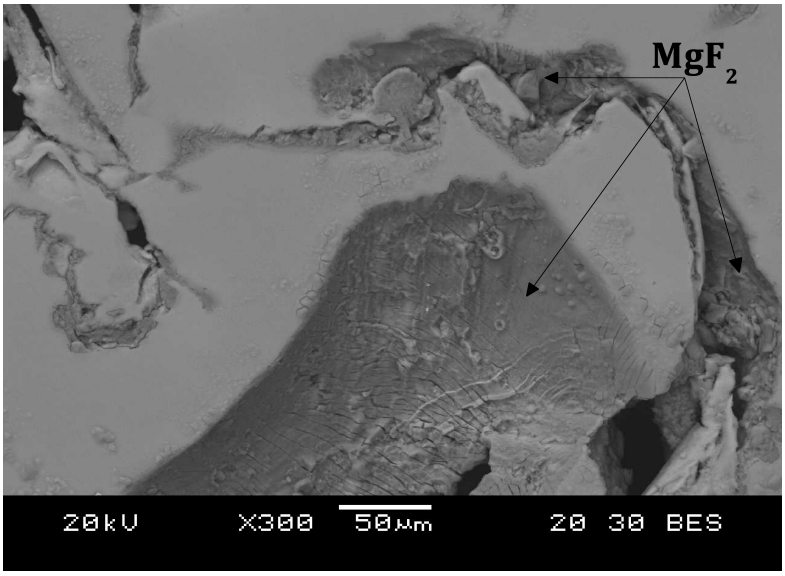

Figure 8.11: Detail of the morphology of coating on ZXM200 alloy

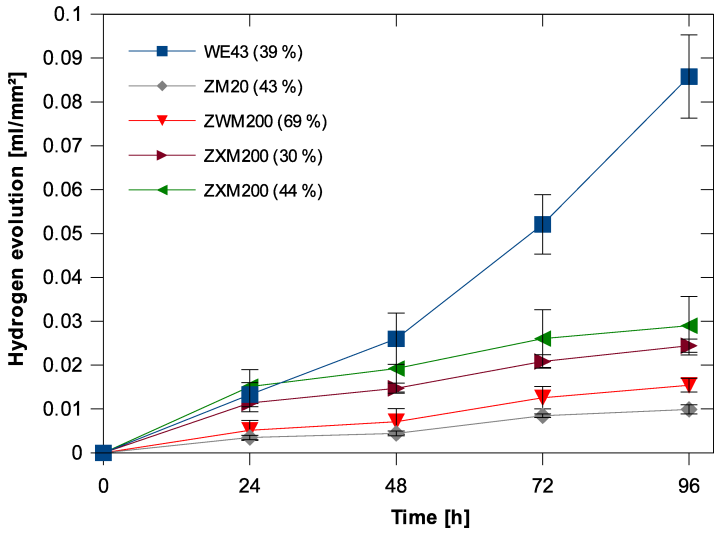

Figure 8.12: Hydrogen evolution of the coated magnesium alloys scaffolds in PBS

8.5 Conclusions

According to the results of the present chapter the following statements were concluded:

- The temperature and infiltration pressure ranges have been defined as being from 740 °C to 755 °C and from 4 to 6 bar respectively. The optimal parameters selection depend on the magnesium alloy to be infiltrated and on the desired porosity.
- The MgF_2 coating presented a good penetration inside the scaffolds. However, the generated MgF_2 coating presented cracks and non-uniform morphology due to the geometry of the scaffolds.
- Despite being high porosity structures, the scaffolds did not present a large hydrogen evolution (0.01-0.09 ml/mm^2 after 96 h of immersion in PBS, figure 8.12). This result makes them a potential application element in tissue engineering. However, more analysis are needed.

Chapter 9

Conclusions and future work

The present chapter describes the conclusions of this research work. The main objective of this work was to develop magnesium scaffolds for their use in tissue engineering. The statements concluded are listed below.

9.1 Conclusions

The main conclusion of the present work is:

- It is stated that magnesium porous scaffolds fabricated by means of replication casting technologies and made of Mg-Zn alloys treated with fluoride can be a good solution for tissue engineering applications.

In Chapter 4 cell cultures were carried out in order to identify problems besides those mentioned in the literature. The principal conclusions drawn from these experiments are:

- Besides to the identified problems of magnesium alloys in regenerative medicine (hydrogen bubbles, pH increase) [Sta06, Zen08], in this work it was also concluded that a high adhesion of crystals on the surface can stop tissue growth, creating a barrier effect. Due to crystal adhesion the samples were only partially covered by a cell layer.

- Despite the hydrogen generation and pH increase cells were able to adhere on the magnesium alloys.

In Chapter 5 and Chapter 6, the corrosion behaviour, cell viability and the influence of the fluoride treatments of AZ31B, WE43 and ZM21 magnesium alloys were also analysed in this work. The main conclusions are:

- AZ31B alloy presented a low cell viability, and it is not recommended for biological applications.
- Despite presenting the highest corrosion rate, ZM21 alloy presented a cell viability similar to WE43. This means that cell viability is not related directly with the corrosion rate. It is likely that the composition of the alloy is more important.
- Fluoride treatment increased corrosion resistance and decreased dramatically the crystal deposition on the surface.
- The decrease of the corrosion rate was directly related with the MgF_2 coating thickness for AZ31B and ZM21 alloys, being more effective when it was applied to the ZM21 alloy for 72 hours.
- Fluoride treatment encapsulated the intermetallic phases in the WE43 alloy reducing the micro-galvanic couples. The decrease of the corrosion rate was not related to the coating thickness.
- Fluoride coating was able to adequate the corrosion rate of magnesium alloys making them available for the future development of temporal implants and scaffolds. A relation between the immersion time in HF and the corrosion rate was established: the higher the immersion time was the lower the corrosion rate was.
- Fluoride treatment increased cell viability in all analysed magnesium alloys.

Taking into account the results of Chapter 4, Chapter 5 and Chapter 6, novel magnesium alloys were developed based on the Mg-Zn system. ZM20 alloy was developed and the influence of the addition of Ca and Y was analysed. The main conclusions are:

- The addition of Y improved slightly the corrosion resistance of the ZM20 alloy.
- The addition of Ca decreased the corrosion resistance of the ZM20 alloy.
- Fluoride treatment improved the corrosion resistance and reduced the adhesion of crystals in all the alloys.
- The addition of Ca or Y did not achieve an increase in the cell viability of the ZM20 alloy.
- Fluoride treatment had a positive effect in the cell viability.
- The ZM20 alloy with additions of Y and Ca and with fluoride treatment presented a cell viability close to that of Ti-6Al-4V, and higher than WE43, implying that coated ZWM200 and ZXM200 alloys can be potential materials for biomedical fields.

Finally, in Chapter 8, magnesium scaffolds were manufactured with the alloys developed in this thesis. Replication casting was used to manufacture the scaffolds. The principal conclusions are listed below.

- Successful scaffolds with required porosity and pore sizes have been achieved.
- The temperature and infiltration pressure ranges were defined as being from 740 °C to 755 °C and from 4 to 6 bar respectively.
- The MgF_2 coating presented a good penetration inside the scaffolds. However, due to the geometry of the scaffolds the generated MgF_2 coating presented cracks and a non uniform morphology.
- Despite being high porosity structures, the scaffolds did not present a large hydrogen evolution during the corrosion test in PBS. This result makes them a potential application element in tissue engineering.

9.2 Future work

This dissertation has demonstrated that magnesium scaffolds with a not large hydrogen generation can be achieved. However, further research work is suggested in order to completely optimize and understand some open questions outlined in this work.

According to the new developed materials, it would be interesting to characterise them beyond their as-cast condition. Taking into account their possible application as screws or plates, the material could be extruded and heat-treated in T4 and T6 conditions. Finally, a corrosion and biological characterisation should be carried out.

In order to analyse more deeply the effect of the fluoride coating more experiments are needed. Fluoride treatment with different immersion time should be carried out in order to achieve the thickest MgF_2 layer optimizing the fluoride treatment time for each alloy. Longer corrosion tests should be carried out in order to analyse the complete dissolution of the MgF_2 coating.

Regarding the crystal deposition, it was concluded that in the cell viability tests less crystals were deposited on the samples. This is likely due to the corrosion medium or even due to the cell activity. In order to analyse the effect of the cell adhesion in corrosion, hydrogen evolution test during cell cultures should be carried out. In the same way, XPS techniques should be used to achieve a better identification of the deposited crystals.

According to the scaffold manufacturing process, residual NaCl in the scaffolds can accelerate the corrosion of the foam. For this reason, it is recommended the use of microtomography techniques to ensure the absence of residual NaCl before the implantation of the foams.

Taking into account the cell viability results, new cell viability tests with human osteoblast should be the next step of this research work. In this case, the test should be carried out with coated and uncoated ZWM200 and ZXM200 alloys because these alloys presented the best cell viability. Finally, *in vivo* tests should be carried out with the developed scaffolds in order to analyse inflammatory responses, hydrogen generation and absorption, magnesium degradation and tissue regeneration.

Acknowledgements - Eskerrak - Agradecimientos

Lau urte t'erdi baino gehiago pasatu dira tesi hau hasi nuenetik eta hitz hauen bidez denbora honetan lagundu didatenei eskerrak eman nahi dizkiet. Lehenengo eta behin, eskerrak eman nahi nizkieke nire tesi zuzendariei, Eneko Sáenz de Argandoña doktoreari eta Gurutze Arruebarrena doktoreari, tesian zehar emandako aholkuengatik eta gidaritzagatik. Mondragon Unibertsitateko Mekanika eta Ekoizpen Industriala sailari eta bere koordinatzaileari, Angel Orunari eta batez ere Materialak Eraldatzeko Prozesu Aurreratuen ikerketa taldea eskertu nahiko nuke, urte hauetan taldearen koordinatzaile izan direnei, Iñaki Hurtado doktoreari eta Zigor Azpilgain doktoreari, tesi hau egiteko aukera emateagatik.

. . . . . .

I would like to thank Dr. Dietmar Letzig and Dr. Joachim Wendt from MagIC at Helmholtz-Zentrum Geesthach for their support in material development.

I would also like to thank Dr. Gwendolen Reilly and William van Grunsven from the University of Sheffield for their support, advise and help in the MG-63 cell cultures. To Dr. Russell Goodall for his contribution and guide in the scaffold development.

. . . . . .

También me gustaría agradecer a la Dra. Ana Conde, Dra. María Ángeles Arenas y al Dr. Ignacio Manuel García del Grupo de Corrosión y Protección de Materiales Metálicos del CENIM, por sus consejos en los ensayos de corrosión.

A la Dra. Clara Isabel Rodríguez y a Garbiñe Ruiz de Eguino del Grupo de Células Madre y Terapia Celular del Hospital de Cruces, por su ayuda y colaboración en los ensayos iniciales de esta tesis. Porque con ellas empecé a entender algo del mundo de la biología.

. . . . . .

Mondragon Uniberstitateko Azalen Teknologiak ikerketa taldeari, batez ere, Wilson Tato doktoreari eta Andrea Aginagalde doktoreari, eskainitako laguntzagatik.

Xabier Gómez doktoreari eta Larraitzi, nire laborategiko entseguetan laguntzeagatik eta bere aholkuengatik. Tailerreko teknikariei, Gotzon, Arkaitz, Iñaki eta Mikel, nire laginak eta prototipoak egiten tailerrean laguntzeagatik.

Nirekin bekadun izan diren ikasle guztiei ere eskertu nahi diet eskainitako laguntzarengatik: Iñigo, Ainara, Eneko eta Julen.

. . . . . .

También le doy gracias a mi madre, Antonia. Le doy gracias por todo lo que me ha dado y por todo lo que me ha aguantado los últimos cuatro años y pico. Aunque nunca tuvo muy claro lo que estaba haciendo. Por ello, esta tesis también va dedicada a ella. También agradecer y dedicar esta tesis a mi padre que siempre me apoyó y me ayudó mientras pudo.

. . . . . .

Agradecer también (¿cómo no?) a toda la gente que ha pasado por Fabri 2 (y por su posterior ubicación) durante estos 4 años y pico. Por ayudarme y compartir risas, desahogos y dolores de cabeza (normalmente provocados por mí). Haciendo el mal... (ya sabéis). A Jokin ("El Grande") por darme a probar burrito. Por sus historias sobre Otxandio y su fauna. Por ser vizcaíno y proteger nuestra frontera con Gipuzkoa. A Joanes por aguantar mis excentricidades, "click-click" (un subrayador puede desquiciar a cualquiera, ahora lo sé). Por los "Mandarina time". A Alain ("Monsieur Magtan"), el mejor responsable de oficina que he tenido nunca. Por sus historias y aventuras que terminaban con una carcajada. A Alaitz por ayudarme con la biología y por enseñarme la importancia de las superficies. A Ione por estar siempre dispuesta a ayudar. Por sus comentarios puntiagudos que me hacían reír. A David ("El Titan") que ya en primero me enseñó que con una regla de tres las cosas salen clavadas. Por ayudarme en todo lo que le pedí. Por darme siempre la bienvenida en su laboratorio cuando me pasaba a por unos minutos de conversación. A Haritz por mostrarme el mundo de la fundición en su estado más científico. Por su forma de ver el mundo siempre enriquecedora. A los nuevos que seguirán nuestros pasos, Aitor y Miren. A Jon Ander, Edurne e Ibai que aunque dejaron Fabri 2 al poco de entrar yo siempre me han ayudado y aconsejado.

A los compañeros que han compartido conmigo cafés, comidas y excursiones. A Nuria por estar siempre dispuesta a ayudar. Por sus consejos en el SEM. Por preocuparse por "Copper Dog". A Kintana por ayudarme en todo lo necesario. Por compartir conmigo los jueves. Por sus consejos y por decir las cosas claras. Por hacerme caso hasta cuando no sé lo que digo. A Nagore por ayudarme a diferenciar la realidad de los rumores. Por ser crítica con el mundo. Por sus venturas y desventuras. A Jon por decir las cosas claras. Por ayudarme con mis historias. A Ainarita por alegrarme con sus historietas. Por ayudarme cuando lo necesité. A Miriam por preocuparse por mí y por mi trabajo. Por ayudarme con la prensa. A Ireneo por hacerme reír contando sus historias de esa forma tan particular. Por hacerme ver que todos somos distintos y a la vez iguales. A Manex por sus consejos y sus ánimos. A Elena que llegó corriendo. A Erik por sus ánimos y por las tardes de jueves.

Agradecer también la peña "tupper", con los que he compartido frustraciones y risas. A Pablo (aunque una vez me atacó con agua), Joseba (buena suerte y buenas olas), Elías, Mikel (MA), Cruzado, Josu, Mikel (MC), Irantzu, Llavori y Chamorro. Gracias por amenizar las comidas. Agradecer a otros doctorandos con los que también tuve el gusto de trabajar. A Christian por sufrir conmigo este mundo de la biología. A Luis por no dejar una pregunta sin respuesta. A Ingo, Pitzo, Tena, Jon Ander, Joseba, Legarda.

. . . . . .

Azkenik eskerrak eman nahi nizkieke Gamboako kide guztiei, gure abentura, abesti eta barre guztiengatik.

References

[Aba05] C. Abad, S. P. nero, T. Proverbio, F. Proverbio, and R. Marín. "Sulfato de magnesio: ¿una panacea?". *INCI*, Vol. 30, No. 9, pp. 36–50, 2005.

[Agh10] E. Aghion, T. Yered, Y. Perez, and Y. Gueta. "The prospects of carrying and releasing drugs via biodegradable magnesium foam". *Advanced Engineering Materials*, Vol. 12, No. 8, pp. B374–B379, 2010.

[Alo12] C. Alonso, J. del Valle, M. Gamero, and M. F. L. de Mele. "Do phosphate ions affect the biodegradation rate of fluoride-treated Mg?". *Materials Letters*, Vol. 68, No. 0, pp. 149–152, 2012.

[Alv10] M. Alvarez-Lopez, M. D. Pereda, J. del Valle, M. Fernandez-Lorenzo, M. Garcia-Alonso, O. Ruano, and M. Escudero. "Corrosion behaviour of AZ31 magnesium alloy with different grain sizes in simulated biological fluids". *Acta Biomaterialia*, Vol. 6, No. 5, pp. 1763–1771, 2010.

[Ara00] P. Aranda, E. Planells, and J. Llopis. "Magnesio". *Ars Pharmaceutica*, Vol. 41, No. 1, pp. 91–100, 2000.

[Atr11] A. Atrens, M. Liu, and N. I. Z. Abidin. "Corrosion mechanism applicable to biodegradable magnesium implants". *Materials Science and Engineering: B*, Vol. 176, No. 20, pp. 1609–1636, 2011.

[Ave99] M. M. Avedesian and H. Baker. *Magnesium and Magnesium Alloys*. ASM International, 1999.

[Bac03] F.-W. Bach, D. Bormann, and P. Wilk. "Cellular Magnesium". In: J. Banhart and N. Fleck, Eds., *Cellular Metals and Metal Foaming Technology*, pp. 215–218, 2003.

[Bac05] F.-W. Bach, D. Bormann, P. Wilk, and R. Kucharski. "Production and Properties of foamed Magnesium". In: R. Singer, C. Körner, and V. Altstädt, Eds., *Cellular Metals and Polymers 2004*, pp. 77–78, 2005.

[Bai12] K. Bai, Y. Zhang, Z. Fu, C. Zhang, X. Cui, E. Meng, S. Guan, and J. Hu. "Fabrication of chitosan/magnesium phosphate composite coating and the in

vitro degradation properties of coated magnesium alloy". *Materials Letters*, Vol. 73, No. 0, pp. 59–61, 2012.

[Ban01] J. Banhart. "Manufacture, characterisation and application of cellular metals and metal foams". *Progress in Materials Science*, Vol. 46, No. 6, pp. 559–632, 2001.

[Bar07] P. Barlis, J. Tanigawa, and C. D. Mario. "Coronary bioabsorbable magnesium stent: 15-month intravascular ultrasound and optical coherence tomography findings". *European Heart Journal*, Vol. 28, No. 19, p. 2319, 2007.

[Bla98] J. Black and G. Hasting. *Handbook of biomaterials properties*. Champman & Hall, 1998.

[Bli08] C. van Blitterswijk, Ed. *Tissue Engineering*. Elsevier Inc., 2008.

[Boy00] B. Boyan and Z. Schwartz. "Modulation of osteogenesis via implant surface design". In: J. Davies, Ed., *Bone engineering*, pp. 232–239, Toronto: em squared Inc., 2000.

[Bra10] H. S. Brar and M. V. Manuel. "The dissolution behavior of a Mg-Zn-Ca alloy for biomedical applications". pp. 647–649, Seattle, WA, United states, 2010.

[Bur09] P. Burke, G. J. Kipouros, D. Fancelli, and V. Laverdiere. "Sintering fundamentals of magnesium powders". *Canadian Metallurgical Quarterly*, Vol. 48, No. 2, pp. 123–132, 2009.

[Cai10] Y. Cai, J. Zhang, S. Zhang, S. Venkatraman, X. Zeng, H. Du, and D. Mondal. "Osteoblastic cell response on fluoridated hydroxyapatite coatings: the effect of magnesium incorporation". *Biomedical Materials*, Vol. 5, No. 5, p. 054114 (7 pp.), 2010.

[Cal95] W. D. Callister. *Introducción a la Ciencia e Ingeniería de los Materiales*. Editorial Reverté, 1995.

[Cao12] J. Cao, N. Kirkland, K. Laws, N. Birbilis, and M. Ferry. "Ca-Mg-Zn bulk metallic glasses as bioresorbable metals". *Acta Biomaterialia*, Vol. 8, No. 6, pp. 2375–2383, 2012.

[Car10a] M. Carboneras, L. Hernandez-Alvarado, Y. E. Mireles, L. S. Hernandez, M. Garcia-Alonso, and M. L. Escudero. "Chemical conversion treatments to protect biodegradable magnesium in applications as temporary implants for bone repair; Tratamientos quimicos de conversion para la proteccion de magnesio biodegradable en aplicaciones temporales de reparacion osea". *Revista de Metalurgia (Madrid)*, Vol. 46, No. 1, pp. 86–92, 2010.

[Car10b] M. Carboneras, R. Lozano, B. Pérez-Maceda, J. del Valle, E. Onofre, L. Hernández, M. García-Alonso, and M. Escudero. "Biomateriales biodegradables de base magnesio: comportamiento mecánico y frente a la corrosión en medio fisiológico con y sin células". In: *XI Congreso Nacional de Materiales*, pp. COM–159, 2010.

[Car11a] M. Carboneras, M. Garcia-Alonso, and M. Escudero. "Biodegradation kinetics of modified magnesium-based materials in cell culture medium". *Corrosion Science*, Vol. 53, No. 4, pp. 1433–1439, 2011.

[Car11b] M. Carboneras, C. Iglesias, B. Pérez-Maceda, J. del Valle, M. García-Alonso, M. Alobera, C. Clemente, J. Rubio, M. Escudero, and R. Lozano. "Corrosion behaviour and in vitro/in vivo biocompatibility of surface-modified AZ31 alloy; Comportamiento frente a la corrosión y biocompatibilidad in vitro/in vivo de la aleación AZ31 modificada superficialmente". *Revista de Metalurgia (Madrid)*, Vol. 47, No. 3, pp. 212–223, 2011.

[Car11c] M. Carboneras, B. Peréz-Maceda, J. del Valle, M. García-Alonso, R. Lozano, and M. Escudero. "In vitro performance of magnesium processed by different routes for bone regeneration applications". *Materials Letters*, Vol. 65, pp. 3020–3023, 2011.

[Cas02] D. G. Castner and B. D. Ratner. "Biomedical surface science: Foundations to frontiers". *Surface Science*, Vol. 500, No. 1-3, pp. 28–60, 2002.

[Cas11] C. Castellani, R. A. Lindtner, P. Hausbrandt, E. Tschegg, S. E. Stanzl-Tschegg, G. Zanoni, S. Beck, and A.-M. Weinberg. "Bone-implant interface strength and osseointegration: Biodegradable magnesium alloy versus standard titanium control". *Acta Biomaterialia*, Vol. 7, No. 1, pp. 432–440, 2011.

[Che11a] S. Chen, S. Guan, B. Chen, W. Li, J. Wang, L. Wang, S. Zhu, and J. Hu. "Corrosion behavior of TiO_2 films on Mg-Zn alloy in simulated body fluid". *Applied Surface Science*, Vol. 257, No. 9, pp. 4464–4467, 2011.

[Che11b] X.-B. Chen, N. Birbilis, and T. Abbott. "A simple route towards a hydroxyapatite-$Mg(OH)_2$ conversion coating for magnesium". *Corrosion Science*, Vol. 53, No. 6, pp. 2263–2268, 2011.

[Cho11] L. Choudhary, J. Szmerling, R. Goldwasser, and R. S. Raman. "Investigations into stress corrosion cracking behaviour of AZ91D magnesium alloy in physiological environment". *Procedia Engineering*, Vol. 10, No. 0, pp. 518–523, 2011.

[Con06] Y. Conde, J.-F. Despois, R. Goodall, A. Marmottant, L. Salvo, C. San-Marchi, and A. Mortensen. "Replication Processing of Highly Porous Materials". *Advanced Engineering Materials*, Vol. 8, No. 9, pp. 795–803, 2006.

[Con10] T. da Conceicao, N. Scharnagl, C. Blawert, W. Dietzel, and K. Kainer. "Surface modification of magnesium alloy AZ31 by hydrofluoric acid treatment and its effect on the corrosion behaviour". *Thin Solid Films*, Vol. 518, No. 18, pp. 5209–5218, 2010.

[Con11] T. F. da Conceicao, N. Scharnagl, W. Dietzel, D. Hoeche, and K. Kainer. "Study on the interface of PVDF coatings and HF-treated AZ31 magnesium alloy: Determination of interfacial interactions and reactions with self-healing properties". *Corrosion Science*, Vol. 53, No. 2, pp. 712–719, 2011.

[Cor07] D. A. Cortés, H. Y. López, and D. Mantovani. "Spontaneous and biomimetic apatite formation on pure magnesium". *Materials Science Forum*, Vol. 539-543, pp. 589–594, 2007.

[Coy10] A. Coy, F. Viejo, P. Skeldon, and G. Thompson. "Susceptibility of rare-earth-magnesium alloys to micro-galvanic corrosion". *Corrosion Science*, Vol. 52, No. 12, pp. 3896–3906, 2010.

[Cur98] J. Currey. *Handbook of biomaterials properties*, Chap. A1, pp. 3–14. Champman & Hall, 1998.

[Den07] B. Denkena and A. Lucas. "Biocompatible magnesium alloys as absorbable implant materials adjusted surface and subsurface properties by machining processes". *CIRP Annals - Manufacturing Technology*, Vol. 56, No. 1, pp. 113–116, 2007.

[Den09] B. Denkena, L. De Leon, and A. Lucas. "Machining processes of degradable implant materials to adjust surface and subsurface properties". pp. 977–979, Munich, Germany, 2009.

[Di 04] C. Di Mario, H. Griffiths, O. Goktekin, N. Peeters, J. Verbist, M. Bosiers, K. Deloose, B. Heublein, R. Rohde, V. Kasese, C. Ilsley, and R. Erbel. "Drug-eluting bioabsorbable magnesium stent". *Journal of Interventional Cardiology*, Vol. 17, No. 6, pp. 391–395, 2004.

[Dom06] M. Dominici, K. L. Blanc, I. Mueller, I. Slaper-Cortenbach, F. M. D. Krause, R. Deans, A. Keating, D. Prockop, and E. Horwitz. "Minimal criteria for defining multipotent mesenchymal stromal cells. The International Society for Cellular Therapy position statemt". *Cytotherapy*, Vol. 8, pp. 315–317, 2006.

[Duy07] O. Duygulu, R. Kaya, G. Oktay, and A. Kaya. "Investigation on the potential of magnesium alloy AZ31 as a bone implant". *Materials Science Forum*, Vol. 546-549, pp. 421–424, 2007.

[El 03] S. El-Rahman. "Neuropathology of aluminum toxicity in rats (glutamate and GABA impairment)". *Pharm Res*, Vol. 47, pp. 189–194, 2003.

[Eli10] A. Eliezer and F. Witte. "Corrosion behavior of magnesium alloys in biomedical environments". pp. 17–20, Beer-Sheva, Israel, 2010.

[Erd10] N. Erdmann, A. Bondarenko, M. Hewicker-Trautwein, N. Angrisani, J. Reifenrath, A. Lucas, and A. Meyer-Lindenberg. "Evaluation of the soft tissue biocompatibility of MgCa0.8 and surgical steel 316L in vivo: A comparative study in rabbits". *BioMedical Engineering OnLine*, p. 63, 2010.

[Eri09] M. Erinc, W. Sillekens, R. Mannens, and R. Werkhoven. "Applicability of existing magnesium alloys as biomedical implant materials". In: *Magnesium Technology*, pp. 209–214, San Francisco, CA, United states, 2009.

[Eur06] EuropeanTechnologyPlatform. "Nanomedicine. Nanotechnology for Health". Tech. Rep., November 2006.

[Fer08] P. Fernandez, L. Cruz, and J. Coleto. "Manufacturing processes of cellular metals. Part I: Liquid route processes". *Revista de Metalurgia (Madrid)*, Vol. 44, No. 6, pp. 540–555, 2008.

[Fer09] P. Fernandez, L. Cruz, and J. Coleto. "Manufacturing processes of cellular metals. Part II. Solid route, metals deposition, other processes". *Revista de Metalurgia (Madrid)*, Vol. 45, No. 2, pp. 124–142, 2009.

[Fey10] F. Feyerabend, J. Fischer, J. Holtz, F. Witte, R. Willumeit, H. Drücker, C. Vogt, and N. Hort. "Evaluation of short-term effects of rare earth and other elements used in magnesium alloys on primary cells and cell lines". *Acta Biomaterialia*, Vol. 6, No. 5, pp. 1834–1842, 2010.

[Fis10] J. Fischer, M. H. Prosenc, M. Wolff, N. Hort, R. Willumeit, and F. Feyerabend. "Interference of magnesium corrosion with tetrazolium-based cytotoxicity assays". *Acta Biomaterialia*, Vol. 6, No. 5, pp. 1813–1823, 2010.

[Gao07] J. Gao, Y. Xue, L. Qiao, Y. Wang, and Y. Zhang. "Surface modification of magnesium with rare earth conversion films for biomedical protection". *Materials Science Forum*, Vol. 546-549, pp. 601–604, 2007.

[Gao10] J. Gao, S. Guan, J. Chen, L. Wang, S. Zhu, J. Hu, and Z. Ren. "Fabrication and characterization of rod-like nano-hydroxyapatite on MAO coating supported on Mg-Zn-Ca alloy". *Applied Surface Science*, Vol. 257, No. 6, pp. 2231–2237, 2010.

[Gao11a] J. Gao, S. Guan, Z. Ren, Y. Sun, S. Zhu, and B. Wang. "Homogeneous corrosion of high pressure torsion treated Mg-Zn-Ca alloy in simulated body fluid". *Materials Letters*, Vol. 65, No. 4, pp. 691–693, 2011.

[Gao11b] J. Gao, X. Shi, B. Yang, S. Hou, E. Meng, F. Guan, and S. Guan. "Fabrication and characterization of bioactive composite coatings on Mg-Zn-Ca alloy by

MAO/sol-gel". *Journal of Materials Science: Materials in Medicine*, Vol. 22, No. 7, pp. 1681–1687, 2011.

[Gar06] W. E. Garrett-Jr., M. F. Swiontkowski, J. N. Weinstein, J. Callaghan, R. N. Rosier, D. J. Berry, J. Harrast, G. P. Derosa, and the Research Committee of The American Board of Orthopaedic Surgery. "American Board of Orthopaedic Surgery Practice of the Orthopaedic Surgeon: Part-II, Certification Examination Case Mix". *The Journal of Bone & Joint Surgery*, Vol. 88, pp. 660–667, 2006.

[Gho10] A. Ghoneim, A. Fekry, and M. Ameer. "Electrochemical behavior of magnesium alloys as biodegradable materials in Hank's solution". *Electrochimica Acta*, Vol. 55, No. 20, pp. 6028–6035, 2010.

[Gib97] L. Gibson and M. Ashby. *Cellular Solids. Cambridge Solid State Science Series*, Cambridge University press, 1997.

[Gon06] J. M. González, M. López, and G. Ruiz. "vt5 - Nanomedicina. Informe de vigilancia tecnológica". http://www.madrimasd.org/informacionidi/biblioteca/publicacion/Vigilancia-Tecnologica/default.asp, 2006.

[Gon12] S. González, E. Pellicer, J. Fornell, A. Blanquer, L. Barrios, E. Ibáñez, P. Solsona, S. Suriñach, M. Baró, C. Nogués, and J. Sort. "Improved mechanical performance and delayed corrosion phenomena in biodegradable Mg-Zn-Ca alloys through Pd-alloying". *Journal of the Mechanical Behavior of Biomedical Materials*, Vol. 6, No. 0, pp. 53–62, 2012.

[Goo13] R. Goodall and A. Mortensen. "Porous Metals". In: K. Hono and D. Laughlin, Eds., *Physical Metallurgy: 5th Edition*, p. (in print), Elsevier, Amsterdam, NL, 2013.

[Gri04] H. Griffiths, P. Peeters, J. Verbist, M. Bosiers, K. Deloose, B. Heublein, R. Rohde, V. Kasese, C. Ilsley, and C. D. Mario. "Future devices: bioabsorbable stents". *The British Journal of Cardiology (Acute & Interventional Carciology)*, Vol. 11, pp. 80–84, 2004.

[Gu09] X. Gu, Y. Zheng, Y. Cheng, S. Zhong, and T. Xi. "In vitro corrosion and biocompatibility of binary magnesium alloys". *Biomaterials*, Vol. 30, No. 4, pp. 484–498, 2009.

[Gu10a] X. Gu, W. Zhou, Y. Zheng, Y. Cheng, S. Wei, S. Zhong, T. Xi, and L. Chen. "Corrosion fatigue behaviors of two biomedical Mg alloys - AZ91D and WE43 - In simulated body fluid". *Acta Biomaterialia*, Vol. 6, No. 12, pp. 4605–4613, 2010.

[Gu10b] X. Gu and Y. Zheng. "A review on magnesium alloys as biodegradable materials". *Frontiers of Materials Science in China*, Vol. 4, No. 2, pp. 111–115, 2010.

[Gu10c] X. Gu, Y. Zheng, S. Zhong, T. Xi, J. Wang, and W. Wang. "Corrosion of, and cellular responses to Mg-Zn-Ca bulk metallic glasses". *Biomaterials*, Vol. 31, No. 6, pp. 1093–1103, 2010.

[Gu10d] X. Gu, W. Zhou, Y. Zheng, L. Dong, Y. Xi, and D. Chai. "Microstructure, mechanical property, bio-corrosion and cytotoxicity evaluations of Mg/HA composites". *Materials Science and Engineering C*, Vol. 30, No. 6, pp. 827–832, 2010.

[Gua11] S. Guan, J. Hu, L. Wang, S. Zhu, H. Wang, J. Wang, W. Li, Z. Ren, S. Chen, E. Meng, J. Gao, S. Hou, B. Wang, and B. Chen. *Magnesium Alloys - Corrosion and Surface Treatments*, Chap. Mg Alloys Development and Surface Modification for Biomedical Application, pp. 109–152. InTech, 2011.

[Gum04] J. Gums. "Magnesium in cardiovascular and other disorders". *American Journal of Health-System Pharmacy*, Vol. 61, No. 15, pp. 1569–1576, 2004.

[Hah11] B. Hahn, D. Park, J. Choi, J. Ryu, W. Yoon, J. Choi, H. Kim, and S. Kim. "Aerosol deposition of hydroxyapatite-chitosan composite coatings on biodegradable magnesium alloy". *Surface and Coatings Technology*, Vol. 205, No. 8-9, pp. 3112–3118, 2011.

[Ham12] C. Hampp, B. Ullmann, J. Reifenrath, N. Angrisani, D. Dziuba, D. Bormann, J.-M. Seitz, and A. Meyer-Lindenberg. "Research on the Biocompatibility of the New Magnesium Alloy LANd442 - An In Vivo Study in the Rabbit Tibia over 26 Weeks". *Advanced Engineering Materials*, Vol. 14, No. 3, pp. B28–B37, 2012.

[Han09] A. C. Hänzi, A. S. Sologubenko, and P. J. Uggowitzer. "Design strategy for microalloyed ultra-ductile magnesium alloys for medical applications". pp. 75–82, Gold Coast, QLD, Australia, 2009.

[Han10] A. C. Hänzi, I. Gerber, M. Schinhammer, J. F. Löffler, and P. J. Uggowitzer. "On the in vitro and in vivo degradation performance and biological response of new biodegradable Mg-Y-Zn alloys". *Acta Biomaterialia*, Vol. 6, No. 5, pp. 1824–1833, 2010.

[Han11] A. C. Hänzi, A. Metlar, M. Schinhammer, H. Aguib, T. C. Lüth, J. F. Löffler, and P. J. Uggowitzer. "Biodegradable wound-closing devices for gastrointestinal interventions: Degradation performance of the magnesium tip". *Materials Science and Engineering: C*, Vol. 31, No. 5, pp. 1098–1103, 2011.

[Hao09] G. L. Hao, F. S. Han, and W. D. Li. "Processing and mechanical properties of magnesium foams". *Journal of Porous Materials*, Vol. 16, No. 3, pp. 251–256, 2009.

[Hen02] L. L. Hench and J. M. Polak. "Third-generation biomedical materials". *Science*, Vol. 295, No. 5557, pp. 1014+1016–1017, 2002.

[Her07a] H. Hermawan, D. Dubé, and D. Mantovani. "Development of Degradable Fe-35Mn Alloy for Biomedical Application". *Advanced Materials Research*, Vol. 15-17, pp. 107–112, 2007.

[Her07b] H. Hermawan, M. Moravej, D. Dubé, M. Fiset, and D. Mantovani. "Degradarion Behaviour of Metallic Biomaterials for Degradable Stents". *Advanced Materials Research*, Vol. 15-17, pp. 113–118, 2007.

[Her10a] H. Hermawan, D. Dubé, and D. Mantovani. "Developments in metallic biodegradable stents". *Acta Biomaterialia*, Vol. 6, No. 5, pp. 1693–1697, 2010.

[Her10b] H. Hermawan, D. Dubé, and D. Mantovani. "Degradable metallic biomaterials: Design and development of Fe-Mn alloys for stents". *Journal of Biomedical Materials Research Part A*, Vol. 93A, No. 1, pp. 1–11, 2010.

[Her10c] H. Hermawan, A. Purnama, D. Dubé, J. Couet, and D. Mantovani. "Fe-Mn alloys for metallic biodegradable stents: Degradation and cell viability studies". *Acta Biomaterialia*, Vol. 6, No. 5, pp. 1852–1860, 2010.

[Heu03] B. Heublein, R. Rohde, V. Kaese, M. Niemeyer, W. Hartung, and A. Haverich. "Biocorrosion of magnesium alloys: a new principle in cardiovascular implant technology?". *Heart*, Vol. 89, pp. 651–656, 2003.

[Hir10a] S. Hiromoto and M. Tomozawa. "Corrosion behavior of magnesium with hydroxyapatite coatings formed by hydrothermal treatment". *Materials Transactions*, Vol. 51, No. 11, pp. 2080–2087, 2010.

[Hir10b] S. Hiromoto and A. Yamamoto. "Control of degradation rate of bioabsorbable magnesium by anodization and steam treatment". *Materials Science and Engineering C*, Vol. 30, No. 8, pp. 1085–1093, 2010.

[Hor10] N. Hort, Y. Huang, D. Fechner, M. Störmer, C. Blawert, F. Witte, C. Vogt, H. Drücker, R. Willumeit, K. Kainer, and F. Feyerabend. "Magnesium alloys as implant materials - Principles of property design for Mg-RE alloys". *Acta Biomaterialia*, Vol. 6, No. 5, pp. 1714–1725, 2010.

[Hou12] S. Hou, R. Zhang, S. Guan, C. Ren, J. Gao, Q. Lu, and X. Cui. "In vitro corrosion behavior of Ti-O film deposited on fluoride-treated Mg-Zn-Y-Nd alloy". *Applied Surface Science*, Vol. 258, No. 8, pp. 3571–3577, 2012.

[Hu02] Y. Hu, D. W. Grainger, S. R. Winn, and J. O. Hollinger. "Fabrication of poly(α-hydroxy acid) foam scaffolds using multiple solvent systems". *J. Biomed. Mater. Res.*, Vol. 59, No. 3, pp. 563–572, 2002.

[Hua07] J. Huang, Y. Ren, Y. Jiang, B. Zhang, and K. Yang. "In vivo study of degradable magnesium and magnesium alloy as bone implant". *Frontiers of Materials Science in China*, Vol. 1, No. 4, pp. 405–409, 2007.

[Hua10] Z. Huan, M. Leeflang, J. Zhou, L. Fratila-Apachitei, and J. Duszczyk. "In vitro degradation behavior and cytocompatibility of Mg-Zn-Zr alloys". *Journal of Materials Science: Materials in Medicine*, Vol. 21, No. 9, pp. 2623–2635, 2010.

[Hus78] E. Huse. "A new ligature?". *Chicago Medical Journal and Examiner*, Vol. 37, pp. 171–172, 1878.

[Ian01] S. Iannello and F. Belfiore. "Hypomagnesemia. A review of pathophysiological, clinical and therapeutical aspects". *Panminerva Medica*, Vol. 43, No. 3, pp. 177–209, 2001.

[Ito08] A. Ito and R. Z. LeGeros. "Magnesium- and Zinc-Substituted Beta-Tricalcium Phosphates As Potential Bone Substitute Biomaterials". *Key Engineering Materials*, Vol. 377, pp. 85–98, 2008.

[Jam11] M. Jamesh, S. Kumar, and T. S. Narayanan. "Corrosion behavior of commercially pure Mg and ZM21 Mg alloy in Ringer's solution - Long term evaluation by EIS". *Corrosion Science*, Vol. 53, No. 2, pp. 645–654, 2011.

[Jo11] J.-H. Jo, B.-G. Kang, K.-S. Shin, H.-E. Kim, B.-D. Hahn, D.-S. Park, and Y.-H. Koh. "Hydroxyapatite coating on magnesium with MgF_2 interlayer for enhanced corrosion resistance and biocompatibility". *Journal of Materials Science: Materials in Medicine*, Vol. 22, No. 11, pp. 2437–2447, 2011.

[Kan08] M. B. Kannan and R. K. S. Raman. "In vitro degradation and mechanical integrity of calcium-containing magnesium alloys in modified-simulated body fluid". *Biomaterials*, Vol. 29, No. 15, pp. 2306–2314, 2008.

[Kan10] S. Kannan, F. Goetz-Neunhoeffer, J. Neubauer, S. Pina, P. Torres, and J. Ferreira. "Synthesis and structural characterization of strontium - and magnesium-co-substituted -tricalcium phosphate". *Acta Biomaterialia*, Vol. 6, No. 2, pp. 571–576, 2010.

[Kan11] M. B. Kannan, R. Singh Raman, F. Witte, C. Blawert, and W. Dietzel. "Influence of circumferential notch and fatigue crack on the mechanical integrity of biodegradable magnesium-based alloy in simulated body fluid". *Journal of Biomedical Materials Research - Part B Applied Biomaterials*, Vol. 96 B, No. 2, pp. 303–309, 2011.

[Kas02] B. Kasemo. "Biological surface science". *Surface Science*, Vol. 500, No. 1-3, pp. 656–677, 2002.

[Kea98] T. Keaveny. *Handbook of biomaterials properties*, Chap. A2 Cancellous bone, pp. 15–23. Champman & Hall, 1998.

[Kei11] S. Keim, J. G. Brunner, B. Fabry, and S. Virtanen. "Control of magnesium corrosion and biocompatibility with biomimetic coatings". *Journal of Biomedical Materials Research - Part B Applied Biomaterials*, Vol. 96 B, No. 1, pp. 84–90, 2011.

[Ken12] A. Kennedy. *Powder Metallurgy*, Chap. Porous Metals and Metal Foams Made from Powders, pp. 31–46. InTech, 2012.

[Kim08] Y. K. Kim, M. H. Lee, M. N. Prasad, I. S. Park, M. H. Lee, K. W. Seol, and T. S. Bae. "Surface characteristics of magnesium alloys treated by anodic oxidation using pulse power". *Advanced Materials Research*, Vol. 47-50, pp. 1290–1293, 2008.

[Kir10] N. T. Kirkland, N. Birbilis, J. Walker, T. Woodfield, G. J. Dias, and M. P. Staiger. "In-vitro dissolution of magnesium-calcium binary alloys: Clarifying the unique role of calcium additions in bioresorbable magnesium implant alloys". *Journal of Biomedical Materials Research - Part B Applied Biomaterials*, Vol. 95, No. 1, pp. 91–100, 2010.

[Kir12] N. Kirkland, N. Birbilis, and M. Staiger. "Assessing the corrosion of biodegradable magnesium implants: A critical review of current methodologies and their limitations". *Acta Biomaterialia*, Vol. 8, No. 3, pp. 925–936, 2012.

[Kra10] A. Krause, N. von der Hoh, D. Bormann, C. Krause, F.-W. Bach, H. Windhagen, and A. Meyer-Lindenberg. "Degradation behaviour and mechanical properties of magnesium implants in rabbit tibiae". *Journal of Materials Science*, Vol. 45, No. 3, pp. 624–632, 2010.

[Kuw00] H. Kuwahara, Y. Al-Abdullat, M. Ohta, S. Tsutsumi, K. Ikeuchi, and T. Aizawa. "Surface Reaction of Magnesium in Hank's Solution". *Materials Science Forum*, Vol. 350-351, pp. 349–358, 2000.

[Lam32] A. Lambotte. "L'utilisation du magnesium comme materiel perdu dans l'osteosynthèse". *Bull Mém Soc Nat Chir*, Vol. 28, pp. 1325–1334, 1932.

[Lau11] D. Laurencin, N. Almora-Barrios, N. H. de Leeuw, C. Gervais, C. Bonhomme, F. Mauri, W. Chrzanowski, J. C. Knowles, R. J. Newport, A. Wong, Z. Gan, and M. E. Smith. "Magnesium incorporation into hydroxyapatite". *Biomaterials*, Vol. 32, No. 7, pp. 1826–1837, 2011.

[Li08] Z. Li, X. Gu, S. Lou, and Y. Zheng. "The development of binary Mg-Ca alloys for use as biodegradable materials within bone". *Biomaterials*, Vol. 29, No. 10, pp. 1329–1344, 2008.

[Li10a] H. Li, Y. Wang, Y. Cheng, and Y. Zheng. "Surface modification of Ca60Mg15Zn25 bulk metallic glass for slowing down its biodegradation rate in water solution". *Materials Letters*, Vol. 64, No. 13, pp. 1462–1464, 2010.

[Li10b] J. Li, Y. Song, S. Zhang, C. Zhao, F. Zhang, X. Zhang, L. Cao, Q. Fan, and T. Tang. "In vitro responses of human bone marrow stromal cells to a fluoridated hydroxyapatite coated biodegradable Mg-Zn alloy". *Biomaterials*, Vol. 31, No. 22, pp. 5782–5788, 2010.

[Li10c] J. Li, P. Cao, X. Zhang, S. Zhang, and Y. He. "In vitro degradation and cell attachment of a PLGA coated biodegradable Mg-6Zn based alloy". *Journal of Materials Science*, Vol. 45, No. 22, pp. 6038–6045, 2010.

[Li10d] Y. Li, M. Li, W. Hu, P. Hodgson, and C. Wen. "Biodegradable Mg-Ca and Mg-Ca-Y alloys for regenerative medicine". pp. 2192–2195, Cairns, QLD, Australia, 2010.

[Li11a] J. Li, P. Han, W. Ji, Y. Song, S. Zhang, Y. Chen, C. Zhao, F. Zhang, X. Zhang, and Y. Jiang. "The in vitro indirect cytotoxicity test and in vivo interface bioactivity evaluation of biodegradable FHA coated Mg-Zn alloys". *Materials Science and Engineering: B*, Vol. 176, No. 20, pp. 1785–1788, 2011.

[Li11b] M. Li, Q. Chen, W. Zhang, W. Hu, and Y. Su. "Corrosion behavior in SBF for titania coatings on Mg-Ca alloy". *Journal of Materials Science*, Vol. 46, No. 7, pp. 2365–2369, 2011.

[Li11c] W. Li, S. Guan, J. Chen, J. Hu, S. Chen, L. Wang, and S. Zhu. "Preparation and in vitro degradation of the composite coating with high adhesion strength on biodegradable Mg-Zn-Ca alloy". *Materials Characterization*, Vol. 62, No. 12, pp. 1158–1165, 2011.

[Lih10] M. Lihe, W. Yulin, W. Yizao, H. Fang, and H. Yuan. "Corrosion Resistance of Ag-ion Implanted Mg-Ca-Zn Alloys in SBF". *Rare Metal Materials and Engineering*, Vol. 39, No. 12, pp. 2075–2078, 2010.

[Liu10a] C. Liu, Y. Wang, R. Zeng, X. Zhang, W. Huang, and P. Chu. "In vitro corrosion degradation behaviour of Mg-Ca alloy in the presence of albumin". *Corrosion Science*, Vol. 52, No. 10, pp. 3341–3347, 2010.

[Liu10b] G. Liu, J. Hu, Z. Ding, and C. Wang. "Bioactive calcium phosphate coating formed on micro-arc oxidized magnesium by chemical deposition". *Applied Surface Science*, Vol. 257, No. 6, pp. 2051–2057, 2010.

[Lu07a] H. Lu, S. Zhang, L. Cheng, P. Chen, W. Zhou, J. Liu, and J. Zhou. "Repair of articular cartilage defect with cell-loaded nano-HA/PLGA composites". *Key Engineering Materials*, Vol. 330-332 II, pp. 1185–1188, 2007.

[Lu07b] S. K. Lu, H. I. Yeh, T. Y. Tian, and W. H. Lee. "Degradation of Magnesium Alloys in Biological Solutions and Reduced Phenotypic Expresions of Endothelial Cell Grown on There Alloys". *International Federation for Medical and Biological Engineering, Proceedings*, Vol. 15, No. IFMBE (2007) Proceedings 15, pp 98-101, pp. 98–101, 2007.

[Lu11] P. Lu, L. Cao, Y. Liu, X. Xu, and X. Wu. "Evaluation of magnesium ions release, biocorrosion, and hemocompatibility of MAO/PLLA-modified magnesium alloy WE42". *Journal of Biomedical Materials Research - Part B Applied Biomaterials*, Vol. 96 B, No. 1, pp. 101–109, 2011.

[Ma10] C. Ma, X. Zhang, L. Qu, and M. Li. "Calcium and Phosphate Biocoatings on Magnesium Alloy Fabricated By Micro-arc Oxidation". *Advanced Materials Research*, Vol. 105-106, pp. 565–568, 2010.

[Ma11a] J. Ma, C. Chen, D. Wang, and J. Hu. "Synthesis, characterization and in vitro bioactivity of magnesium-doped sol-gel glass and glass-ceramics". *Ceramics International*, Vol. 37, No. 5, pp. 1637–1644, 2011.

[Ma11b] X. Ma, Y. Lv, Z. Gao, and G. Cheng. "Surface modification of biomedical magnesium alloys by PHB". *Advanced Materials Research*, Vol. 146-147, pp. 1170–1173, 2011.

[Man07] G. Mani, M. D. Feldman, D. Patel, and C. M. Agrawal. "Coronary stents: A materials perspective". *Biomaterials*, Vol. 28, No. 9, pp. 1689–1710, 2007.

[Mar06] G. Marco. *Evaluación de la humectabilidad y de la rugosidad de superficies de titanio con diferentes tratamientos y su relación con la adhesión celular*. PhD thesis, Universidad de Granada, 2006.

[Mat01] H. Matsuno, A. Yokoyama, F. Watari, M. Uo, and T. Kawasaki. "Biocompatibility and osteogenesis of refractory metal implants, titanium, hafnium, niobium, tantalum and rhenium". *Biomaterials*, Vol. 22, No. 11, pp. 1253–1262, 2001.

[Men11] E. Meng, S. Guan, H. Wang, L. Wang, S. Zhu, J. Hu, C. Ren, J. Gao, and Y. Feng. "Effect of electrodeposition modes on surface characteristics and corrosion properties of fluorine-doped hydroxyapatite coatings on Mg-Zn-Ca alloy". *Applied Surface Science*, Vol. 257, No. 11, pp. 4811–4816, 2011.

[Mic05] A. Michiardi. *Nuevo tratamiento de oxidación en aleaciones de NiTi para aplicaciones biomédicas. Caracterización superficial y respuesta biológica in vitro*. PhD thesis, Universitat Politècnica de Catalunya, 2005.

[MIT06a] MIT. MIT Open Course Ware "Design of Medical Device and Implants". http://ocw.mit.edu/courses/mechanical-engineering/2-782j-design-of-medical-devices-and-implants-spring-2006/lecture-notes/ [last checked 2013/09/01] 2006.

[MIT06b] MIT. MIT Open Course Ware "Molecular principles of biomaterials". http://ocw.mit.edu/courses/biological-engineering/20-462j-molecular-principles-of-biomaterials-spring-2006/index.htm [last checked 2013/09/01] 2006.

[Mor09] E. Mora, G. Garcés, E. O. norbe, P. Pérez, and P. Adeva. "High-strength Mg-Zn-Y alloys produced by powder metallurgy". *Scripta Materialia*, Vol. 60, No. 9, pp. 776–779, 2009.

[Mor10a] M. Moravej, F. Prima, M. Fiset, and D. Mantovani. "Electroformed iron as new biomaterial for degradable stents: Development process and structure-properties relationship". *Acta Biomaterialia*, Vol. 6, No. 5, pp. 1726–1735, 2010.

[Mor10b] M. Moravej, A. Purnama, M. Fiset, J. Couet, and D. Mantovani. "Electroformed pure iron as a new biomaterial for degradable stents: In vitro degradation and preliminary cell viability studies". *Acta Biomaterialia*, Vol. 6, No. 5, pp. 1843–1851, 2010.

[Mor11] M. Moravej and D. Mantovani. "Biodegradable Metals for Cardiovascular Stent Application: Interests and New Opportunities". *International Journal of Molecular Sciences*, Vol. 12, pp. 4250–4270, 2011.

[Mro10] W. Mroz, A. Bombalska, S. Burdynska, M. Jedynski, A. Prokopiuk, B. Budner, A. Slosarczyk, A. Zima, E. Menaszek, A. Scisowska-Czarnecka, and K. Niedzielski. "Structural studies of magnesium doped hydroxyapatite coatings after osteoblast culture". *Journal of Molecular Structure*, Vol. 977, No. 1-3, pp. 145–152, 2010.

[Mue10] W.-D. Mueller, M. L. Nascimento, and M. F. L. de Mele. "Critical discussion of the results from different corrosion studies of Mg and Mg alloys for biomaterial applications". *Acta Biomaterialia*, Vol. 6, No. 5, pp. 1749–1755, 2010.

[Nag03] J. Nagels, M. Stokdijk, and P. Rozing. "Stress shielding and bone resorption in shoulder arthroplasty". *J Shoulder Elbow Surg*, Vol. 12, pp. 35–39, 2003.

[Ng10] W. Ng, K. Chiu, and F. Cheng. "Effect of pH on the in vitro corrosion rate of magnesium degradable implant material". *Materials Science and Engineering: C (Materials for Biological Applications)*, Vol. 30, No. 6, pp. 898–903, 2010.

[Nii01] T. Niinimäki, J. Junila, and P. Jalovaara. "A proximal fixed anatomic femoral stem reduces stress shielding". *International Orthopaedics*, Vol. 25, pp. 85–88, 2001.

[Ohb09] S. Ohba, F. Yano, and U. Chung. "Tissue Engineering of Bone and Cartilage". *IBMS BoneKey*, Vol. 6, No. 11, pp. 405–419, 2009.

[Oza08] S. Ozan and S. Bilhan. "Effect of fabrication parameters on the pore concentration of the aluminum metal foam, manufactured by powder metallurgy process". *International Journal of Advanced Manufacturing Technology*, Vol. 39, No. 3-4, pp. 257–260, 2008.

[Pee05] P. Peeters, M. Bosiers, J. Verbist, K. Deloose, and B. Heublein. "Preliminary Results After Application of Absorbable Metal Stents in Patients With Critical Limb Ischemia". *Journal of Endovascular Therapy*, Vol. 12, pp. 1–5, 2005.

[Pen10] Q. Peng, Y. Huang, L. Zhou, N. Hort, and K. Kainer. "Preparation and properties of high purity Mg-Y biomaterials". *Biomaterials*, Vol. 31, No. 3, pp. 398–403, 2010.

[Per10] M. Pereda, C. Alonso, L. Burgos-Asperilla, J. del Valle, O. Ruano, P. Perez, and M. F. L. de Mele. "Corrosion inhibition of powder metallurgy Mg by fluoride treatments". *Acta Biomaterialia*, Vol. 6, No. 5, pp. 1772–1782, 2010.

[Per11] M. Pereda, C. Alonso, M. Gamero, J. del Valle, and M. F. L. de Mele. "Comparative study of fluoride conversion coatings formed on biodegradable powder metallurgy Mg: The effect of chlorides at physiological level". *Materials Science and Engineering C*, Vol. 31, No. 5, pp. 858–865, 2011.

[Peu03a] M. Peuster, C. Fink, and C. Von Schnakenburg. "Biocompatibility of corroding tungsten coils: In vitro assessment of degradation kinetics and cytotoxicity on human cells". *Biomaterials*, Vol. 24, No. 22, pp. 4057–4061, 2003.

[Peu03b] M. Peuster, C. Fink, P. Wohlsein, M. Bruegmann, A. Gunther, V. Kaese, M. Niemeyer, H. Haferkamp, and C. V. Schnakenburg. "Degradation of tungsten coils implanted into the subclavian artery of New Zealand white rabbits is not associated with local or systemic toxicity". *Biomaterials*, Vol. 24, No. 3, pp. 393–399, 2003.

[Peu03c] M. Peuster, V. Kaese, G. Wuensch, C. Von Schnakenburg, M. Niemeyer, C. Fink, H. Haferkamp, and G. Hausdorf. "Composition and In Vitro Biocompatibility of Corroding Tungsten Coils". *Journal of Biomedical Materials Research - Part B Applied Biomaterials*, Vol. 65, No. 1, pp. 211–216, 2003.

[Pie08] A. Pietak, P. Mahoney, G. Dias, and M. Staiger. "Bone-like matrix formation on magnesium and magnesium alloys". *Journal of Materials Science: Materials in Medicine*, Vol. 19, No. 1, pp. 407–415, 2008.

[Pul10] Z. Puliang, L. Bin, Z. Dong, T. Yongwei, Y. Shengrong, and W. Jinqing. "Ceramic coatings of magnesium alloy for biomaterial applications". *Key Engineering Materials*, Vol. 434-435, pp. 634–637, 2010.

[Qu11] Q. Qu, J. Ma, L. Wang, L. Li, W. Bai, and Z. Ding. "Corrosion behaviour of AZ31B magnesium alloy in NaCl solutions saturated with CO_2". *Corrosion Science*, Vol. 53, No. 4, pp. 1186–1193, 2011.

[Ral10] K. Ralston and N. Birbilis. "Effect fo Grain Size on Corrosion: A Review". *Corrosion*, Vol. 66, No. 7, pp. 075005–1 – 075005–13, 2010.

[Raz10] M. Razavi, M. Fathi, and M. Meratian. "Microstructure, mechanical properties and bio-corrosion evaluation of biodegradable AZ91-FA nanocomposites for biomedical applications". *Materials Science and Engineering A*, Vol. 527, No. 26, pp. 6938–6944, 2010.

[Rei10] J. Reifenrath, A. Krause, D. Bormann, B. Von Rechenberg, H. Windhagen, and A. Meyer-Lindenberg. "Profound differences in the in-vivo-degradation and biocompatibility of two very similar rare-earth containing Mg-alloys in a rabbit model". pp. 1054–1061, P.O. Box 101161, Weinheim, D-69451, Germany, 2010.

[Ren07a] Y. Ren, J. Huang, B. Zhang, and K. Yang. "Preliminary study of biodegradation of AZ31B magnesium alloy". *Front. Mater. Sci.*, Vol. 1, No. 4, pp. 401–404, 2007.

[Ren07b] Y. Ren, H. Wang, J. Huang, B. Zhang, and K. Yang. "Study of biodegradation of pure magnesium". *Key Engineering Materials*, Vol. 342-343, No. Key Engineering Materials, pp. 601–604, 2007.

[Sab09] M. I. Sabir, X. Xu, and L. Li. "A review on biodegradable polymeric materials for bone tissue engineering applications". *Journal of Materials Science*, Vol. 44, No. 21, pp. 5713–5724, 2009.

[Sar00] N.-E. L. Saris, E. Mervaala, H. Karppanen, J. A. Khawaja, and A. Lewenstam. "Magnesium. An update on physiological, clinical and analytical aspects". *Clinica Chimica Acta*, Vol. 294, pp. 1–26, 2000.

[Sch10] C. Schille, H.-P. Reichel, N. Hort, and J. Geis-Gerstorfer. "Corrosion of Experimental Magnesium Alloys for use as a Possible Bone Replacement Material". In: *Magnesium: 8th International Conference on Magnesium Alloys and their Applications*, pp. 1195–1200, Weinheim, Germany, 2010.

[Sea10] M. Sealy and Y. Guo. "Surface integrity and process mechanics of laser shock peening of novel biodegradable magnesium-calcium (Mg-Ca) alloy". *Journal of the Mechanical Behavior of Biomedical Materials*, Vol. 3, No. 7, pp. 488–496, 2010.

[Sei10] J.-M. Seitz, D. Bormann, J. Stahl, S. Schumacher, M. Kietzmann, S. Kramer, B. Schwab, T. Lenarz, and F.-W. Bach. "The Potential for Magnesium Alloys Containing Neodymium in Medical Engineering". pp. 1193–1194, Weinheim, Germany, 2010.

[Sei11] J.-M. Seitz, K. Collier, E. Wulf, D. Bormann, and F.-W. Bach. "Comparison of the Corrosion Behavior of Coated and Uncoated Magnesium Alloys in an In Vitro Corrosion Environment". *Advanced Engineering Materials*, Vol. 13, No. 9, pp. B313–B323, 2011.

[Shi09] P. Shi, W. Ng, M. Wong, and F. Cheng. "Improvement of corrosion resistance of pure magnesium in Hanks' solution by microarc oxidation with sol-gel TiO_2 sealing". *Journal of Alloys and Compounds*, Vol. 469, No. 1-2, pp. 286–292, 2009.

[Shi10] Z. Shi, M. Liu, and A. Atrens. "Measurement of the corrosion rate of magnesium alloys using Tafel extrapolation". *Corrosion Science*, Vol. 52, No. 2, pp. 579–588, 2010.

[Sil00] C. Silvestre, L. Fagoaga, M. GarciandÃa, I. Lanzeta, M. Mateo, and M. Zapata. "Sterilisation". *ANALES Sis San Navarra*, Vol. 23 (Suppl. 2), pp. 95–103, 2000.

[Smo12] B. Smola, L. Joska, V. Březina, I. Stulíková, and F. Hnilica. "Microstructure, corrosion resistance and cytocompatibility of Mg-5Y-4Rare Earth-0.5Zr (WE54) alloy". *Materials Science and Engineering: C*, Vol. 32, No. 4, pp. 659–664, 2012.

[Son99] G. L. Song and A. Atrens. "Corrosion Mechanisms of Magnesium Alloys". *Advanced Engineering Materials*, Vol. 1, No. 1, pp. 11–33, 1999.

[Son03] G. Song and A. Atrens. "Understanding magnesium corrosion. A framework for improved alloy performance". *Advanced Engineering Materials*, Vol. 5, No. 12, pp. 837–858, 2003.

[Son05] G. Song. "Recent progress in corrosion and protection of magnesium alloys". *Advanced Engineering Materials*, Vol. 7, No. 7, pp. 563–586, 2005.

[Son07a] G. Song. "Control of biodegradation of biocompatible magnesium alloys". *Corrosion Science*, Vol. 49, No. 4, pp. 1696–1701, 2007.

[Son07b] G. Song. "Control of Degradation of Biocompatible Magnesium in a Pseudo-Physiological Environment by a Ceramic like Anodized Coating". *Advanced Materials Research*, Vol. 29-30, pp. 95–98, 2007.

[Son07c] G. Song and S. Song. "A possible biodegradable magnesium implant material". *Advanced Engineering Materials*, Vol. 9, No. 4, pp. 298–302, 2007.

[Son08] Y. W. Song, D. Y. Shan, and E. H. Han. "Electrodeposition of hydroxyapatite coating on AZ91D magnesium alloy for biomaterial application". *Materials Letters*, Vol. 62, No. 17-18, pp. 3276–3279, 2008.

[Son10] Y. Song, S. Zhang, J. Li, C. Zhao, and X. Zhang. "Electrodeposition of Ca-P coatings on biodegradable Mg alloy: In vitro biomineralization behavior". *Acta Biomaterialia*, Vol. 6, No. 5, pp. 1736–1742, 2010.

[Sta06] M. P. Staiger, A. M. Pietak, J. Huadmai, and G. Dias. "Magnesium and its alloys as orthopedic biomaterials: A review". *Biomaterials*, Vol. 27, No. 9, pp. 1728–1734, 2006.

[Suc04] W. L. Suchanek, K. Byrappa, P. Shuk, R. E. Riman, V. F. Janas, and K. S. Tenhuisen. "Preparation of magnesium-substituted hydroxyapatite powders by the mechanochemical-hydrothermal method". *Biomaterials*, Vol. 25, No. 19, pp. 4647–4657, 2004.

[Swa03] R. Swaminathan. "Magnesium Metabolism and its Disorders". *Clin Biochem Rev.*, Vol. 24, pp. 47–66, 2003.

[Tan10] L.-L. Tan, Q. Wang, F. Geng, X.-S. Xi, J.-H. Qiu, and K. Yang. "Preparation and characterization of Ca-P coating on AZ31 magnesium alloy". *Transactions of Nonferrous Metals Society of China (English Edition)*, Vol. 20, No. SUPPL. 2, pp. s648–s654, 2010.

[Tie10] D. Tie, F. Feyerabend, N. Hort, R. Willumeit, and D. Hoeche. "XPS studies of magnesium surfaces after exposure to Dulbecco's modified eagle medium, Hank's buffered salt solution, and simulated body fluid". *Advanced Engineering Materials*, Vol. 12, No. 12, pp. B699–B704, 2010.

[Tir02] M. Tirrell, E. Kokkoli, and M. Biesalski. "The role of surface science in bio-engineered materials". *Surface Science*, Vol. 500, No. 1-3, pp. 61–83, 2002.

[Toj10] C. Tojal, J. Devaud, V. Amigó, and J. A. Calero. "Caracterización mecánica de aleaciones porosas base Ti producidas mediante la técnica de sinterización con espaciador". In: F. P. nalba, Ed., *XII Congreso Nacional de Propiedades Mecánicas de Sólidos*, pp. 116–122 (MET–07), 2010.

[Vog98] E. A. Vogler. "Structure and reactivity of water at biomaterial surfaces". *Advances in Colloid and Interface Science*, Vol. 74, pp. 69–117, 1998.

[Vog10] C. Vogt, K. Bechstein, S. Gruhl, M. Lange, H. Drucker, F. Witte, and J. Vogt. "Investigation of the Degradation of Biodegradable Mg Implant Alloys in vitro and in vivo by Analytical Methods". In: *Magnesium. 8th International Conference on Magnesium Alloys and their Applications*, pp. 1162–1174, Weinheim, Germany, 2010.

[Wan08] H. Wang, Z. M. Shi, and K. Yang. "Magnesium and Magnesium Alloys as Degradable Metallic Biomaterials". *Advanced Materials Research*, Vol. 32, pp. 207–210, 2008.

[Wan09] J. Wang, R. Zeng, J. Chen, and R. Chen. "Corrosion Behavior of Magnesium Alloy AX53 in Simulated Body Fluids". *Materials Science Forum*, Vol. 610-613, pp. 1174–1178, 2009.

[Wan10a] H. Wang, S. Guan, X. Wang, C. Ren, and L. Wang. "In vitro degradation and mechanical integrity of Mg-Zn-Ca alloy coated with Ca-deficient hydroxyapatite by the pulse electrodeposition process". *Acta Biomaterialia*, Vol. 6, No. 5, pp. 1743–1748, 2010.

[Wan10b] J. Wang, L. Wang, S. Guan, S. Zhu, C. Ren, and S. Hou. "Microstructure and corrosion properties of as sub-rapid solidification Mg-Zn-Y-Nd alloy in dynamic simulated body fluid for vascular stent application". *Journal of Materials Science: Materials in Medicine*, Vol. 21, No. 7, pp. 2001–2008, 2010.

[Wan11a] Y. Wang, X. Xie, H. Li, X. Wang, M. Zhao, E. Zhang, Y. Bai, and Y. Zheng. "Biodegradable CaMgZn bulk metallic glass for potential skeletal application". *Acta Biomaterialia*, Vol. 7, No. 8, pp. 3196–3208, 2011.

[Wan11b] Y. Wang, C. S. Lim, C. V. Lim, M. S. Yong, E. K. Teo, and L. N. Moh. "In vitro degradation behavior of M1A magnesium alloy in protein-containing simulated body fluid". *Materials Science and Engineering C*, Vol. 31, No. 3, pp. 579–587, 2011.

[Wei10] J. Wei, J. Jia, F. Wu, S. Wei, H. Zhou, H. Zhang, J.-W. Shin, and C. Liu. "Hierarchically microporous/macroporous scaffold of magnesium-calcium phosphate for bone tissue regeneration". *Biomaterials*, Vol. 31, No. 6, pp. 1260–1269, 2010.

[Wen00] C. Wen, Y. Yamada, K. Shimojima, M. Mabuchi, M. Nakamura, and T. Asahina. "Mechanical properties of cellular magnesium materials". *Materials Science Forum*, Vol. 350, pp. 359–364, 2000.

[Wen01] C. E. Wen, M. Mabuchi, Y. Yamada, K. Shimojima, Y. Chino, and T. Asahina. "Processing of biocompatible porous Ti and Mg". *Scripta Materialia*, Vol. 45, No. 10, pp. 1147–1153, 2001.

[Wen04] C. E. Wen, Y. Yamada, K. Shimojima, Y. Chino, H. Hosokawa, and M. Mabuchi. "Compressibility of porous magnesium foam: Dependency on porosity and pore size". *Materials Letters*, Vol. 58, No. 3-4, pp. 357–360, 2004.

[Wen07] G. Wen, J. Wang, M. Li, and X. Meng. "Study on tissue engineering scaffolds of silk fibroin-chitosan/nano- hydroxyapatite composite". pp. 971–974, Laubisrutistr.24, Stafa-Zuerich, CH-8712, Switzerland, 2007.

[Wen10] Z. Wen, C. Wu, C. Dai, and F. Yang. "Corrosion behaviors of Mg and its alloys with different Al contents in a modified simulated body fluid". *Journal of Alloys and Compounds*, Vol. 488, No. 1, pp. 392–399, 2010.

[Wil05] C. Wilson. *Mediation of Osteoblast Responses to Titanium Roughness by Adsorbed Proteins*. PhD thesis, Queensland University of Technology, 2005.

[Wil06] D. Williams. "New Interests in Magnesium". *European Medical Device Technology*, Vol. http://emdt.co.uk/article/new-interests-magnesium [Last checked 2013/09/01], 2006.

[Wil11] E. Willbold, A. Kaya, R. Kaya, F. Beckmann, and F. Witte. "Corrosion of magnesium alloy AZ31 screws is dependent on the implantation site". *Materials Science and Engineering: B*, Vol. 176, No. 20, pp. 1835–1840, 2011.

[Wit05] F. Witte, V. Kaese, H. Haferkamp, E. Switzer, A. Meyer-Lindenberg, C. J. Wirth, and H. Windhagen. "In vivo corrosion of four magnesium alloys and the associated bone response". *Biomaterials*, Vol. 26, No. 17, pp. 3557–3563, 2005.

[Wit06] F. Witte, J. Fisher, J. Nellesen, H. A. Crostack, V. Kaese, A. Pisch, F. Beckmann, and H. Windhagen. "In vitro and in vivo corrosion measurements of magnesium alloys". *Biomaterials*, Vol. 27, No. 7, pp. 1013–1018, 2006.

[Wit07a] F. Witte, H. Ulrich, C. Palm, and E. Willbold. "Biodegradable magnesium scaffolds: Part II: Peri-implant bone remodeling". *Journal of Biomedical Materials Research - Part A*, Vol. 81, No. 3, pp. 757–765, 2007.

[Wit07b] F. Witte, H. Ulrich, M. Rudert, and E. Willbold. "Biodegradable magnesium scaffolds: Part I: Appropriate inflammatory response". *Journal of Biomedical Materials Research - Part A*, Vol. 81, No. 3, pp. 748–756, 2007.

[Wit07c] F. Witte, F. Feyerabend, P. Maier, J. Fischer, M. Stormer, C. Blawert, W. Dietzel, and N. Hort. "Biodegradable magnesium-hydroxyapatite metal matrix composites". *Biomaterials*, Vol. 28, No. 13, pp. 2163–2174, 2007.

[Wit10a] F. Witte, J. Fischer, J. Nellesen, C. Vogt, J. Vogt, T. Donath, and F. Beckmann. "In vivo corrosion and corrosion protection of magnesium alloy LAE442". *Acta Biomaterialia*, Vol. 6, No. 5, pp. 1792–1799, 2010.

[Wit10b] F. Witte. "The history of biodegradable magnesium implants: A review". *Acta Biomaterialia*, Vol. 6, No. 5, pp. 1680–1692, 2010.

[Wol03] F. I. Wolf and A. Cittadini. "Chemistry and biochemistry of magnesium". *Molecular Aspects of Medicine*, Vol. 24, pp. 3–9, 2003.

[Won10] H. M. Wong, K. W. K. Yeung, K. O. Lam, V. Tam, P. K. Chu, K. D. K. Luk, and K. M. C. Cheung. "A biodegradable polymer-based coating to control the performance of magnesium alloy orthopaedic implants". *Biomaterials*, Vol. 31, No. 8, pp. 2084–2096, 2010.

[Wu07] C. Wu, J. Chang, W. Zhai, and S. Ni. "A novel bioactive porous bredigite ($Ca_7MgSi_4O_{16}$) scaffold with biomimetic apatite layer for bone tissue engineering". *Journal of Materials Science: Materials in Medicine*, Vol. 18, No. 5, pp. 857–864, 2007.

[Wu10] W. Wu, L. Petrini, D. Gastaldi, T. Villa, M. Vedani, E. Lesma, B. Previtali, and F. Migliavacca. "Finite element shape optimization for biodegradable magnesium alloy stents". *Annals of Biomedical Engineering*, Vol. 38, No. 9, pp. 2829–2840, 2010.

[Wu11] G. Wu, L. Gong, K. Feng, S. Wu, Y. Zhao, and P. K. Chu. "Rapid degradation of biomedical magnesium induced by zinc ion implantation". *Materials Letters*, Vol. 65, No. 4, pp. 661–663, 2011.

[Xia12] Y. Xia, B. Zhang, Y. Wang, M. Qian, and L. Geng. "In-vitro cytotoxicity and in-vivo biocompatibility of as-extruded Mg-4.0Zn-0.2Ca alloy". *Materials Science and Engineering: C*, Vol. 32, No. 4, pp. 665–669, 2012.

[Xin09] R. Xin, M. Wang, J. Gao, P. Liu, and Q. Liu. "Effect of Microstructure and Texture on Corrosion Resistance of Magnesium Alloy". *Materials Science Forum*, Vol. 610-613, No. Materials Science Forum Vols. 610-613 (2009) pp 1160-1163, pp. 1160–1163, 2009.

[Xin11a] Y. Xin, T. Hu, and P. Chu. "In vitro studies of biomedical magnesium alloys in a simulated physiological environment: A review". *Acta Biomaterialia*, Vol. 7, No. 4, pp. 1452–1459, 2011.

[Xin11b] Y. Xin, T. Hu, and P. K. Chu. "Degradation behaviour of pure magnesium in simulated body fluids with different concentrations of HCO^{3-}". *Corrosion Science*, Vol. 53, pp. 1522–1528, 2011.

[Xu08] L. Xu, E. Zhang, D. Yin, S. Zeng, and K. Yang. "In vitro corrosion behaviour of Mg alloys in a phosphate buffered solution for bone implant application". *Journal of Materials Science*, Vol. 19, No. 3, pp. 1017–1025, 2008.

[Xu09a] L. Xu, F. Pan, G. Yu, L. Yang, E. Zhang, and K. Yang. "In vitro and in vivo evaluation of the surface bioactivity of a calcium phosphate coated magnesium alloy". *Biomaterials*, Vol. 30, No. 8, pp. 1512–1523, 2009.

[Xu09b] L. Xu, E. Zhang, and K. Yang. "Phosphating treatment and corrosion properties of Mg-Mn-Zn alloy for biomedical application". *Journal of Materials Science: Materials in Medicine*, Vol. 20, No. 4, pp. 859–867, 2009.

[Xu12] L. Xu and A. Yamamoto. "In vitro degradation of biodegradable polymer-coated magnesium under cell culture condition". *Applied Surface Science*, Vol. 258, No. 17, pp. 6353–6358, 2012.

[Xue11] D. Xue, Y. Yun, M. J. Schulz, and V. Shanov. "Corrosion protection of biodegradable magnesium implants using anodization". *Materials Science and Engineering: C*, Vol. 31, No. 2, pp. 215–223, 2011.

[Xue12] D. Xue, Y. Yun, Z. Tan, Z. Dong, and M. J. Schulz. "In Vivo and In Vitro Degradation Behavior of Magnesium Alloys as Biomaterials". *Journal of Materials Science & Technology*, Vol. 28, No. 3, pp. 261–267, 2012.

[Yam99] Y. Yamada, K. Shimojima, Y. Sakaguchi, M. Mabuchi, M. Nakamura, T. Asahina, T. Mukai, H. Kanahashi, and K. Higashi. "Processing of an open-cellular AZ91 magnesium alloy with a low density of 0.05 g/cm^3". *Journal of Materials Science Letters*, Vol. 18, No. 18, pp. 1477–1480, 1999.

[Yan08] J. xin Yang, Y. peng Jiao, Q. shui Yin, Y. Zhang, and T. Zhang. "Calcium phosphate coating on magnesium alloy by biomimetic method: investigation of morphology, composition and formation process". *Frontiers of Materials Science in China*, Vol. 2, No. 2, pp. 149–155, 2008.

[Yan10] T. Yan, L. Tan, D. Xiong, X. Liu, B. Zhang, and K. Yang. "Fluoride treatment and in vitro corrosion behavior of an AZ31B magnesium alloy". *Materials Science and Engineering C*, Vol. 30, No. 5, pp. 740–748, 2010.

[Yin08] D.-s. Yin, E.-l. Zhang, and S.-y. Zeng. "Effect of Zn on mechanical property and corrosion property of extruded Mg-Zn-Mn alloy". *Transactions of Nonferrous Metals Society of China (English Edition)*, Vol. 18, No. 4, pp. 763–768, 2008.

[Yos03] H. Yoshimoto, Y. Shin, H. Terai, and J. Vacanti. "A biodegradable nanofiber scaffold by electrospinning and its potential for bone tissue engineering". *Biomaterials*, Vol. 24, No. 12, pp. 2077–2082, 2003.

[Yue08] C. Yuen and W. Ip. "Resorbable metallic implant: Findings from an animal model". *Advanced Materials Research*, Vol. 47-50, pp. 604–607, 2008.

[Zbe09] B. Zberg, P. Uggowitzer, and J. Loffler. "MgZnCa glasses without clinically observable hydrogen evolution for biodegradable implants". *Nature Materials*, Vol. 8, No. 11, pp. 887–891, 2009.

[Zen08] R. Zeng, W. Dietzel, F. Witte, N. Hort, and C. Blawert. "Progress and challenge for magnesium alloys as biomaterials". *Advanced Engineering Materials*, Vol. 10, No. 8, pp. B3–B14, 2008.

[Zha07] X. P. Zhang, Z. P. Zhao, F. M. Wu, Y. L. Wang, and J. Wu. "Corrosion and wear resistance of AZ91D magnesium alloy with and without microarc oxidation coating in Hank's solution". *Journal of Materials Science*, Vol. 42, pp. 8523–8528, 2007.

[Zha08] E. Zhang, W. He, H. Du, and K. Yang. "Microstructure, mechanical properties and corrosion properties of Mg-Zn-Y alloys with low Zn content". *Materials Science and Engineering: A*, Vol. 488, No. 1-2, pp. 102–111, 2008.

[Zha10] S. Zhang, X. Zhang, C. Zhao, J. Li, Y. Song, C. Xie, H. Tao, Y. Zhang, Y. He, Y. Jiang, and Y. Bian. "Research on an Mg-Zn alloy as a degradable biomaterial". *Acta Biomaterialia*, Vol. 6, No. 2, pp. 626–640, 2010.

[Zha11a] B. Zhang, Y. Hou, X. Wang, Y. Wang, and L. Geng. "Mechanical properties, degradation performance and cytotoxicity of Mg-Zn-Ca biomedical alloys with different compositions". *Materials Science and Engineering: C*, Vol. 31, No. 8, pp. 1667–1673, 2011.

[Zha11b] W. Zhang, Y. Shen, H. Pan, K. Lin, X. Liu, B. W. Darvell, W. W. Lu, J. Chang, L. Deng, D. Wang, and W. Huang. "Effects of strontium in modified biomaterials". *Acta Biomaterialia*, Vol. 7, No. 2, pp. 800–808, 2011.

[Zhe10] Y. Zheng, X. Gu, Y. Xi, and D. Chai. "In vitro degradation and cytotoxicity of Mg/Ca composites produced by powder metallurgy". *Acta Biomaterialia*, Vol. 6, No. 5, pp. 1783–1791, 2010.

[Zre03] H. Zreiqat, C. R. Howlett, A. Zannettino, P. Evans, C. Knabe, G. Schulze-Tanzil, and G. M. Shakibaei. "Surface modification of bioceramics affect osteoblastic cells response". *Key Engineering Materials*, Vol. 240-242, pp. 707–710, 2003.

Appendix A

Scientific contribution

A.1 Publications in scientific journals

J. Trinidad, G. Arruebarrena, E. Sáenz de Argandoña, G. Ruiz De Eguino, A. Infante, C. I. Rodríguez "Evaluation of magnesium alloys with alternative surface finishing for the proliferation and chondro-differentiation of human mesenchymal stem cells" *J. Phys.: Conf. Ser.* 252 012010

J. Trinidad, G. Arruebarrena, I. Marco, I. Hurtado, E. Sáenz de Argandoña "Effectivity of fluoride treatment on hydrogen and corrosion products generation in temporal implants for different magnesium alloys" Journal of Engineering in Medicine (Accepted)

J. Trinidad, I. Marco, G. Arruebarrena, J. Wendt, D. Letzig, E. Sáenz de Argandoña, and R. Goodall "Processing of Magnesium Porous Structures by Infiltration Casting for Biomedical Applications" Adv. Eng. Mater., 2012, 10.1002/adem.201300236 (Accepted)

J. Trinidad, G. Arruebarrena, W. van Grunsven, R. Goodall, E. Sáenz de Argandoña, G. C. Reilly "Corrosion and cell viability characterisation of Mg-Zn alloys for medical applications" (Under review)

A.2 Publications and presentations in conferences

J. Trinidad, G. Arruebarrena, E. Sáenz de Argandoña, G. Ruiz de Eguino, A. Infante, C. I. Rodríguez "Cultivo y diferenciación a cartílago de células madre mesenquimales

sobre aleaciones de magnesio" *XI Congreso Nacional de Materiales*, Zaragoza, June 23-25, 2010, COM-121

J. Trinidad, G. Arruebarrena, E. Sáenz de Argandoña, G. Ruiz de Eguino, A. Infante, C. I. Rodríguez "Evaluation of magnesium alloys with alternative surface finishing for the proliferation and chondro-differentiation of human mesenchymal stem cells" *BIOCOAT*, Zaragoza, June 24, 2010, SM-4

J. Trinidad, E. Sáenz de Argandoña, G. Arruebarrena "Fabricación de scaffolds de magnesio para aplicaciones biomédicas" *18 Congreso de Máquinas-Herramienta y Tecnologías de Fabricación*, Donostia-San Sebastián, 10-12 nov 2010

Appendix B

Scheme of the corrosion test

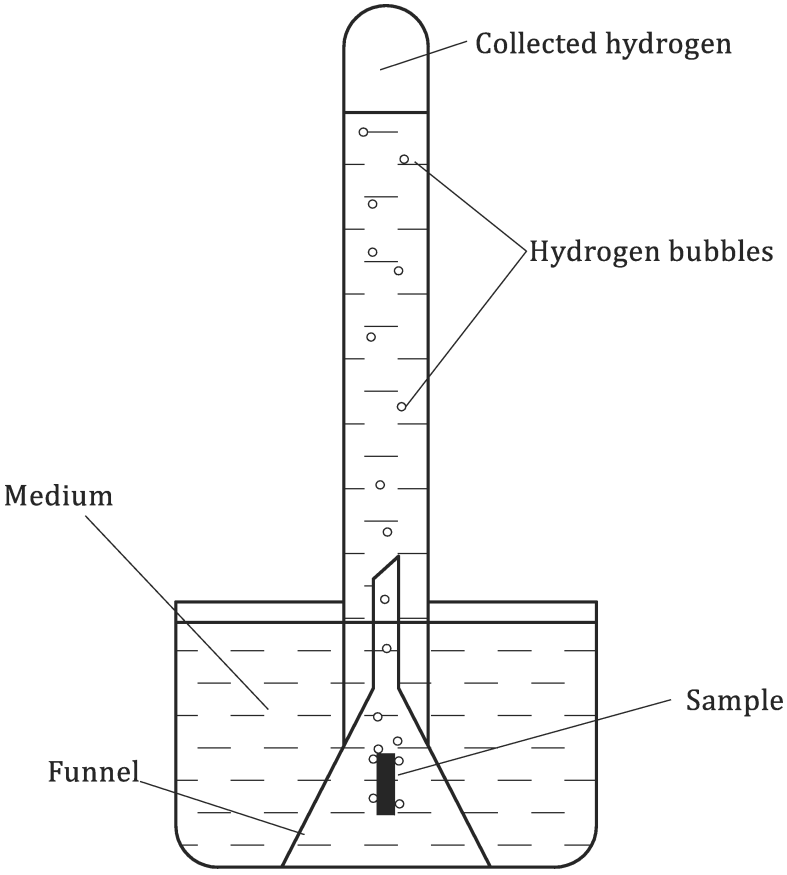

Figure B.1: Scheme of the hydrogen evolution test

Appendix C

Data of the corrosion tests

In this appendix, the data of the different corrosion tests carried out in Chapter 5, Chapter 6 and Chapter 7 are shown. Sample 5 and sample 6 were removed from the experiment at 24 and 72 hours respectively for SEM analysis.

Table C.1: Hydrogen evolution data of AZ31B in PBS [ml/mm^2]

	Sample 1	**Sample 2**	**Sample 3**	**Sample 4**	**Sample 5**	**Sample 6**
24 h	0.0043	0.0044	0.0036	0.0040	0.0040	0.0043
48 h	0.0055	0.0055	0.0056	0.0060	0.0056	-
72 h	0.0090	0.0079	0.0092	0.0096	0.0088	-
96 h	0.0110	0.0095	0.0112	0.0120	-	-

Table C.2: Hydrogen evolution data of AZ31BHF24h in PBS [ml/mm^2]

	Sample 1	**Sample 2**	**Sample 3**	**Sample 4**	**Sample 5**	**Sample 6**
24 h	0.0022	0.0028	0.0024	0.0018	0.0025	0.0018
48 h	0.0036	0.0039	0.0042	0.0028	0.0036	-
72 h	0.0068	0.0064	0.0081	0.0060	0.0058	-
96 h	0.0082	0.0078	0.0095	0.0071	-	-

Table C.3: Hydrogen evolution data of AZ31BHF72h in PBS [ml/mm^2]

	Sample 1	Sample 2	Sample 3	Sample 4	Sample 5	Sample 6
24 h	0.0007	0.0007	0.0007	0.0007	0.0007	0.007
48 h	0.0021	0.0021	0.0021	0.0022	0.0022	-
72 h	0.0039	0.0039	0.0042	0.0043	0.0043	-
96 h	0.0050	0.0050	0.0061	0.0051	-	-

Table C.4: Hydrogen evolution data of WE43 in PBS [ml/mm^2]

	Sample 1	Sample 2	Sample 3	Sample 4	Sample 5	Sample 6
24 h	0.0032	0.0037	0.0040	0.0040	0.0043	0.0041
48 h	0.0035	0.0037	0.0044	0.0052	0.0055	-
72 h	0.0074	0.0070	0.0072	0.0080	0.0094	-
96 h	0.0106	0.0092	0.0080	0.0092	-	-

Table C.5: Hydrogen evolution data of WE43HF24h in PBS [ml/mm^2]

	Sample 1	Sample 2	Sample 3	Sample 4	Sample 5	Sample 6
24 h	0.0025	0.0021	0.0021	0.0018	0.0014	0.0021
48 h	0.0032	0.0028	0.0029	0.0029	0.0024	-
72 h	0.0056	0.0049	0.0050	0.0047	0.0039	-
96 h	0.0060	0.0059	0.0061	0.0054	-	-

Table C.6: Hydrogen evolution data of WE43HF72h in PBS [ml/mm^2]

	Sample 1	Sample 2	Sample 3	Sample 4	Sample 5	Sample 6
24 h	0.0011	0.0011	0.0011	0.0011	-	0.0011
48 h	0.0021	0.0018	0.0018	0.0021	-	-
72 h	0.0039	0.0036	0.0036	0.0039	-	-
96 h	0.0050	0.0043	0.0040	0.0054	-	-

Table C.7: Hydrogen evolution data of ZM21 in PBS [ml/mm^2]

	Sample 1	Sample 2	Sample 3	Sample 4	Sample 5	Sample 6
24 h	0.0054	0.0058	0.0045	0.0047	0.0063	-
48 h	0.0083	0.0082	0.0075	0.0069	0.0086	-
72 h	0.0141	0.0152	0.0124	0.0128	0.0153	-
96 h	0.0157	0.0169	0.0146	0.0146	-	-

Table C.8: Hydrogen evolution data of ZM21HF24h in PBS [ml/mm^2]

	Sample 1	Sample 2	Sample 3	Sample 4	Sample 5	Sample 6
24 h	0.0014	0.0011	0.0011	0.0011	0.0011	0.0014
48 h	0.0036	0.0039	0.0029	0.0039	0.0033	-
72 h	0.0087	0.0086	0.0065	0.0078	0.0065	-
96 h	0.0109	0.0111	0.0083	0.0103	-	-

Table C.9: Hydrogen evolution data of ZM21HF72h in PBS [ml/mm^2]

	Sample 1	Sample 2	Sample 3	Sample 4	Sample 5	Sample 6
24 h	0.0007	0.0007	0.0007	0.0007	0.0007	0.0007
48 h	0.0011	0.0011	0.0011	0.0011	0.0011	-
72 h	0.0025	0.0025	0.0029	0.0028	0.0028	-
96 h	0.0040	0.0032	0.0043	0.0039	-	-

Table C.10: Hydrogen evolution data of ZM20 in PBS [ml/mm^2]

	Sample 1	Sample 2	Sample 3	Sample 4	Sample 5	Sample 6
24 h	0.0043	0.0039	0.0024	0.0036	0.0034	0.0046
48 h	0.0075	0.0071	0.0052	0.0064	0.0068	-
72 h	0.0121	0.0124	0.0114	0.0114	0.0136	-
96 h	0.0160	0.0156	0.0169	0.0150	-	-

Table C.11: Hydrogen evolution data of ZM20HF72h in PBS [ml/mm^2]

	Sample 1	Sample 2	Sample 3	Sample 4	Sample 5	Sample 6
24 h	0.0010	0.0010	0.0010	0.0010	0.0010	0.0017
48 h	0.0024	0.0019	0.0022	0.0023	0.0023	-
72 h	0.0054	0.0055	0.0061	0.0056	0.0065	-
96 h	0.0078	0.0075	0.0083	0.0076	-	-

Table C.12: Hydrogen evolution data of ZWM200 in PBS [ml/mm^2]

	Sample 1	Sample 2	Sample 3	Sample 4	Sample 5	Sample 6
24 h	0.0031	0.0038	0.0022	0.0025	0.0023	0.0019
48 h	0.0062	0.0066	0.0049	0.0050	0.0042	-
72 h	0.0119	0.0105	0.0099	0.0100	0.0113	-
96 h	0.0156	0.0126	0.0130	0.0144	-	-

Table C.13: Hydrogen evolution data of ZWM200HF72h in PBS [ml/mm^2]

	Sample 1	Sample 2	Sample 3	Sample 4	Sample 5	Sample 6
24 h	0.0010	0.0010	0.0010	0.0006	0.0010	0.0010
48 h	0.0014	0.0013	0.0015	0.0009	0.0015	-
72 h	0.0037	0.0029	0.0039	0.0025	0.0040	-
96 h	0.0048	0.0036	0.0048	0.0031	-	-

Table C.14: Hydrogen evolution data of ZXM200 in PBS [ml/mm^2]

	Sample 1	Sample 2	Sample 3	Sample 4	Sample 5	Sample 6
24 h	0.0030	0.0026	0.0034	0.0027	0.0036	0.0038
48 h	0.0043	0.0057	0.0052	0.0043	0.0062	-
72 h	0.0128	0.0124	0.0130	0.0112	0.0140	-
96 h	0.0230	0.0201	0.0248	0.0238	-	-

Table C.15: Hydrogen evolution data of ZXM200HF72h in PBS [ml/mm^2]

	Sample 1	Sample 2	Sample 3	Sample 4	Sample 5	Sample 6
24 h	0.0010	0.0010	0.0010	0.0011	0.0009	0.0009
48 h	0.0017	0.0020	0.0016	0.0018	0.0022	-
72 h	0.0049	0.0050	0.0042	0.0049	0.0057	-
96 h	0.0063	0.0060	0.0054	0.0067	-	-

Table C.16: Hydrogen evolution data of WE43HF72h foam (39 %) in PBS [ml/mm^2]

	Sample 1	Sample 2	Sample 3
24 h	0.0164	0.0113	0.0121
48 h	0.0327	0.0227	0.0226
72 h	0.0598	0.0473	0.0492
96 h	0.0911	0.0748	0.0914

Table C.17: Hydrogen evolution data of ZM20HF72h foam (43 %) in PBS [ml/mm^2]

	Sample 1	Sample 2	Sample 3
24 h	0.0040	0.0034	0.0031
48 h	0.0047	0.0048	0.0038
72 h	0.0081	0.0089	0.0084
96 h	0.0087	0.0103	0.0107

Table C.18: Hydrogen evolution data of ZWM200HF72h foam (69 %) in PBS [ml/mm^2]

	Sample 1	Sample 2	Sample 3
24 h	0.0040	0.0036	0.0077
48 h	0.0065	0.0045	0.0103
72 h	0.0113	0.0108	0.0155
96 h	0.0146	0.0144	0.0172

Table C.19: Hydrogen evolution data of ZXM200HF72h foam (30 %) in PBS [ml/mm^2]

	Sample 1	**Sample 2**	**Sample 3**
24 h	0.0093	0.0115	0.0133
48 h	0.0135	0.0148	0.0158
72 h	0.0195	0.0205	0.0225
96 h	0.0228	0.0246	0.0258

Table C.20: Hydrogen evolution data of ZXM200HF72h foam (44 %) in PBS [ml/mm^2]

	Sample 1	**Sample 2**	**Sample 3**
24 h	0.0135	0.0123	0.0195
48 h	0.0180	0.0145	0.0251
72 h	0.0240	0.0207	0.0334
96 h	0.0278	0.0230	0.0362

List of Figures

List of Tables